USGS
science for a changing world

Alkalic-Type Epithermal Gold Deposit Model

Chapter R of
Mineral Deposit Models for Resource Assessment

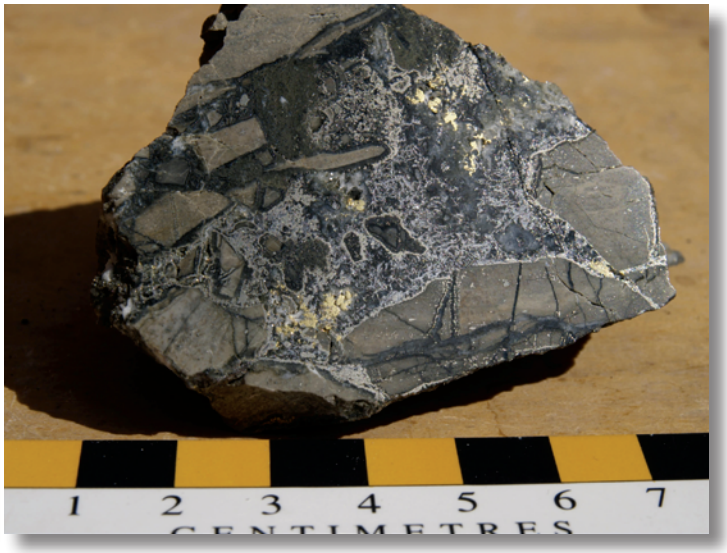

Scientific Investigations Report 2010–5070–R

U.S. Department of the Interior
U.S. Geological Survey

Cover. Photographs of alkalic-type epithermal gold deposits and ores. Upper left: Cripple Creek, Colorado—One of the largest alkalic-type epithermal gold deposits in the world showing the Cresson open pit looking southwest. Note the green funnel-shaped area along the pit wall is lamprophyre of the Cresson Pipe, a common alkaline rock type in these deposits. The Cresson Pipe was mined by historic underground methods and produced some of the richest ores in the district. The holes that are visible along several benches in the pit (bottom portion of photograph) are historic underground mine levels. (Photograph by Karen Kelley, USGS, April, 2002). Upper right: High-grade gold ore from the Porgera deposit in Papua New Guinea showing native gold intergrown with gold-silver telluride minerals (silvery) and pyrite. (Photograph by Jeremy Richards, University of Alberta, Canada, 2013, used with permission). Lower left: Mayflower Mine, Montana—High-grade hessite, petzite, benleonardite, and coloradoite in limestone. (Photograph by Paul Spry, Iowa State University, 1995, used with permission). Lower right: View of north rim of Navilawa Caldera, which hosts the Banana Creek prospect, Fiji, from the portal of the Tuvatu prospect. (Photograph by Paul Spry, Iowa State University, 2007, used with permission).

Alkalic-Type Epithermal Gold Deposit Model

By Karen D. Kelley, Paul G. Spry, Virginia T. McLemore, David L. Fey, and Eric D. Anderson

Chapter R of
Mineral Deposit Models for Resource Assessment

Scientific Investigations Report 2010–5070—R

U.S. Department of the Interior
U.S. Geological Survey

U.S. Department of the Interior
DAVID BERNHARDT, Secretary

U.S. Geological Survey
James F. Reilly II, Director

U.S. Geological Survey, Reston, Virginia: 2020

Suggested citation:
Kelley, K.D., Spry, P.G., McLemore, V.T., Fey, D.L., and Anderson, E.D., 2020, Alkalic-type epithermal gold deposit model: U.S. Geological Survey Scientific Investigations Report 2010–5070–R, 74 p., https://doi.org/10.3133/sir20105070R.

ISSN 2328-0328 (online)

Acknowledgments

We thank Antonio Arribas (University of Texas, El Paso) and Jeremy Richards (University of Alberta, Canada, deceased in 2019) who provided photographs, and Eric Jensen (EMX Royalty Corporation), who provided stimulating discussions about alkalic-type epithermal gold deposits. Ed du Bray (Emeritus, U.S. Geological Survey) and Jim Saunders (Consultant) reviewed the manuscript, which greatly improved the content.

Contents

Figures

Tables

Conversion Factors

U.S. customary units to International System of Units

Multiply	By	To obtain
	Length	
foot (ft)	0.3048	meter (m)
	Volume	
gallon (gal)	3.785	liter (L)
	Mass	
ounce, avoirdupois (oz)	28.35	gram (g)

International System of Units to U.S. customary units

Multiply	By	To obtain
	Length	
centimeter (cm)	0.3937	inch (in.)
millimeter (mm)	0.03937	inch (in.)
meter (m)	3.281	foot (ft)
kilometer (km)	0.6214	mile (mi)
	Area	
hectare (ha)	2.471	acre
square kilometer (km^2)	247.1	acre
	Volume	
liter (L)	33.81402	ounce, fluid (fl. oz)
liter (L)	0.2642	gallon (gal)
cubic meter (m^3)	35.31	cubic foot (ft^3)
cubic meter (m^3)	1.308	cubic yard (yd^3)
	Mass	
gram (g)	0.03527	ounce, avoirdupois (oz)
kilogram (kg)	2.205	pound avoirdupois (lb)
metric ton (t)	1.102	ton, short [2,000 lb]
metric ton (t)	0.9842	ton, long [2,240 lb]
	Energy	
joule (J)	0.0000002	kilowatt hour (kWh)
(Megajoule (MJ) equals 1,000,000 joules)		

Temperature in degrees Celsius (°C) may be converted to degrees Fahrenheit (°F) as
$°F = (1.8 \times °C) + 32$.

Temperature in degrees Fahrenheit (°F) may be converted to degrees Celsius (°C) as
$°C = (°F - 32) / 1.8$.

Elements

Ag	silver
Al	aluminum
Ar	argon
As	arsenic
Au	gold
Ba	barium
Bi	bismuth
Ca	calcium
Co	cobalt
Cu	copper
Cr	chromium
F	fluorine
Fe	iron
Hg	mercury
K	potassium
Mg	magnesium
Mn	manganese
Mo	molybdenum
Nb	niobium
Nd	neodymium
Ni	nickel
Pb	lead
Sb	antimony
Se	selenium
Si	silica
Sm	samarium
Sr	strontium
Te	tellurium
Th	thorium
Ti	titanium
U	uranium
V	vanadium
Y	yttrium
Zn	zinc
Zr	zirconium

Abbreviations

~	about
>	greater than
<	less than
fO_2	oxygen fugacity
AP	acid potential
CO_2	carbon dioxide
EM	electromagnetic
Ga.	billion years
HCN	hydrogen cyanide gas
HREE	heavy rare earth element
K_2O	potassium oxide
LREE	light rare earth element
Ma	million years ago (mega-annum)
m.y.	million years
Na_2O	sodium oxide
NAP	net acid production
NNP	net neutralization potential
NP	neutralization potential
NPR	neutralization potential ratio
per mil	one part per thousand
PGE	platinum group element
PNG	Papua New Guinea
ppb	parts per billion
ppm	parts per million
Q	Koenigsberger Ratio
REE	rare earth element
SI	magnetic susceptibility
SiO_2	silicon dioxide
wt%	weight percent

Alkalic-Type Epithermal Gold Deposit Model

By Karen D. Kelley,[1] Paul G. Spry,[2] Virginia T. McLemore,[3] David L. Fey,[1] and Eric D. Anderson[1]

Abstract

This report summarizes the primary characteristics of alkalic-type epithermal gold (Au) deposits and provides an updated descriptive model. These deposits, primarily of Mesozoic to Neogene age, are among the largest epithermal gold deposits in the world. Considered a subset of low-sulfidation epithermal deposits, they are spatially and genetically linked to small stocks or clusters of intrusions containing high alkali-element contents. Deposits occur as disseminations, breccia-fillings, and veins and may be spatially and genetically related to skarns and low-grade porphyry copper (Cu) or molybdenum (Mo) systems. Gold commonly occurs as native gold, precious metal tellurides, and as sub-micron gold in arsenian pyrite. Quartz, carbonate, fluorite, adularia, and vanadian muscovite/roscoelite are the most common gangue minerals. Alkalic-type gold deposits form in a variety of geological settings including continent-arc collision zones and back-arc or post-subduction rifts that are invariably characterized by a transition from convergent to extensional or transpressive tectonics.

The geochemical compositions of alkaline igneous rocks spatially linked with these deposits span the alkaline-subalkaline transition. Their alkali enrichment may be masked by potassic alteration, but the unaltered or least altered rocks (1) have chondrite normalized patterns that are commonly light rare earth element (LREE) enriched, (2) are heavy rare earth element (HREE) depleted, and (3) have high large ion lithophile contents and variable enrichment of high-field strength elements. Radiogenic isotopes suggest a mantle derivation for the alkalic magmas but allow crustal contamination.

Oxygen and hydrogen isotope compositions show that the fluids responsible for deposit formation are dominantly magmatic, although meteoric or other external fluids (seawater, evolved groundwater) also contributed to the ore-forming fluids responsible for these deposits. Carbon and sulfur isotope compositions in vein-hosted carbonates and sulfide gangue minerals, respectively, coincide with magmatic values, although a sedimentary source of carbon and sulfur is evident in several deposits.

Deep-seated structures are critical for the upwelling of hydrous alkalic magmas and for focusing magmatic-hydrothermal fluids to the site of precious metal deposition. The source of gold, silver (Ag), tellurium (Te), vanadium (V), and fluorine (F) was probably the alkalic igneous rocks themselves, and the coexistence of native gold, gold tellurides, and roscoelite in several deposits is primarily a function of similar physicochemical conditions during deposition (for example, overlapping pH and oxygen fugacity (fO_2).

Potential environmental impacts related to the mining and processing of alkalic-type epithermal gold deposits include acid mine drainage with high levels of metals, especially zinc (Zn), copper, lead (Pb), and arsenic. However, because alkalic-type gold deposits typically contain carbonates, which contribute calcium and magnesium ions that increase water hardness, aquatic life may be afforded some protection. Impacts vary widely as a function of host rocks, climate, topography, and mining methods.

Geologic mapping to (1) highlight the distribution of potassic alteration; (2) define fault density and orientation of structures; (3) determine the distribution of alkaline rocks and hydrothermal breccias; and (4) identify uniquely colored gangue minerals, such as fluorite and roscoelite, will be critical to exploration and future discoveries. Geophysical techniques that identify potassium (K) anomalies (for example, radiometric and spectroscopic surveys), as well as magnetic, resistivity, aeromagnetic, and gravity surveys, may help locate zones of high-permeability that control advecting hydrothermal fluids. Geochemical surveys that include analyses for Au, Ag, barium, Te, K, F, V, Mo, and mercury, which are key elements in these deposits, should be undertaken along with the measurement of other pathfinder elements such as arsenic, bismuth, Cu, iron, nickel, Pb, antimony, selenium, and Zn.

Introduction

Gold deposits related to alkaline igneous rocks have been referred to in many ways, including “alkaline igneous rock-related epithermal gold deposits,” “alkalic-related epithermal gold deposits,” and “alkalic-type epithermal deposits.” This report refers to these deposits as “alkalic-type epithermal deposits.” These epithermal deposits are found

[1]U.S. Geological Survey.

[2]Iowa State University.

[3]New Mexico Bureau of Geology and Mineral Resources.

throughout the world (fig. 1; table 1). Some porphyry deposits (Galore Creek and Mount Milligan in Canada, and Cadia and Goonumbla in Australia) that are transitional to or spatially associated with alkalic-type epithermal deposits are also included. The largest of the epithermal deposits (greater than [>] 100 metric tons gold) occur in Fiji, Papua New Guinea (PNG), and North America (fig. 2). This report is part of a U.S. Geological Survey Mineral Resources Program effort to update existing, and develop new, mineral deposit models. This effort by the U.S. Geological Survey is intended to supplement previously published models (Cox and Singer, 1986; du Bray, 1995) for use in mineral-resource and mineral-environmental assessments. This document is dependent on previous summary articles including those by Mutschler and others (1985), Mutschler and Mooney (1995), Richards (1995), Jensen and Barton (2000), and Kelley and Spry (2016).

Alkalic-type epithermal gold deposits are part of a family of epithermal deposits, and in fact are considered a subset of low-sulfidation epithermal gold deposits. Alkalic-type deposits are distinct enough in their characteristics, however, to warrant a separate model. The model for all other epithermal gold deposits is detailed in John and others (2018).

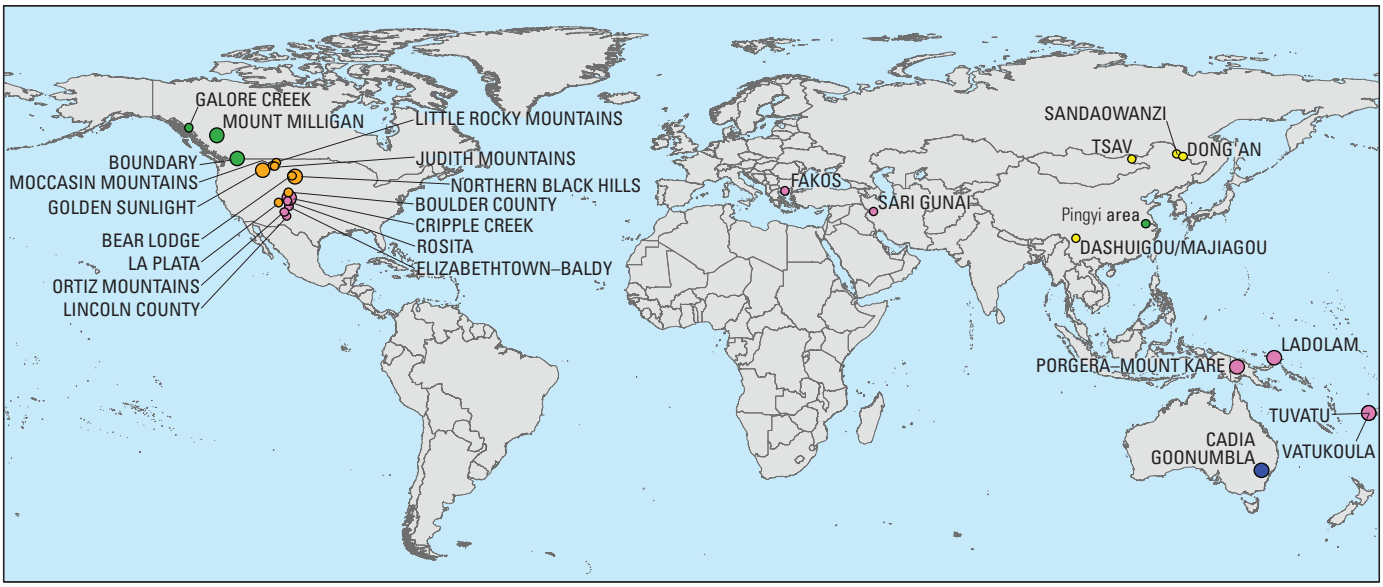

Base from U.S. Geological Survey Global 20 arc-second elevation data, 1996

EXPLANATION

LINCOLN COUNTY — **Gold deposit or district with identifier**

Geologic Age

- Oligocene and younger
- Late Cretaceous, Paleocene, or Eocene
- Early to middle Cretaceous
- Triassic to Jurassic
- Ordovician

Gold tonnage

- Less than 100 metric tons
- Greater than 100 metric tons

Figure 1. Locations of alkalic-type epithermal gold deposits. Deposits or districts (made up of several deposits) containing greater than 100 metric tons of gold are shown as large solid circles. The color of each circle corresponds to the age of the deposit or age of associated alkaline igneous rocks.

Table 1. Characteristics of selected alkalic-type epithermal gold deposits and related porphyry deposits.

[Table modified from Jensen and Barton (2000). Grade/tonnage and contained gold (Au) for many U.S. deposits from Mutschler (1992). ~, approximately; >, greater than; %, percent; ±, plus or minus; act, acanthite; Ag, silver; alt, altaite; ar, argentite; As, arsenic; aspy, arsenopyrite; avg, average; Ba, barium; bar, barite; bas, bastnaesite, bi, bismuthinite; Bi, bismuth; bn, bornite; born, bournonite; calc, calcite; carb, carbonates; cc, chalcocite; cn, cinnabar; cm, centimeter; co, coloradoite; cpy, chalcopyrite; Cu, copper; cv, calaverite; do, dolomite; em, empressite; en, enargite; epith, epithermal; F, fluorine; Fe, iron; fl, fluorite; fr, freibergite; gn, galena; g/t, grams per metric ton; hm, hematite; hs, hessite; K, potassium; km, kilometer; kr, krennerite; m, meter; Ma, millions of years ago; mc, marcasite; me, mernskyite; ml, melonite; mo, molybdenite; Mo, molybdenum; mrc, marcasite; mt, magnetite; Pb, lead; Pd, palladium; PGE, platinum group elements; po, pyrrhotite; porph, porphyry; ppm, parts per million; py, pyrite; pyr, pyrargyrite/proustite; pz, petzite; qtz, quartz; REE, rare earth elements; Sb, antimony; sch, scheelite; Se, selenium; ser, sericite; Si, silica; sp, sphalerite; spy, sperrylite; st, stuetzite; stb, stibnite; sy, sylvanite; TE, tellurium; Th, thorium; tn, tennantite; tour, tourmaline; tt, tetrahedrite; U, uranium; V, vanadium; W, tungsten; wo, wolframite; wt. %, weight percent; Zn, zinc]

District, location Type	Gold endowment: tonnage and grade Contained Au (million metric tons or Mt)	Age (millions of years ago or Ma)	Alkaline igneous rocks	Tectonic/geologic setting	Mineralization style/structure	Metallic minerals	Trace element association	Reference(s)
Porgera, Papua New Guinea Epithermal Au	51 Mt at 7 g/t Au 387 metric tons	5 Ma	Mafic alkaline volcanics; hawaiite-mugearite	Intrusive complex in fold-thrust belt formed by continent-island arc collision. Intrusions/mineralization controlled by crustal suture	Disseminated Au-pyrite with Au-Te epithermal veins controlled by normal faults	aspy, cpy, electrum, gn, hm, native Au, po, py, sp, tt, tellurides	Ag, Au, Te, V	Richards, 1990; Richards and others, 1991; Richards and Kerrich, 1993; Jensen and Barton, 2000; Ronacher and others, 2004
Mount Kare, Papua New Guinea Epithermal Au	51.5 Mt at 6.5 g/t Au 335 metric tons	5.5±0.1 Ma	Mafic alkaline volcanics; tephrite-basanite, alkali basalt, phonotephrite, mugearite	Intrusive complex in fold-thrust belt formed by continent-island arc collision. Intrusions/mineralization controlled by crustal suture	Metallic mineralization hosted in quartz-roscoelite veins and breccias whose emplacement was controlled by a steeply-dipping shear zone. Secondary Au found in colluvial deposits	Au-Ag alloy, gn native Au, py, pyr, sp, tt	Ag, Au, Pb, V, Zn	Richards and Ledlie, 1993
Ladolam, Lihir Island, Papua New Guinea Epithermal Au(±Cu)	29.1 Mt at >1 g/t Au 497 metric ton	0.18–1.5 Ma	Trachybasalts intruded by monzonite, syenite, and latite porphyry dikes	Eruptions of trachybasaltic and trachyandesitic volcanics followed emplacement of tholeiitic magmatism that resulted from oceanic subduction. Incipient rift formed after subduction, yielded shoshonitic volcanics	Deep stockwork qtz veins overlain by breccias hosting high Au	cn, cpy, gn, mc, native Au, py, sp, tellurides	Ag, Au, Sb, Te	Jensen and Barton, 2000; Müller and others, 2001; Carman, 2003

Table 1. Characteristics of selected alkalic-type epithermal gold deposits and related porphyry deposits.—Continued

[Table modified from Jensen and Barton (2000). Grade/tonnage and contained gold (Au) for many U.S. deposits from Mutschler (1992). ~, approximately; >, greater than; %, percent; ±, plus or minus; act, acanthite; Ag, silver; alt, altaite; ar, argentite; As, arsenic; aspy, arsenopyrite; avg, average; Ba, barium; bar, barite; bas, bastnaesite, bi, bismuthinite; Bi, bismuth; bn, bornite; born, bournonite; calc, calcite; carb, carbonates; cc, chalcocite; cn, cinnabar; cm, centimeter; co, coloradoite; cpy, chalcopyrite; Cu, copper; cv, calaverite; do, dolomite; em, empressite; en, enargite; epith, epithermal; F, fluorine; Fe, iron; fl, fluorite; fr, freibergite; gn, galena; g/t, grams per metric ton; hm, hematite; hs, hessite; K, potassium; km, kilometer; kr, krennerite; m, meter; Ma, millions of years ago; mc, marcasite; me, mernskyite; ml, melonite; mo, molybdenite; Mo, molybdenum; mrc, marcasite; mt, magnetite; Pb, lead; Pd, palladium; PGE, platinum group elements; po, pyrrhotite; porph, porphyry; ppm, parts per million; py, pyrite; pyr, pyrargyrite/proustite; pz, petzite; qtz, quartz; REE, rare earth elements; Sb, antimony; sch, scheelite; Se, selenium; ser, sericite; Si, silica; sp, sphalerite; spy, sperrylite; st, stuetzite; stb, stibnite; sy, sylvanite; TE, tellurium; Th, thorium; tn, tennantite; tour, tourmaline; tt, tetrahedrite; U, uranium; V, vanadium; W, tungsten; wo, wolframite; wt. %, weight percent; Zn, zinc]

District, location Type	Gold endowment: tonnage and grade Contained Au (million metric tons or Mt)	Age (millions of years ago or Ma)	Alkaline igneous rocks	Tectonic/geologic setting	Mineralization style/structure	Metallic minerals	Trace element association	Reference(s)
Tuvatu, Fiji Epithermal Au-Te transitional to porphyry Cu	Unknown tonnage and grade 13 metric tons	5.4–4.6 Ma	Shoshonites intruded by monzonite stocks	Adjacent to eroded shoshonite volcano along the >250 km northeast-trending Viti-Levu lineament; alkaline volcanism following island-arc magmatism, during waning stages of subduction; faults are north-northeast	Flat-lying Au-Te veins, stockworks, hydrothermal breccias. Multiple stages of veining; porphyry Cu style mineralization is adjacent to epithermal deposits	bi, en, gn, hm, mt, native Au, native bi, py, sp, tellurides, tt-tn	Au, F, Te, V	Scherbarth and Spry, 2006
Vatukoula (Emperor), Fiji Epithermal Au-Te(±Cu) transitional to porphyry Cu	14.7 Mt at 8.1 g/t Au 280 metric tons	3.8–4.8 Ma	Mafic alkaline volcanics intruded by monzonite stocks	Alkalic volcanism following island-arc magmatism. Emplaced during waning stages of subduction. Intrusions and mineralization controlled by large-scale regional structure	High grade Au-Te epithermal veins overlying deep Cu-porphyry mineralization	aspy, gn, hm, mt, native Au, py, sp, telluride minerals, tt-tn	Ag, As, Au, Cu, Te	Ahmad and others, 1987; Begg, 1996; Pals and Spry, 2003
Cadia, New South Wales Porphyry Cu-Au	530 Mt at 0.55 g/t Au 585 metric tons	Ordovician	Shoshonitic volcanic rocks intruded by quartz monzonite dikes and stocks	Island arc tectonic setting within Lachlan Fold Belt	Sheeted and stockwork quartz-sulfide veins and locally as disseminated and skarn mineralization	bn, cpy, native Au	Au, Cu, PGE	Holliday and others, 2002; Cooke and others, 2007

Table 1. Characteristics of selected alkalic-type epithermal gold deposits and related porphyry deposits.—Continued

[Table modified from Jensen and Barton (2000). Grade/tonnage and contained gold (Au) for many U.S. deposits from Mutschler (1992). ~, approximately; >, greater than; %, percent; ±, plus or minus; act, acanthite; Ag, silver; alt, altaite; ar, argentite; As, arsenic; aspy, arsenopyrite; avg, average; Ba, barium; bar, barite; bas, bastnaesite, bi, bismuthinite; Bi, bismuth; bn, bornite; born, bournonite; calc, calcite; carb, carbonates; cc, chalcocite; cn, cinnabar; cm, centimeter; co, coloradoite; cpy, chalcopyrite; Cu, copper; cv, calaverite; do, dolomite; em, empressite; en, enargite; epith, epithermal; F, fluorine; Fe, iron; fl, fluorite; fr, freibergite; gn, galena; g/t, grams per metric ton; hm, hematite; hs, hessite; K, potassium; km, kilometer; kr, krennerite; m, meter; Ma, millions of years ago; mc, marcasite; me, mernskyite; ml, melonite; mo, molybdenite; Mo, molybdenum; mrc, marcasite; mt, magnetite; Pb, lead; Pd, palladium; PGE, platinum group elements; po, pyrrhotite; porph, porphyry; ppm, parts per million; py, pyrite; pyr, pyrargyrite/proustite; pz, petzite; qtz, quartz; REE, rare earth elements; Sb, antimony; sch, scheelite; Se, selenium; ser, sericite; Si, silica; sp, sphalerite; spy, sperrylite; st, stuetzite; stb, stibnite; sy, sylvanite; TE, tellurium; Th, thorium; tn, tennantite; tour, tourmaline; tt, tetrahedrite; U, uranium; V, vanadium; W, tungsten; wo, wolframite; wt. %, weight percent; Zn, zinc]

District, location Type	Gold endowment: tonnage and grade Contained Au (million metric tons or Mt)	Age (millions of years ago or Ma)	Alkaline igneous rocks	Tectonic/geologic setting	Mineralization style/structure	Metallic minerals	Trace element association	Reference(s)
Goonumbla, New South Wales, Australia Porphyry Cu-Au	30 Mt at 0.5 g/t Au, 0.91 percent Cu	Ordovician	Alkaline volcanics intruded by diorite, monzonite, quartz monzonite, and post-ore syenite porphyries. Late mafic dikes (lamprophyre?)	Intrusions follow ring fracture in caldera within Lachlan Fold Belt	Disseminated Cu(Au) mineralization; stockwork quartz/sulfide veins in core	bn, cc, cpy, native Au, tellurides	Au, Cu, Te	Heithersay and Walshe, 1995
Tsav, Eastern Mongolia Epithermal Ag-Pb-Zn	Tonnage unknown 7.21 wt. % Pb, 3.42 wt. % Zn, 0.23 wt. % Cu; 141 g/t Ag	Late Mesozoic	Hypabyssal shoshonites to high-K calcalkaline volcanic rocks	Veins controlled by vertical northwest faults in extensional environment	3–4.5 km long, 0.3–3 m wide, banded qtz veins and veinlets	ar, aspy, cpy, electrum, gn, hm, fr, native Au, py, sp, tt	Ag, Au, As, Cu, Pb, Zn	Gantumur and others, 2005
Dong'an (=Eastern Dragon), northeast China Epithermal Au	14 Mt at 5.04 g/t 63.8 metric tons	108.1±2.4 Ma	Shoshonites to high-K calc-alkaline subvolcanics	Collisional belt with Andean type magmatic arcs formed as a result of subduction. Veins and intrusions controlled by post orogenic tensile shears and faults	1–7 m wide qtz veins with massive gangue minerals, disseminated ore minerals	ar, aspy, carb, cpy, electrum, gn, hm, py, sp	Ag, As, Au, Cu, Pb, Zn	Zhang and others, 2010

Table 1. Characteristics of selected alkalic-type epithermal gold deposits and related porphyry deposits.—Continued

[Table modified from Jensen and Barton (2000). Grade/tonnage and contained gold (Au) for many U.S. deposits from Mutschler (1992). ~, approximately; >, greater than; %, percent; ±, plus or minus; act, acanthite; Ag, silver; alt, altaite; ar, argentite; As, arsenic; aspy, arsenopyrite; avg, average; Ba, barium; bar, barite; bas, bastnaesite, bi, bismuthinite; Bi, bismuth; bn, bornite; born, bournonite; calc, calcite; carb, carbonates; cc, chalcocite; cn, cinnabar; cm, centimeter; co, coloradoite; cpy, chalcopyrite; Cu, copper; cv, calaverite; do, dolomite; em, empressite; en, enargite; epith, epithermal; F, fluorine; Fe, iron; fl, fluorite; fr, freibergite; gn, galena; g/t, grams per metric ton; hm, hematite; hs, hessite; K, potassium; km, kilometer; kr, krennerite; m, meter; Ma, millions of years ago; mc, marcasite; me, mernskyite; ml, melonite; mo, molybdenite; Mo, molybdenum; mrc, marcasite; mt, magnetite; Pb, lead; Pd, palladium; PGE, platinum group elements; po, pyrrhotite; porph, porphyry; ppm, parts per million; py, pyrite; pyr, pyrargyrite/proustite; pz, petzite; qtz, quartz; REE, rare earth elements; Sb, antimony; sch, scheelite; Se, selenium; ser, sericite; Si, silica; sp, sphalerite; spy, sperrylite; st, stuetzite; stb, stibnite; sy, sylvanite; TE, tellurium; Th, thorium; tn, tennantite; tour, tourmaline; tt, tetrahedrite; U, uranium; V, vanadium; W, tungsten; wo, wolframite; wt. %, weight percent; Zn, zinc]

District, location Type	Gold endowment: tonnage and grade Contained Au (million metric tons or Mt)	Age (millions of years ago or Ma)	Alkaline igneous rocks	Tectonic/geologic setting	Mineralization style/structure	Metallic minerals	Trace element association	Reference(s)
Sandaowanzi, northeast China Low sulfide Au-Te(-Ag)	15 tons Au at average 8.03 g/t	135.3±3.9 to 124.7±2.9 Ma	Trachytes, trachytic andesites, basalts, andesites, rhyolites overlying a 181.6±3.4 Ma monzogranite. Host rocks and ore veins crosscut by 116.6±2.4 Ma diabase, syenite, and syenodiorite dikes	Mesozoic oceanic subduction followed by regional extension provided for magmatism and volcanism. Igneous activity controlled by large-scale extensional structures	West-northwest trending qtz veins containing Au-tellurides (up to 3 cm) with lesser sulfides. Fine disseminations of ore minerals found in host rock surrounding metalliferous veins	alt, carb, co, cpy, em, gn, hs, kr, native Au, py, pz, sp, st, sy	Ag, Au, Cu, Pb, Te, Zn	Liu and others, 2011
Pingyi area (Guilaizuiang, Lifanggou, and Mofanggou deposits), western Shandong, eastern China	45 total tons Au at grades averaging 4.9–11.54 g/t (total of three deposits)	175.7±3.8 Ma	Diorite porphyry and pyroxene-hornblende monzosyenite porphyry	Mesozoic oceanic subduction followed by regional extension provided for magmatism and volcanism. Igneous activity controlled by large-scale extensional structures	Guilaizuiang: qtz veins and mineralized breccias hosted in limestone/dolostone. Controlled by east-west fault; steeply dipping to the south. Lifanggou and Mofanggou: Stratiform ore bodies hosted in limestone/dolostone. Parallel to sedimentary bedding and dip gently west-northwest	alt, cv, electrum, ml, pz, tellurides	Unknown	Hu and others, 2006

Table 1. Characteristics of selected alkalic-type epithermal gold deposits and related porphyry deposits.—Continued

[Table modified from Jensen and Barton (2000). Grade/tonnage and contained gold (Au) for many U.S. deposits from Mutschler (1992). ~, approximately; >, greater than; %, percent; ±, plus or minus; act, acanthite; Ag, silver; alt, altaite; ar, argentite; As, arsenic; aspy, arsenopyrite; avg, average; Ba, barium; bar, barite; bas, bastnaesite, bi, bismuthinite; Bi, bismuth; bn, bornite; born, bournonite; calc, calcite; carb, carbonates; cc, chalcocite; cn, cinnabar; cm, centimeter; co, coloradoite; cpy, chalcopyrite; Cu, copper; cv, calaverite; do, dolomite; em, empressite; en, enargite; epith, epithermal; F, fluorine; Fe, iron; fl, fluorite; fr, freibergite; gn, galena; g/t, grams per metric ton; hm, hematite; hs, hessite; K, potassium; km, kilometer; kr, krennerite; m, meter; Ma, millions of years ago; mc, marcasite; me, mernskyite; ml, melonite; mo, molybdenite; Mo, molybdenum; mrc, marcasite; mt, magnetite; Pb, lead; Pd, palladium; PGE, platinum group elements; po, pyrrhotite; porph, porphyry; ppm, parts per million; py, pyrite; pyr, pyrargyrite/proustite; pz, petzite; qtz, quartz; REE, rare earth elements; Sb, antimony; sch, scheelite; Se, selenium; ser, sericite; Si, silica; sp, sphalerite; spy, sperrylite; st, stuetzite; stb, stibnite; sy, sylvanite; TE, tellurium; Th, thorium; tn, tennantite; tour, tourmaline; tt, tetrahedrite; U, uranium; V, vanadium; W, tungsten; wo, wolframite; wt. %, weight percent; Zn, zinc]

District, location Type	Gold endowment: tonnage and grade Contained Au (million metric tons or Mt)	Age (millions of years ago or Ma)	Alkaline igneous rocks	Tectonic/geologic setting	Mineralization style/structure	Metallic minerals	Trace element association	Reference(s)
Dashuigou and Majiagou, southwest China Epithermal Te (Au)	Unknown Au tonnage; Dashuigou contains estimated 30,200 tons of ore (indicated and inferred) grading 1.09% Te; Majiagou contains 13,400 at 3.26%	Late Triassic to mid-Cretaceous	Permian-Triassic basalt and metabasalt/marble intruded by syenite and quartz diorite	Western margin of Yangtze craton that has been tectonically active since Late Paleozoic; continental rifting in Permian, followed by compression in Late Jurassic-Cretaceous	Series of 13 subparallel veins within metabasalt that end at contact with marble; intense wall-rock alteration is associated with veins	bi, carb, cpy, do, fl, hm, native bi, po, py, qtz, ser, sp, tt, tour	Au, Ag, bi, Cu, F, Se, Te; noted for its extreme Te enrichment	Mao and others, 2002; Zhang and others, 2018
Sari Gunai, northwest Iran Epithermal Au	52 Mt at 1.77 g/t Au 92 metric tons	11.7–11.0 Ma	Mildly alkaline latites and trachytes	Epithermal veins overprinting early, barren, porphyry veins. Structural lineament trending north-northwest controls volcanic centers	Qtz veins, massive sulfides, vuggy infillings and disseminations	aspy, cn, gn, mrc, py, sp, stb	As, Au, Pb, Sb, Zn	Richards and others, 2006

Table 1. Characteristics of selected alkalic-type epithermal gold deposits and related porphyry deposits.—Continued

[Table modified from Jensen and Barton (2000). Grade/tonnage and contained gold (Au) for many U.S. deposits from Mutschler (1992). ~, approximately; >, greater than; %, percent; ±, plus or minus; act, acanthite; Ag, silver; alt, altaite; ar, argentite; As, arsenic; aspy, arsenopyrite; avg, average; Ba, barium; bar, barite; bas, bastnaesite, bi, bismuthinite; Bi, bismuth; bn, bornite; born, bournonite; calc, calcite; carb, carbonates; cc, chalcocite; cn, cinnabar; cm, centimeter; co, coloradoite; cpy, chalcopyrite; Cu, copper; cv, calaverite; do, dolomite; em, empressite; en, enargite; epith, epithermal; F, fluorine; Fe, iron; fl, fluorite; fr, freibergite; gn, galena; g/t, grams per metric ton; hm, hematite; hs, hessite; K, potassium; km, kilometer; kr, krennerite; m, meter; Ma, millions of years ago; mc, marcasite; me, mernskyite; ml, melonite; mo, molybdenite; Mo, molybdenum; mrc, marcasite; mt, magnetite; Pb, lead; Pd, palladium; PGE, platinum group elements; po, pyrrhotite; porph, porphyry; ppm, parts per million; py, pyrite; pyr, pyrargyrite/proustite; pz, petzite; qtz, quartz; REE, rare earth elements; Sb, antimony; sch, scheelite; Se, selenium; ser, sericite; Si, silica; sp, sphalerite; spy, sperrylite; st, stuetzite; stb, stibnite; sy, sylvanite; TE, tellurium; Th, thorium; tn, tennantite; tour, tourmaline; tt, tetrahedrite; U, uranium; V, vanadium; W, tungsten; wo, wolframite; wt. %, weight percent; Zn, zinc]

District, location Type	Gold endowment: tonnage and grade Contained Au (million metric tons or Mt)	Age (millions of years ago or Ma)	Alkaline igneous rocks	Tectonic/geologic setting	Mineralization style/structure	Metallic minerals	Trace element association	Reference(s)
Fakos, Aegean Sea, Greece Pophyry Cu-Au(Mo) to Epithermal Au-Te	Tonnage unknown. Bulk rock samples up to 13 ppm Au, 780 ppm Cu, 83 ppm Mo	18–21 Ma	Quartz monzonite, late-stage dikes with shoshonitic affinities	Magmatism/volcanism as a result of alpine collision and oceanic subduction followed by regional extension. Late-stage epithermal veins overprinting porphyry veins related to volcanic arc volcanism/plutonism during tectonic extension	1–10 cm qtz veins. Orientation controlled by normal fault orientation. Cross-cut earlier porphyry mineralization and alteration	Porphyry: bn, cpy, gn, hm, mo, mt, py, sp Epithermal: alt, born, electrum, en, hs, native Au, pz, pyr, tn-tt	As, Au, Cu, Pb, PGE, Sb, Zn	Fornadel and others, 2012
Mount Milligan, Quesnal Terrane, British Columbia Porphyry Cu-Au; Late stage Au-Te-Bi-PGE	706 Mt at 0.33 g/t 232 metric tons	183±4 Ma	Monzonite, monzodiorite, syenite with shoshonitic affinities	Silica-saturated magmatic arc complex with intrusives and volcanics. Regional northwest-southeast and north-northeast, south-southwest faults and structures	Late-stage epithermal veins overprinting porphyry veins. 0.5–1 cm qtz veins in five stages. Cross-cut earlier porphyry mineralization and potassic alteration	Porphyry: cpy, electrum, hm, mt; subepithermal: aspy, electrum, gn, me, naldrettite-stibiopalladinite, pz, sp, spy, st, tellurides, tn-tt	Au, Cu, Pb, Pd	LeFort and others, 2011; Jago and others, 2014

Table 1. Characteristics of selected alkalic-type epithermal gold deposits and related porphyry deposits.—Continued

[Table modified from Jensen and Barton (2000). Grade/tonnage and contained gold (Au) for many U.S. deposits from Mutschler (1992). ~, approximately; >, greater than; %, percent; ±, plus or minus; act, acanthite; Ag, silver; alt, altaite; ar, argentite; As, arsenic; aspy, arsenopyrite; avg, average; Ba, barium; bar, barite; bas, bastnaesite, bi, bismuthinite; Bi, bismuth; bn, bornite; born, bournonite; calc, calcite; carb, carbonates; cc, chalcocite; cn, cinnabar; cm, centimeter; co, coloradoite; cpy, chalcopyrite; Cu, copper; cv, calaverite; do, dolomite; em, empressite; en, enargite; epith, epithermal; F, fluorine; Fe, iron; fl, fluorite; fr, freibergite; gn, galena; g/t, grams per metric ton; hm, hematite; hs, hessite; K, potassium; km, kilometer; kr, krennerite; m, meter; Ma, millions of years ago; mc, marcasite; me, mernskyite; ml, melonite; mo, molybdenite; Mo, molybdenum; mrc, marcasite; mt, magnetite; Pb, lead; Pd, palladium; PGE, platinum group elements; po, pyrrhotite; porph, porphyry; ppm, parts per million; py, pyrite; pyr, pyrargyrite/proustite; pz, petzite; qtz, quartz; REE, rare earth elements; Sb, antimony; sch, scheelite; Se, selenium; ser, sericite; Si, silica; sp, sphalerite; spy, sperrylite; st, stuetzite; stb, stibnite; sy, sylvanite; TE, tellurium; Th, thorium; tn, tennantite; tour, tourmaline; tt, tetrahedrite; U, uranium; V, vanadium; W, tungsten; wo, wolframite; wt. %, weight percent; Zn, zinc]

District, location Type	Gold endowment: tonnage and grade Contained Au (million metric tons or Mt)	Age (millions of years ago or Ma)	Alkaline igneous rocks	Tectonic/geologic setting	Mineralization style/structure	Metallic minerals	Trace element association	Reference(s)
Galore Creek, British Columbia Porphyry Cu-Au	125 Mt at 0.4 g/t 50 metric tons	Jurassic	Alkaline volcanics, syenite, monzonite and late alkalic basalts and lamprophyres	Quesnellia and Stikinia terranes; intrusions emplaced in intraoceanic island arc terranes prior to or during accretion onto North American continent; intrusions hosted by Upper Triassic volcanic and sedimentary rocks	Disseminated Cu(Au) porphyry with peripheral Fe-skarns. Post-ore faults with small displacement throughout	bn, cpy, native Au, mt, py, tellurides, tt	Au, Ag, Cu	Enns and others, 1995; Lang and others, 1995
Boundary area (Republic, Dusty Mac, Shasket Creek, Sappho), Washington, U.S.A.; British Columbia, Canada Epithermal Au (±Ag, Te, Se) and porphyry Cu-Ag-PGE (±Au)	13.5 at avg 11 g/t 192 metric tons	Jurassic-Cretaceous (Sappho, Shasket Creek) and Tertiary (Dusty Mac, Republic)	Alkaline igneous intrusions (dikes, plugs, sills, porphyry), including quartz monzonite and syenite	Part of the Quesnellia terrane, an accreted magmatic-arc terrane; intrusions hosted by greenstone and sedimentary and igneous rocks of Permian and Triassic age. North-northeast-trending extensional faults and grabens served to localize alkaline intrusions and associated mineralization	Epithermal: disseminated in breccias and veins with some replacement mineralization in sedimentary rocks (Dusty Mac) Porphyry: semi-massive to massive veins and sulfide disseminations	Porphyry: cpy, mt, py; epithermal: bn, cpy, gn, native Ag, py, selenide minerals (Republic), tellurides	Porphyry: Ag, Au, Cu, PGE; epithermal: Ag, Au, Cu, Se, Te	Mutschler and others, 1985; Zhang and others, 1989; Nixon and Archibald, 2001

Table 1. Characteristics of selected alkalic-type epithermal gold deposits and related porphyry deposits.—Continued

[Table modified from Jensen and Barton (2000). Grade/tonnage and contained gold (Au) for many U.S. deposits from Mutschler (1992). ~, approximately; >, greater than; %, percent; ±, plus or minus; act, acanthite; Ag, silver; alt, altaite; ar, argentite; As, arsenic; aspy, arsenopyrite; avg, average; Ba, barium; bar, barite; bas, bastnaesite, bi, bismuthinite; Bi, bismuth; bn, bornite; born, bournonite; calc, calcite; carb, carbonates; cc, chalcocite; cn, cinnabar; cm, centimeter; co, coloradoite; cpy, chalcopyrite; Cu, copper; cv, calaverite; do, dolomite; em, empressite; en, enargite; epith, epithermal; F, fluorine; Fe, iron; fl, fluorite; fr, freibergite; gn, galena; g/t, grams per metric ton; hm, hematite; hs, hessite; K, potassium; km, kilometer; kr, krennerite; m, meter; Ma, millions of years ago; mc, marcasite; me, mernskyite; ml, melonite; mo, molybdenite; Mo, molybdenum; mrc, marcasite; mt, magnetite; Pb, lead; Pd, palladium; PGE, platinum group elements; po, pyrrhotite; porph, porphyry; ppm, parts per million; py, pyrite; pyr, pyrargyrite/proustite; pz, petzite; qtz, quartz; REE, rare earth elements; Sb, antimony; sch, scheelite; Se, selenium; ser, sericite; Si, silica; sp, sphalerite; spy, sperrylite; st, stuetzite; stb, stibnite; sy, sylvanite; TE, tellurium; Th, thorium; tn, tennantite; tour, tourmaline; tt, tetrahedrite; U, uranium; V, vanadium; W, tungsten; wo, wolframite; wt. %, weight percent; Zn, zinc]

District, location Type	Gold endowment: tonnage and grade Contained Au (million metric tons or Mt)	Age (millions of years ago or Ma)	Alkaline igneous rocks	Tectonic/geologic setting	Mineralization style/structure	Metallic minerals	Trace element association	Reference(s)
Zortman-Landusky, Montana, U.S.A. Epithermal Au-Te	109 Mt at 0.55 g/t 59.4 metric tons	67–60 Ma	Stocks and laccoliths of syenite porphyry; breccia pipes and breccia dikes were emplaced in altered syenite porphyry	Igneous activity coincided with Laramide subduction; ore bodies formed as a result of repeated fault movement or reopening along intrusive contact; passive hot spot beneath the Great Falls tectonic zone may have resulted from oblique subduction	Vein, disseminated, and stockwork mineralization in syenite; higher grade zones are localized in regional shears	act, cpy, gn, goethite, hm, native Au, py, sp, sulfosalts, tellurides	Au, Ag, Mo, Te	Wilson and Kyser, 1988
Judith Mountains (Spotted Horse, Gies, New Year, Warm Springs deposits), Montana, U.S.A. Epithermal Au-Te	Tonnage and grades unknown 21.5 metric tons	Late Cretaceous (69–62 Ma) to Eocene (47 Ma)	Stocks, laccoliths, sills, and dikes of qtz diorite, monzonite, syenite, alkali syenite, and tinguaite; some breccia pipes intrude alkaline igneous rocks	Igneous activity coincided with Laramide subduction; ore bodies formed as a result of repeated fault movement or reopening along intrusive contact; passive hot spot beneath northeast-trending Great Falls tectonic zone may have resulted from oblique subduction	Mineralized breccia at contact between limestone and monzonite porphyry, and within limestone and porphyry. Fissure fillings, stockwork veins, breccia cement and replacement styles are common. Minor associated skarns. Four stages recognized (Gies deposit); latest stage is Au-Te stage	gn, native Au, py, sp, tellurides	Au, Ag, F, Te, V	Mutschler and others, 1991; Woodward and Giles, 1993; Zhang and Spry, 1994; Woodward, 1995

Table 1. Characteristics of selected alkalic-type epithermal gold deposits and related porphyry deposits.—Continued

[Table modified from Jensen and Barton (2000). Grade/tonnage and contained gold (Au) for many U.S. deposits from Mutschler (1992). ~, approximately; >, greater than; %, percent; ±, plus or minus; act, acanthite; Ag, silver; alt, altaite; ar, argentite; As, arsenic; aspy, arsenopyrite; avg, average; Ba, barium; bar, barite; bas, bastnaesite, bi, bismuthinite; Bi, bismuth; bn, bornite; born, bournonite; calc, calcite; carb, carbonates; cc, chalcocite; cn, cinnabar; cm, centimeter; co, coloradoite; cpy, chalcopyrite; Cu, copper; cv, calaverite; do, dolomite; em, empressite; en, enargite; epith, epithermal; F, fluorine; Fe, iron; fl, fluorite; fr, freibergite; gn, galena; g/t, grams per metric ton; hm, hematite; hs, hessite; K, potassium; km, kilometer; kr, krennerite; m, meter; Ma, millions of years ago; mc, marcasite; me, mernskyite; ml, melonite; mo, molybdenite; Mo, molybdenum; mrc, marcasite; mt, magnetite; Pb, lead; Pd, palladium; PGE, platinum group elements; po, pyrrhotite; porph, porphyry; ppm, parts per million; py, pyrite; pyr, pyrargyrite/proustite; pz, petzite; qtz, quartz; REE, rare earth elements; Sb, antimony; sch, scheelite; Se, selenium; ser, sericite; Si, silica; sp, sphalerite; spy, sperrylite; st, stuetzite; stb, stibnite; sy, sylvanite; TE, tellurium; Th, thorium; tn, tennantite; tour, tourmaline; tt, tetrahedrite; U, uranium; V, vanadium; W, tungsten; wo, wolframite; wt. %, weight percent; Zn, zinc]

District, location Type	Gold endowment: tonnage and grade Contained Au (million metric tons or Mt)	Age (millions of years ago or Ma)	Alkaline igneous rocks	Tectonic/geologic setting	Mineralization style/structure	Metallic minerals	Trace element association	Reference(s)
Moccasin Mountains (Kendall, Muleshoe deposits), Montana, U.S.A. Epithermal Au-Te	4 Mt at 1.7 g/t 20.8 metric tons	Late Cretaceous (66–65 Ma)	Laccolith complex (including sills and dikes) of alkali syenite, qtz monzonite, and syenite porphyry; development of breccia pipes within syenite porphyry	Igneous activity coincided with Laramide subduction; ore bodies formed as a result of repeated fault movement or reopening along intrusive contact; passive hot spot beneath northeast-trending Great Falls tectonic zone may have resulted from oblique subduction	Disseminated and stockwork veins; replacement in carbonate sedimentary rocks along contact with intrusive syenite	gn, native Au, py, sp, tellurides	Au, Ag, F, Te, V	Lindsey, 1985; Lindsey and Fisher, 1985; Lindsey and Naeser, 1985; Mutschler and Mooney, 1995
Golden Sunlight, Montana, U.S.A. Porphyry Mo; Epithermal Au-Ag telluride	70.8 Mt at 0.054 g/t 107.7 metric tons	Late Cretaceous (~79 Ma)	Dikes, sills, and stock-like bodies of quartz monzodiorite, latite porphyry, and lamprophyres	Pre-Laramide dextral strike-slip faulting; formation of northeast transtensional Great Falls tectonic zone. Alkaline magmas, Mineral Hill porphyry system, and Mineral Hill breccia pipe developed along zone	In chronological order: Proterozoic stratabound sulfides, low grade porphyry Mo, and epithermal Au in Mineral Hill breccia pipe. Au occurs in disseminations and structurally controlled veins with four stages identified	Breccia pipe: aspy, bn, cpy, gn, native Au, py, sp, tellurides (including Bi), sulfosalts	Au, Ag, Bi, Cu, Mo, Te	Porter and Ripley, 1985; Spry and others, 1996, 1997

Table 1. Characteristics of selected alkalic-type epithermal gold deposits and related porphyry deposits.—Continued

[Table modified from Jensen and Barton (2000). Grade/tonnage and contained gold (Au) for many U.S. deposits from Mutschler (1992). ~, approximately; >, greater than; %, percent; ±, plus or minus; act, acanthite; Ag, silver; alt, altaite; ar, argentite; As, arsenic; aspy, arsenopyrite; avg, average; Ba, barium; bar, barite; bas, bastnaesite, bi, bismuthinite; Bi, bismuth; bn, bornite; born, bournonite; calc, calcite; carb, carbonates; cc, chalcocite; cn, cinnabar; cm, centimeter; co, coloradoite; cpy, chalcopyrite; Cu, copper; cv, calaverite; do, dolomite; em, empressite; en, enargite; epith, epithermal; F, fluorine; Fe, iron; fl, fluorite; fr, freibergite; gn, galena; g/t, grams per metric ton; hm, hematite; hs, hessite; K, potassium; km, kilometer; kr, krennerite; m, meter; Ma, millions of years ago; mc, marcasite; me, mernskyite; ml, melonite; mo, molybdenite; Mo, molybdenum; mrc, marcasite; mt, magnetite; Pb, lead; Pd, palladium; PGE, platinum group elements; po, pyrrhotite; porph, porphyry; ppm, parts per million; py, pyrite; pyr, pyrargyrite/proustite; pz, petzite; qtz, quartz; REE, rare earth elements; Sb, antimony; sch, scheelite; Se, selenium; ser, sericite; Si, silica; sp, sphalerite; spy, sperrylite; st, stuetzite; stb, stibnite; sy, sylvanite; TE, tellurium; Th, thorium; tn, tennantite; tour, tourmaline; tt, tetrahedrite; U, uranium; V, vanadium; W, tungsten; wo, wolframite; wt. %, weight percent; Zn, zinc]

District, location Type	Gold endowment: tonnage and grade Contained Au (million metric tons or Mt)	Age (millions of years ago or Ma)	Alkaline igneous rocks	Tectonic/geologic setting	Mineralization style/structure	Metallic minerals	Trace element association	Reference(s)
Northern Black Hills (Gilt Edge, Annie Creek, Foley Ridge, Golden Reward; Richmond Hill), South Dakota, U.S.A. Epithermal Au-Ag	88.5 Mt at 1.4 g/t 208.3 metric tons	40–60 Ma	Quartz monzonites, latites, rhyolites, trachytes, and phonolites	Black Hills uplift occurred during Laramide basement deformation. In Paleocene-Eocene time, east-west localization of alkaline sills and lacolliths, and subvertical fractures localized mineralization	Disseminated and stockwork veins; replacement in carbonate sedimentary rocks	Intrusion/breccia-hosted: bar, cpy, fl, gn, native Au, mo, mt, py, sy; sedimentary replacement deposits adjacent to intrusions: gn, native Au, sch, sp, sy, wo	Au, Ag, Cu, F, As, Te (Pb, W, Mo)	Lisenbee, 1981; Paterson and others, 1989; Mutschler, 1992
Bear Lodge Wyoming, U.S.A. Epithermal Au; REE	Unknown	60–38 Ma	Trachyte and phonolite stocks, sills, and laccoliths and minor carbonatite	Black Hills uplift occurred during Laramide basement deformation. In Paleocene-Eocene time, the Bear Lodge alkalic complex (one of the bodies similar to the Northern Black Hills) intruded Paleozoic, Mesozoic, and Cenozoic sedimentary rocks	High to low grade veins and mineralized intrusive and volcanic breccias; deep base metal-Ag mineralization associated with fenite. Carbonatite dikes and breccias have REE mineralization	bas, native Au	As, Au, Ba, Mo, REE, Sb, Te	Staatz, 1983

Table 1. Characteristics of selected alkalic-type epithermal gold deposits and related porphyry deposits.—Continued

[Table modified from Jensen and Barton (2000). Grade/tonnage and contained gold (Au) for many U.S. deposits from Mutschler (1992). ~, approximately; >, greater than; %, percent; ±, plus or minus; act, acanthite; Ag, silver; alt, altaite; ar, argentite; As, arsenic; aspy, arsenopyrite; avg, average; Ba, barium; bar, barite; bas, bastnaesite, bi, bismuthinite; Bi, bismuth; bn, bornite; born, bournonite; calc, calcite; carb, carbonates; cc, chalcocite; cn, cinnabar; cm, centimeter; co, coloradoite; cpy, chalcopyrite; Cu, copper; cv, calaverite; do, dolomite; em, empressite; en, enargite; epith, epithermal; F, fluorine; Fe, iron; fl, fluorite; fr, freibergite; gn, galena; g/t, grams per metric ton; hm, hematite; hs, hessite; K, potassium; km, kilometer; kr, krennerite; m, meter; Ma, millions of years ago; mc, marcasite; me, mernskyite; ml, melonite; mo, molybdenite; Mo, molybdenum; mrc, marcasite; mt, magnetite; Pb, lead; Pd, palladium; PGE, platinum group elements; po, pyrrhotite; porph, porphyry; ppm, parts per million; py, pyrite; pyr, pyrargyrite/proustite; pz, petzite; qtz, quartz; REE, rare earth elements; Sb, antimony; sch, scheelite; Se, selenium; ser, sericite; Si, silica; sp, sphalerite; spy, sperrylite; st, stuetzite; stb, stibnite; sy, sylvanite; TE, tellurium; Th, thorium; tn, tennantite; tour, tourmaline; tt, tetrahedrite; U, uranium; V, vanadium; W, tungsten; wo, wolframite; wt. %, weight percent; Zn, zinc]

District, location Type	Gold endowment: tonnage and grade Contained Au (million metric tons or Mt)	Age (millions of years ago or Ma)	Alkaline igneous rocks	Tectonic/geologic setting	Mineralization style/structure	Metallic minerals	Trace element association	Reference(s)
Cripple Creek, Colorado, U.S.A. Epithermal Au-Te	>800 metric tons (including vein and disseminated with different average grades)	32–27 Ma	Diatreme and hydrothermal breccias, phonolite, tephriphonolite, lamprophyre	Emplaced during incipient phases of crustal extension (Rio Grande rift that bisects New Mexico and southern Colorado). Extension followed major regional compression related to the ca. 70–40 Ma Laramide orogeny. Diatreme emplaced at junction of four Precambrian units, 40 km off axis of Rio Grande Rift	High grade Au-telluride veins with K-alteration halos containing disseminated native gold and tellurides. Deep, high-temp, base metal-rich mineralization. Sub-radial pattern to vein orientations at district scale, merging with north-northwest-south-southeast and northeast-southwest regional Precambrian (?) trends	Vein-style: cpy, cv, do, fl, gn, hm, kr, mo, native Au, pz, py, sp, stb, sy, tt; disseminated Au: auriferous py	Vein-style: Ag, Au, F, Mo, Te, V; disseminated: Au, Te	Thompson and others, 1985; Kelley and others, 1998; Jensen and Barton, 2000; Jensen, 2003; Kelley and others, 2020

Table 1. Characteristics of selected alkalic-type epithermal gold deposits and related porphyry deposits.—Continued

[Table modified from Jensen and Barton (2000). Grade/tonnage and contained gold (Au) for many U.S. deposits from Mutschler (1992). ~, approximately; >, greater than; %, percent; ±, plus or minus; act, acanthite; Ag, silver; alt, altaite; ar, argentite; As, arsenic; aspy, arsenopyrite; avg, average; Ba, barium; bar, barite; bas, bastnaesite, bi, bismuthinite; Bi, bismuth; bn, bornite; born, bournonite; calc, calcite; carb, carbonates; cc, chalcocite; cn, cinnabar; cm, centimeter; co, coloradoite; cpy, chalcopyrite; Cu, copper; cv, calaverite; do, dolomite; em, empressite; en, enargite; epith, epithermal; F, fluorine; Fe, iron; fl, fluorite; fr, freibergite; gn, galena; g/t, grams per metric ton; hm, hematite; hs, hessite; K, potassium; km, kilometer; kr, krennerite; m, meter; Ma, millions of years ago; mc, marcasite; me, mernskyite; ml, melonite; mo, molybdenite; Mo, molybdenum; mrc, marcasite; mt, magnetite; Pb, lead; Pd, palladium; PGE, platinum group elements; po, pyrrhotite; porph, porphyry; ppm, parts per million; py, pyrite; pyr, pyrargyrite/proustite; pz, petzite; qtz, quartz; REE, rare earth elements; Sb, antimony; sch, scheelite; Se, selenium; ser, sericite; Si, silica; sp, sphalerite; spy, sperrylite; st, stuetzite; stb, stibnite; sy, sylvanite; TE, tellurium; Th, thorium; tn, tennantite; tour, tourmaline; tt, tetrahedrite; U, uranium; V, vanadium; W, tungsten; wo, wolframite; wt. %, weight percent; Zn, zinc]

District, location Type	Gold endowment: tonnage and grade Contained Au (million metric tons or Mt)	Age (millions of years ago or Ma)	Alkaline igneous rocks	Tectonic/geologic setting	Mineralization style/structure	Metallic minerals	Trace element association	Reference(s)
Boulder County (Jamestown, Ward, Gold Hill, Central City[1]), Colorado, U.S.A. Epithermal Au-Te	Tonnage and grade unknown 67.3 metric tons (~30 from Jamestown, Gold Hill, Ward; ~37.3 from alkaline-related Au deposits from Central City)	59–52 Ma	Stocks, sills, and dikes of primarily leucocratic granodiorite, and monzonite, and bostonite porphyry intrude Precambrian rocks (Central City); 45–44 Ma monzonite and syenite stocks and dikes (Ward, Gold Hill, Jamestown)	Emplaced during the Laramide orogeny as subduction waned and slab flattened to low angle; immediately preceded extension and formation of the Rio Grande Rift	Sulfide and (or) telluride-bearing quartz veins; spatially (and genetically?) associated porphyry Mo (Central City, Jamestown)	gn, fr, native Au, native Te, py, sp, tellurides, wo	Ba, Au, Te, V, F	Kelly and Goddard, 1969; Rice and others, 1985; Saunders, 1991; Geller, 1994; Kelley and Ludington, 2002
La Plata Colorado, U.S.A. Porphyry Cu, Epithermal Au-Te	32.1 Mt at 37 g/t (epith) and 0.069 g/t (porph) 13.7 metric tons	65–70 Ma	Alkaline diorite, monzonites, syenites (+lamprophyres?)	Formed during episode of Late Cretaceous/Paleocene alkaline magmatism (after onset of the Laramide orogeny). Contemporaneous with low angle (?) subduction; Intrusions occupy a 25-km structural dome and are hosted by Permian-Jurassic metasedimentary rocks	Cu (Au)± PGE porphyry-style mineralization with superimposed high grade, epithermal gold telluride veins. Mineralization directed by concentric/radial faults and structures related to early intrusions	Epithermal: bn, cpy, gn, native Au, py, sp, tellurides, tt; porphyry: bn, cpy, native Au, py tellurides	Au, Te, Ba, Cu, F, V	Eckel, 1949; Werle and others, 1984

[1]The Central City deposits are southwest of Boulder County in Gilpin County but along the trend of deposits that define the Boulder County deposits.

Table 1. Characteristics of selected alkalic-type epithermal gold deposits and related porphyry deposits.—Continued

[Table modified from Jensen and Barton (2000). Grade/tonnage and contained gold (Au) for many U.S. deposits from Mutschler (1992). ~, approximately; >, greater than; %, percent; ±, plus or minus; act, acanthite; Ag, silver; alt, altaite; ar, argentite; As, arsenic; aspy, arsenopyrite; avg, average; Ba, barium; bar, barite; bas, bastnaesite, bi, bismuthinite; Bi, bismuth; bn, bornite; born, bournonite; calc, calcite; carb, carbonates; cc, chalcocite; cn, cinnabar; cm, centimeter; co, coloradoite; cpy, chalcopyrite; Cu, copper; cv, calaverite; do, dolomite; em, empressite; en, enargite; epith, epithermal; F, fluorine; Fe, iron; fl, fluorite; fr, freibergite; gn, galena; g/t, grams per metric ton; hm, hematite; hs, hessite; K, potassium; km, kilometer; kr, krennerite; m, meter; Ma, millions of years ago; mc, marcasite; me, mernskyite; ml, melonite; mo, molybdenite; Mo, molybdenum; mrc, marcasite; mt, magnetite; Pb, lead; Pd, palladium; PGE, platinum group elements; po, pyrrhotite; porph, porphyry; ppm, parts per million; py, pyrite; pyr, pyrargyrite/proustite; pz, petzite; qtz, quartz; REE, rare earth elements; Sb, antimony; sch, scheelite; Se, selenium; ser, sericite; Si, silica; sp, sphalerite; spy, sperrylite; st, stuetzite; stb, stibnite; sy, sylvanite; TE, tellurium; Th, thorium; tn, tennantite; tour, tourmaline; tt, tetrahedrite; U, uranium; V, vanadium; W, tungsten; wo, wolframite; wt. %, weight percent; Zn, zinc]

District, location Type	Gold endowment: tonnage and grade Contained Au (million metric tons or Mt)	Age (millions of years ago or Ma)	Alkaline igneous rocks	Tectonic/geologic setting	Mineralization style/structure	Metallic minerals	Trace element association	Reference(s)
Rosita Colorado, U.S.A. Epithermal Au-Ag-Te	Tonnage and grades unknown 3 metric tons	33–27 Ma	Syenogabbro-diorite-monzonite-tracyte plutons; lamprophyry dikes. Coeval high-Si rhyolites and other calc-alkaline intrusions. Host rocks are Precambrian metasedimentary rocks	Emplaced during incipient phases of crustal extension (Rio Grande Rift) following major regional compression related to the 70–40 Ma Laramide orogeny	Veins and disseminated in breccia pipe, following lamprophyre emplacement	cpy, gn, mo, py, tt, tn, stephanite, Sb-Ag sulfosalts	Au, Ag, Ba, Te	McEwan and others, 1996
Ortiz Mountains (Cunningham Hill, Dolores, Lukas Canyon, Carache Canyon) New Mexico, U.S.A. Epithermal Au, skarn	15.3 Mt at 1.5 g/t 29.5 metric tons	36–28 Ma	Nepheline-bearing monzodiorite to monzonite stocks, phreatic breccia pipes, and trachyte dikes	Emplaced during incipient phases of crustal extension (Rio Grande Rift) following major regional compression related to the 70–40 Ma Laramide orogeny	Au-bearing breccias, Au-bearing skarns, Au-bearing Cu skarns, plymetallic veins	gn, native Au, py, sch, sp	Au, W	Schutz, 1995; McLemore, 1996; Kelley and Ludington, 2002

Table 1. Characteristics of selected alkalic-type epithermal gold deposits and related porphyry deposits.—Continued

[Table modified from Jensen and Barton (2000). Grade/tonnage and contained gold (Au) for many U.S. deposits from Mutschler (1992). ~, approximately; >, greater than; %, percent; ±, plus or minus; act, acanthite; Ag, silver; alt, altaite; ar, argentite; As, arsenic; aspy, arsenopyrite; avg, average; Ba, barium; bar, barite; bas, bastnaesite, bi, bismuthinite; Bi, bismuth; bn, bornite; born, bournonite; calc, calcite; carb, carbonates; cc, chalcocite; cn, cinnabar; cm, centimeter; co, coloradoite; cpy, chalcopyrite; Cu, copper; cv, calaverite; do, dolomite; em, empressite; en, enargite; epith, epithermal; F, fluorine; Fe, iron; fl, fluorite; fr, freibergite; gn, galena; g/t, grams per metric ton; hm, hematite; hs, hessite; K, potassium; km, kilometer; kr, krennerite; m, meter; Ma, millions of years ago; mc, marcasite; me, mernskyite; ml, melonite; mo, molybdenite; Mo, molybdenum; mrc, marcasite; mt, magnetite; Pb, lead; Pd, palladium; PGE, platinum group elements; po, pyrrhotite; porph, porphyry; ppm, parts per million; py, pyrite; pyr, pyrargyrite/proustite; pz, petzite; qtz, quartz; REE, rare earth elements; Sb, antimony; sch, scheelite; Se, selenium; ser, sericite; Si, silica; sp, sphalerite; spy, sperrylite; st, stuetzite; stb, stibnite; sy, sylvanite; TE, tellurium; Th, thorium; tn, tennantite; tour, tourmaline; tt, tetrahedrite; U, uranium; V, vanadium; W, tungsten; wo, wolframite; wt. %, weight percent; Zn, zinc]

District, location Type	Gold endowment: tonnage and grade Contained Au (million metric tons or Mt)	Age (millions of years ago or Ma)	Alkaline igneous rocks	Tectonic/geologic setting	Mineralization style/structure	Metallic minerals	Trace element association	Reference(s)
Lincoln County (Jicarilla, White Oaks, Gallinas Mountains, Nogal deposits) New Mexico, U.S.A. Epithermal Au, REE (Gallinas Mountains)	Nogal: 0.6 Mt at 4.5 g/t 0.55 metric tons (all deposits combined)	38–26 Ma	Syenodirorite, syenogabbro to monzonite, trachyte	Emplaced during incipient phases of crustal extension (Rio Grande Rift) following major regional compression related to the 70–40 Ma Laramide orogeny	Veins and disseminated in breccias, Au placers	carb, cpy, gn, native Au, py, sp	Ag, Ag, Cu, F, Pb, Zn, REE (U, Th)	Griswold, 1959; McLemore, 1996
Elizabethtown-Baldy and Red River Districts (Jicarilla, White Oaks, Gallinas Mountains, Nogal deposits) New Mexico, U.S.A. Epithermal Au, REE (Gallinas Mountains)	0.13 Mt at 29.5 g/t 15 metric tons	29–26 Ma	Quartz monzonite to monzonite stocks	Emplaced during incipient phases of crustal extension (Rio Grande rift) following major regional compression related to the 70–40 Ma Laramide orogeny	Veins and Au-Cu skarns with molybdenite mineralization at depth; 20 km east of Questa porphyry Mo deposit	Auriferous py	Au, Cu, W	McLemore, 1996, 2001, 2010

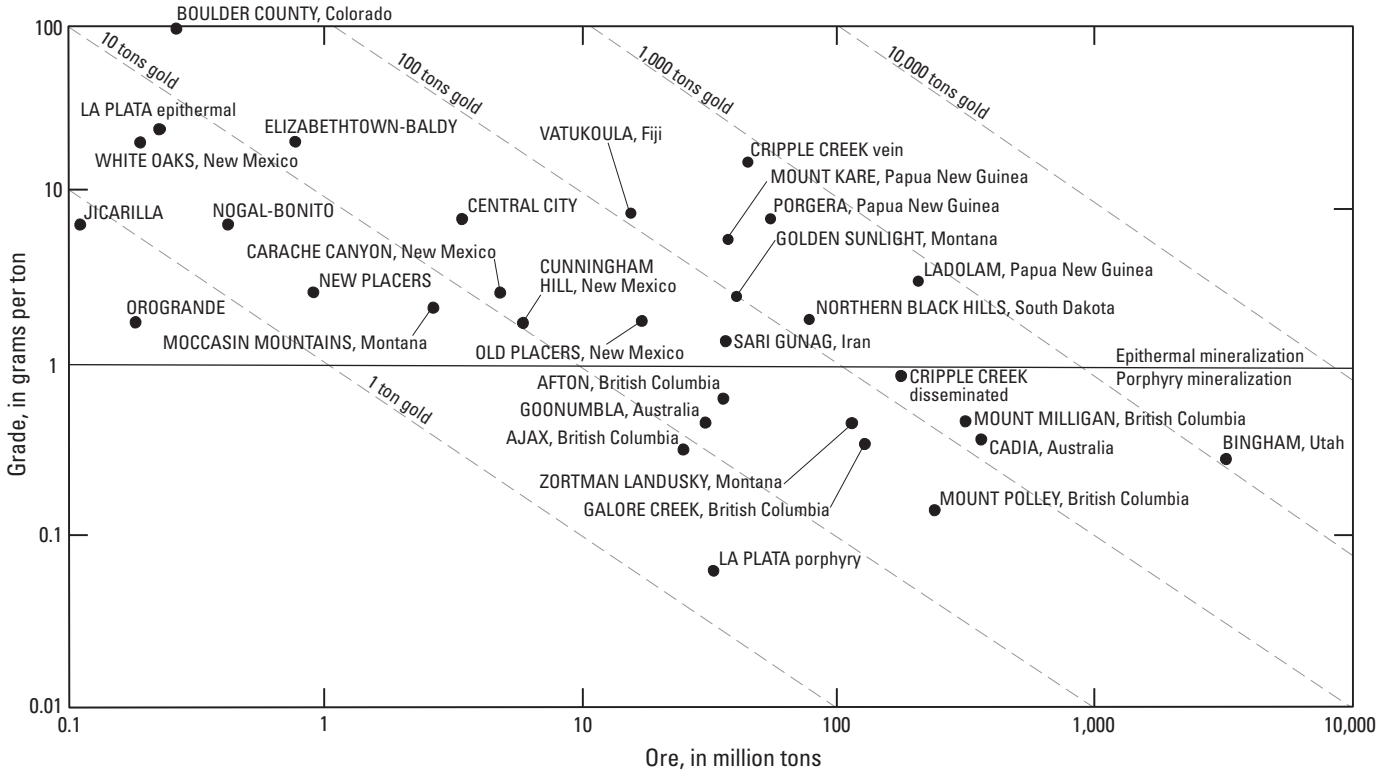

Figure 2. Grade-tonnage diagram of alkalic-type epithermal gold deposits (modified from Kelley and Ludington, 2002).

Deposit Type and Associated Commodities

Name

Alkalic-type epithermal gold deposits

Synonyms

Alkalic-related epithermal gold deposits; alkaline-related epithermal deposits; alkaline igneous rock-related epithermal gold deposits; subset of low-sulfidation epithermal gold deposits; Great Plains Margin deposits (in New Mexico only; McLemore 1996, 2015).

Brief Description

Alkalic-type epithermal deposits, primarily of Mesozoic to Neogene age, range widely in size (some contain between 100 and 1000 metric tons of gold) and grade (0.054 to >8 grams per metric ton [g/t] Au), are hosted in spatially, temporally, and genetically related alkaline igneous rocks and adjacent wall rocks, and occur as disseminated, breccia- and vein-hosted gold (Mutschler and others, 1985; Richards, 1995; Jensen and Barton, 2000; Kelley and Spry, 2016). They typically form at shallow crustal levels (less than [<] 1–2 kilometers [km]) from low temperature (<300 degrees Celsius [°C]) fluids. Native gold, arsenian pyrite, and a variety of tellurides are the dominant ore minerals.

Alkaline igneous rocks spatially linked with these deposits generally form small and isolated intrusions or clusters of stocks, laccoliths, dikes, and sills. These rocks include syenite, nepheline syenite, monzonite, alkali basalt, diorite, latite, phonolite, vogesite, banakite, hawaiite, monchiquite, andesite, trachyte, bostonite, absarokite, and shoshonite (Mutschler and others, 1985; Mutschler, 1992). Most of these rocks are alkaline, but in general, their geochemical compositions span the alkaline-subalkaline transition (Le Bas and others, 1986). Their alkali enrichment may be masked by potassic alteration, but the unaltered or least altered rocks (1) have chondrite normalized rare-earth element (REE) patterns that are commonly light rare earth element enriched, (2) are heavy rare earth element depleted, and (3) have high large ion lithophile contents and variable enrichment of high field strength elements, all characteristics of igneous rocks with an alkaline affinity (Richards and Ledlie, 1993; Müller and others, 2001; Scherbarth and Spry, 2006).

Alkalic-type gold deposits form in a variety of geological settings including continent-arc collision zones and back-arc or post-subduction rifts that are invariably

characterized by a transition from convergent to extensional or transpressive tectonics, and are spatially related to deep-seated regional-scale faults (Richards, 1995; Begg and Gray, 2002; Scherbarth and Spry, 2006; Richards, 2009).

The most important consistent characteristics of alkalic-type epithermal gold deposits are that they (1) typically occur in areas affected by multiple episodes of intrusive activity (locally including more silicic or calc-alkaline intrusions); (2) are dominated by the products of magmatic-hydrothermal activity (for example, breccia pipes, porphyry-type stockworks); and (3) for the most part display a consistent mineral paragenesis, with early base metal sulfides followed by gold or gold-bearing minerals. Gold commonly occurs as native gold, electrum, precious metal tellurides, and as sub-micron gold in arsenian pyrite, and is associated with minor amounts of galena, sphalerite, chalcopyrite, hematite and various sulfosalts and tellurides. Quartz-carbonate-fluorite-adularia-vanadian muscovite/roscoelite alteration is characteristically intergrown with metallic minerals. Notably, some epithermal gold-silver deposits that are associated with calc-alkaline rocks also contain high concentrations of tellurium (see Cook and others, 2009; John and others, 2018), including those in the Baguio district, Philippines (Cooke and McPhail, 2001); the Golden Quadrilateral, Romania (for example, Săcărâmb; Alderton and Fallick, 2000; Cook and others, 2004); Uzbekistan (Kovalenker and others, 1997, 2003); and the Kassiteres, Pefka, Petrota, and Pagoni Rachi deposits in northern Greece (Voudouris, 2006). Many of these deposits are included in the summary by John and others (2018).

Associated Deposit Types

A number of deposit types are either spatially, temporally, or genetically related to alkalic-type epithermal gold deposits. The most common types of associated deposits, and the primary metals (in parentheses) typically recovered from these deposits are listed below:

- Skarns (including copper, gold, iron, and zinc types)
- Porphyry deposits (copper, gold, and molybdenum types related to alkaline igneous rocks)
- Polymetallic replacement deposits (copper, gold, lead, silver, zinc)
- Fluorspar vein and breccia deposits
- Tungsten-bearing veins
- Locally, carbonatites (niobium, REEs)
- Fluorite veins (±niobium, REEs, uranium)

The presence of these deposits does not necessarily indicate the existence of nearby alkalic-type epithermal deposits, nor does their absence preclude the occurrence of nearby epithermal deposits.

Primary Commodities

Gold is the primary commodity in almost all alkalic-type epithermal deposits. Tellurium, however, is a primary product in the Dashigou and Majiagou deposits in China, thus classification of these deposits as alkalic-type epithermal gold deposits is not entirely certain (Zhang and others, 2018).

Byproduct Commodities

Currently, no byproducts are recovered from alkalic-type epithermal gold deposits. However, fluorspar, silver, and tungsten were byproducts of historical mining, although it is unclear how these elements relate temporally or genetically to vein-hosted gold. The Jamestown district in Colorado produced several hundred thousand metric tons of fluorspar between 1940 and 1973 (Kelly and Goddard, 1969; Nash and Cunningham, 1973). Fluorite occurs as a primary mineral in phases of the sodic granite stock and in breccia zones, stockworks, and pipe-shaped bodies in and adjacent to the stock. Gold and tellurides occur with and without fluorite in veins peripheral to the stock (Nash and Cunningham, 1973).

Some alkalic-type epithermal gold deposits also contain tungsten-bearing minerals, including scheelite, ferberite, or wolframite. Small ferberite- and scheelite-bearing orebodies in Boulder County were mined historically (Kelly and Goddard, 1969), and notably were the chief source of tungsten in the United States from about 1900 to 1918 (Lovering and Tweto, 1953). In Boulder County, the tungsten ores largely form a belt that is separate and distinct from the telluride belt, but where they overlap, some tungsten minerals occur in gold-telluride veins. Micron-sized gold in the Ortiz Mountains deposits in New Mexico contain scheelite but there is no record of tungsten production from these deposits (Maynard, 1995; Schutz, 1995; McLemore, 1996, 2015). Tungsten was also produced from alkalic-type epithermal gold deposits in the White Oaks district, New Mexico.

Trace Constituents

In addition to gold, many of these deposits are also enriched in barium, fluorine, silver, tellurium, uranium, and vanadium, and less commonly molybdenum and tungsten. High concentrations of antimony and arsenic, and enrichments in base metals characterize some deposits, and a few contain anomalous platinum group element (PGE) concentrations (Mutschler and others, 1985) and elevated REE contents (Kelley and Spry, 2016). As stated above, fluorine and tungsten have been produced from some of these deposits. The best examples of REE enrichments are the Bear Lodge Mountains deposit in Wyoming, which contains total REE abundances of 0.23 to 9.8 percent (Staatz, 1983), and Cu-REE-F (±Ag, Au) vein deposits in the Gallinas Mountains, New Mexico, which have REE contents that range from <1 to 5.6 percent (Griswold, 1959; McLemore, 2010).

Example Deposits

Numerous compilation papers include descriptions and (or) grade and tonnage estimates of alkalic-type epithermal gold deposits. Cox and Bagby (1986) provide a descriptive model (Model 22b) of gold-silver-tellurium vein deposits, citing six examples, but grade and tonnage information are lacking. Mutschler and others (1985) and Mutschler and Mooney (1995) provide the first major compilation of precious metal deposits (epithermal, porphyry, massive sulfide) related to alkaline rocks in the North America Cordillera, including some grade and tonnage information for many of the Montana and Colorado deposits. Richards (1995) prepared a global review of alkalic-type epithermal deposits and compiled the characteristics common to these deposits; the publication also includes descriptions of well-known examples: Porgera, PNG; Vatukoula (formerly called Emperor), Fiji; Ladolam, (Lihir Island), PNG; Montana alkalic province, U.S.A.; and Cripple Creek and the Colorado Mineral Belt, U.S.A. Jensen and Barton (2000) prepared another review with updated grade and tonnage estimates. The main characteristics of well-known examples of alkalic-type epithermal gold deposits are well established (modified from Kelley and Spry, 2016), but importantly this group of deposits is also characterized by considerable diversity.

Historical Evolution of Descriptive and Genetic Knowledge and Concepts

The association between gold-tellurium epithermal deposits and alkaline rocks was first suggested by Bonham and Giles (1983). Contrasts between these deposits and those of the more clearly defined acid-sulfate and quartz-adularia-sericite epithermal systems (John and others, 2018) became increasingly evident (Heald-Wetlaufer and others, 1983; Hayba and others, 1985; Heald and others, 1987) and formed the basis for the initial "alkalic-type" gold-silver deposits designation (Bonham, 1984, 1986). The presence of magmatic-hydrothermal breccias and porphyritic textures indicates that many of the associated intrusions were emplaced at shallow crustal depths. The common presence of fluorite, tellurides, and vanadium-rich mica (roscoelite) further distinguish these deposits from other epithermal deposits. Bonham (1984) also noted the relationship between epithermal ores, localized in stockwork veins and hydrothermal breccias, and deeper alkalic porphyry-type activity (fig. 3). Descriptions of gold-silver-tellurium veins (Cox and Bagby, 1986; Model 22b) more completely defined the deposit model, particularly with regard to the composition of diorites and lamprophyres present in some of these districts. In the late 1980s and early 1990s, application of the term "sulfidation," initially used to describe the oxidation state of aqueous sulfur species of deep ore-forming solutions (Hedenquist, 1987; White and Hedenquist, 1990), was combined with the observation that certain minerals are diagnostic of particular sulfidation states (Barton and Skinner, 1967). The high sulfidation (that is, acid sulfate) and low sulfidation (that is, quartz-adularia-sericite) terminology remains the most useful classification for epithermal deposits (Simmons and others, 2005). Alkalic-type epithermal gold deposits form a subtype of low sulfidation deposits, an inference borne out by similar gangue mineralogy (quartz -calcite-adularia-illite); however, the two deposit types are distinguished by other distinctive features (Richards, 1995; Jensen and Barton, 2000; Kelley and Spry, 2016).

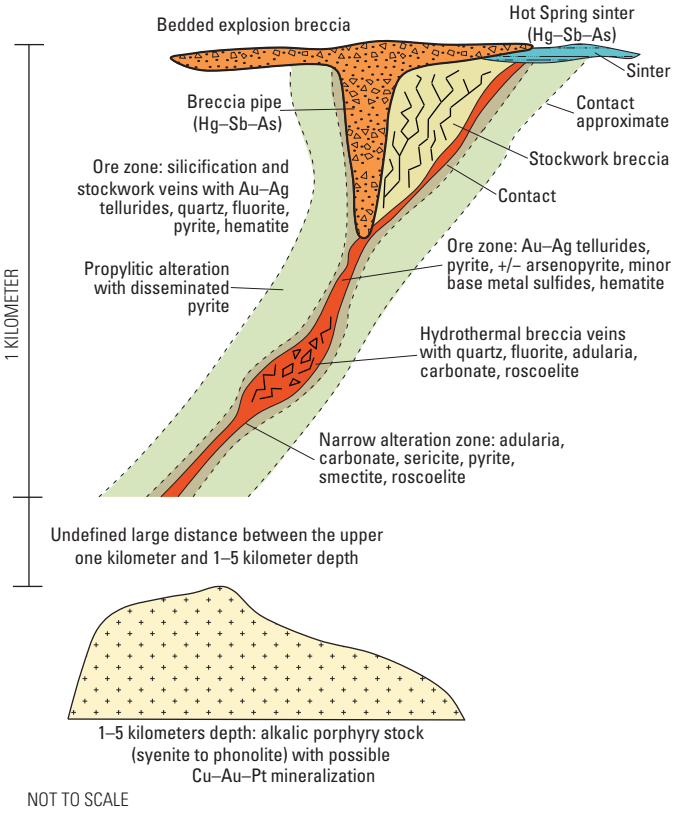

Figure 3. Generalized early model of an alkalic-type epithermal gold deposit (from Bonham, 1986). Note the depiction of possible alkalic-type porphyry deposits at depth, which has been documented for some deposits. (Ag, silver; As, arsenic; Au, gold; Cu, copper; Hg, mercury; Pt, platinum; Sb, antimony)

Regional Environment

Geotectonic Environment

Assuming a direct genetic relationship between alkalic-type epithermal gold deposits and hydrous alkalic magmatism, establishing the tectonic environment in which these magmas are generated is important. Alkaline igneous rocks are commonly associated with rifting, convergent margins, and intraplate environments (Jensen and Barton, 2000). Most alkaline rock provinces consist of low-volume magmatic systems; consequently, these systems form isolated or small clustered magmatic centers that are not regionally extensive (Richards, 1995).

Alkalic-type gold deposits form in a variety of settings, including continent-arc collision zones (for example, Porgera and Mount Kare [Richards, 1990; Richards and Ledlie, 1993]), back-arc rift settings (for example, Cripple Creek [Jensen and Barton, 2000]), and post-subduction rifts (for example, Vatukoula [Eaton and Setterfield, 1993; Begg and Gray, 2002; Begg and others, 2007]; Fakos, Greece [Fornadel and others, 2012]; Ladolam [Carman, 2003]). Regardless of setting, the deposits are invariably associated with the transition from convergent tectonic processes to extensional or transpressive tectonics (Richards, 1995; Jensen and Barton, 2000; McLemore, 2018), and are spatially related to deep-seated regional-scale faults (Richards, 1995; Begg and Gray, 2002; Scherbarth and Spry, 2006).

Alkalic-type epithermal gold deposits in the western United States form a discontinuous belt along the east side of the Rocky Mountains, from New Mexico to northern Montana near the border with Canada (for example, Mutschler and others, 1985; Kelley and Ludington, 2002). Similar deposits extend into west Texas and eastern Mexico (McLemore, 2018). These deposits formed during two distinct time periods: (1) the Laramide orogeny (about 70–40 million years ago [Ma]); and (2) early in the development of the Rio Grande Rift system, during the transition from a compressional to an extensional tectonic regime (about 35–27 Ma).

Temporal (Secular) Relations

Alkaline igneous rocks are as old as late Archean (Sorensen, 1974), but known alkalic-type epithermal gold deposits are no older than Mesozoic (fig. 1). Owing to their formation at shallow crustal levels and in tectonically active convergent plate margins, many older deposits may have been exhumed and eroded. John and others (2018) note that some strongly metamorphosed Au-Ag deposits, inferred to represent high-sulfidation epithermal deposits based on their major element compositions, are >250 Ma old. Other than alkalic-type porphyry deposits, however, the oldest described alkalic-type epithermal deposit is the Triassic to Early Jurassic Mount Milligan deposit in British Columbia, which consists of Au-Cu porphyry and "subepithermal" deposits (LeFort and others, 2011; Jago and others, 2014). The subepithermal deposit consists of transitional (post-porphyry, pre-epithermal) veins formed by fluids highly enriched in As, Au, B, Bi, PGE, Sb, and Te. The Mount Milligan and other porphyry deposits in the region formed in a Late Triassic to Early Jurassic magmatic arc complex along the western North American continental margin. Many other alkalic-type porphyry deposits are known, but none of these have associated epithermal mineralization.

The Late Cretaceous deposits in China are hosted in and post-date Early Cretaceous volcanism (Zhang and others, 2010; Liu and others, 2013); the deposits are interpreted to have formed during regional extension associated with rollback of a slab that was subducting beneath the Eurasian plate (Liu and others, 2011, 2013). A similar post-subduction origin is postulated for alkalic-type epithermal gold deposits in North America. Many of the Boulder County deposits and those in the La Plata Mountains formed along the Colorado Mineral Belt toward the end of the Laramide orogeny. Ages indicate that alkaline magmas at Cripple Creek and at other coeval deposits formed immediately following subduction-related, calc-alkaline magmatism, and at the beginning of bimodal magmatism that accompanied the development of the Rio Grande Rift (Kelley and Ludington, 2002; Kelley and others, 2020). Similar ages characterize deposits in New Mexico, west Texas, and eastern Mexico (McLemore, 2018).

Duration of Magmatic-Hydrothermal System and (or) Mineralizing Processes

Understanding the duration of mineralizing processes is critical for determining how deposits form and for development of genetic models. Isotopic dating of igneous and hydrothermal minerals definitively establish that magmatic-hydrothermal systems associated with individual porphyry copper deposits generally have lifetimes equal to or less than (≤) 1 million years (m.y.) (Chiaradia and others, 2013; Buret and others, 2016). However, most epithermal deposits form episodically, and a single deposit may represent multiple mineralizing episodes as well as multiple intrusive events. Examples include the El Indio (7.8 to about [~] 5 Ma) and Veladero (~12–11 Ma) high sulfidation deposits in Argentina (Bissig and others, 2001; Holley and others, 2016). The Yanacocha high sulfidation epithermal deposit in Peru formed by episodic hydrothermal activity over a 5.4 m.y. period (Longo and others, 2010). Similarly, the alkalic-type epithermal gold deposit at Cripple Creek formed over an interval of about 2 m.y. (Kelley and others, 1998; Kelley and others, 2020), and the low sulfidation epithermal deposits in the Cerro Bayo district in Chile are associated with episodic magmatism during a 33 m.y. time period; individual pulses spanned 2–3 m.y. (Poblete and others, 2014).

The most accurate way to determine the duration of epithermal systems is by analyses of fluids associated with modern hydrothermal systems. The Ladolam deposit is the only known active hydrothermal alkalic-type gold deposit. Several deep (>1 km) geothermal wells were drilled at Ladolam to sample magmatic geothermal brine (Simmons and Brown, 2006). The gold concentration of the brines (~15 parts per billion) and the calculated gold flux suggest that the Ladolam deposit could have formed in ~55,000 years (Simmons and Brown, 2006). Factors that were important in forming the giant Ladolam deposit in this brief time interval in a compact volume of rock were a steady upward flux of gold and efficient deposition at shallow depths, between <100 and 500 meters (m) (Simmons and Brown, 2006). However, these factors may not pertain to most other modern and ancient epithermal systems.

The true duration of ancient epithermal systems is difficult to assess due to the lack of minerals for direct dating of mineralizing events. Many of the age ranges listed above (for example, Yanacocha at >5.4 m.y. and Cripple Creek at >2 m.y.) are based on dates for gangue minerals (for example, adularia) that may have formed either before or after mineralizing fluids deposited gold. Nonetheless, the ages broadly constrain the duration of deposit formation.

Relations to Structures

Some of the largest deposits (for example, Cripple Creek, Golden Sunlight) in the western United States are spatially associated with regional lineaments, the Colorado Mineral Belt and Great Falls tectonic zone, that constitute first-order structural controls on localization of alkalic-type epithermal gold and other hydrothermal deposits. Chapin (2012) proposed that the Colorado Mineral Belt is coincident with extension related to a northeast-trending segment boundary within the underlying, shallowly subducted Farallon slab. However, the location of the belt and the partially cospatial Rio Grande Rift may reflect reactivation of Precambrian basement structures (Richards, 1995); a similar scenario was proposed by Foster and Childs (1993) for the origin of the Great Falls tectonic zone and spatially associated alkalic-type epithermal gold deposits in Montana.

The two largest alkalic-type epithermal gold deposits in Fiji, Vatukoula and Tuvatu, occur along the >250 km long east-northeast-trending Viti-Levu lineament and local faults that parallel this orientation (for example, Begg and Gray, 2002; Scherbarth and Spry, 2006; Forsythe and others, 2019). This lineament reflects a northeast-southeast extension caused by a reversal of subduction direction during initial formation of the Vanuatu trench (Begg and Gray, 2002). The east-west trending faults spatially associated with the alkalic-type Fakos porphyry-epithermal system in Greece are parallel to and at the western end of the major east-west trending Intra-Pontide suture zone that extends from the northeastern part of the Aegean Sea eastward into Turkey. Similarly, the Porgera and Mount Kare deposits are located 25 and 40 km, respectively, south of a major suture zone, the Stolle-Lagaip Fault. In places, these large-scale faults may facilitate the formation of cross-orogen faults that are oblique to the stress direction (for example, Porgera, Golden Sunlight, Cripple Creek [Richards, 1995]). At the deposit scale, mineralization may be focused at the intersection of major faults (for example, Vatukoula; Begg, 1996), in vertical or steeply dipping structures (for example, Mayflower, Montana [Cocker, 1993]; Gies, Montana [Zhang and Spry, 1994]), or along shallowly dipping structures (for example, Tuvatu, Vatukoula). Brecciation zones are commonly the locus of high-grade mineralization (for example, Gies, Vatukoula).

Structural trends in some districts are radially or concentrically oriented and may reflect stress fields generated during the shallow emplacement of alkaline intrusions. The intersections of regional basement structures and fractures that were developed effectively localize mineralizing fluids and deposit formation (for example, Vatukoula, Fiji, is located at the intersection of a caldera boundary fault and a major shear zone).

Relations to Igneous Rocks

By definition, all alkalic-type epithermal gold deposits are associated with coeval igneous (volcanic or intrusive) rocks with an alkalic affinity; these rocks can be either silica saturated or unsaturated. Deposits are hosted by a variety of types of magmatic centers, including calderas (Vatukoula, Ladolam, Tuvatu), diatremes (Golden Sunlight, Ortiz Mountains, Cripple Creek), and hypabyssal intrusive rocks (Porgera; Boulder County, Colorado; Montana alkalic province). In general, alkaline igneous rocks associated with epithermal gold deposits have relatively high sodium oxide plus potassium oxide (Na_2O+K_2O) contents and most also contain relatively high volatile abundances (Richards, 1995). Alkaline igneous rocks associated with well-known alkalic-type epithermal deposits are compositionally diverse (fig. 4). Silica contents of unaltered igneous rocks associated with alkalic-type epithermal gold deposits span the range from <40 wt. percent to about 77 wt. percent SiO_2, and K_2O+Na_2O contents range from <2 to ~16 wt. percent. Many rocks associated with large deposits have K_2O+Na_2O contents that approximate the alkaline-subalkaline boundary (Irvine and Baragar, 1971) and are coincident with the ultrapotassic, shoshonitic, and calc-alkaline fields mentioned by Peccerillo and Taylor (1976). This compositional variability is especially typical of the igneous rocks spatially associated with the Fakos and Ladolam epithermal deposits, where ultrapotassic, shoshonitic, and calc-alkaline rock compositions are all present (Müller and others, 2001; Fornadel and others, 2012). The Na:K ratio of these rocks can be highly variable within a district (see Jensen and Barton, 2000). In many cases, highly variable Na_2O and K_2O contents likely reflect alteration of the igneous rocks (Jensen and Barton, 2000).

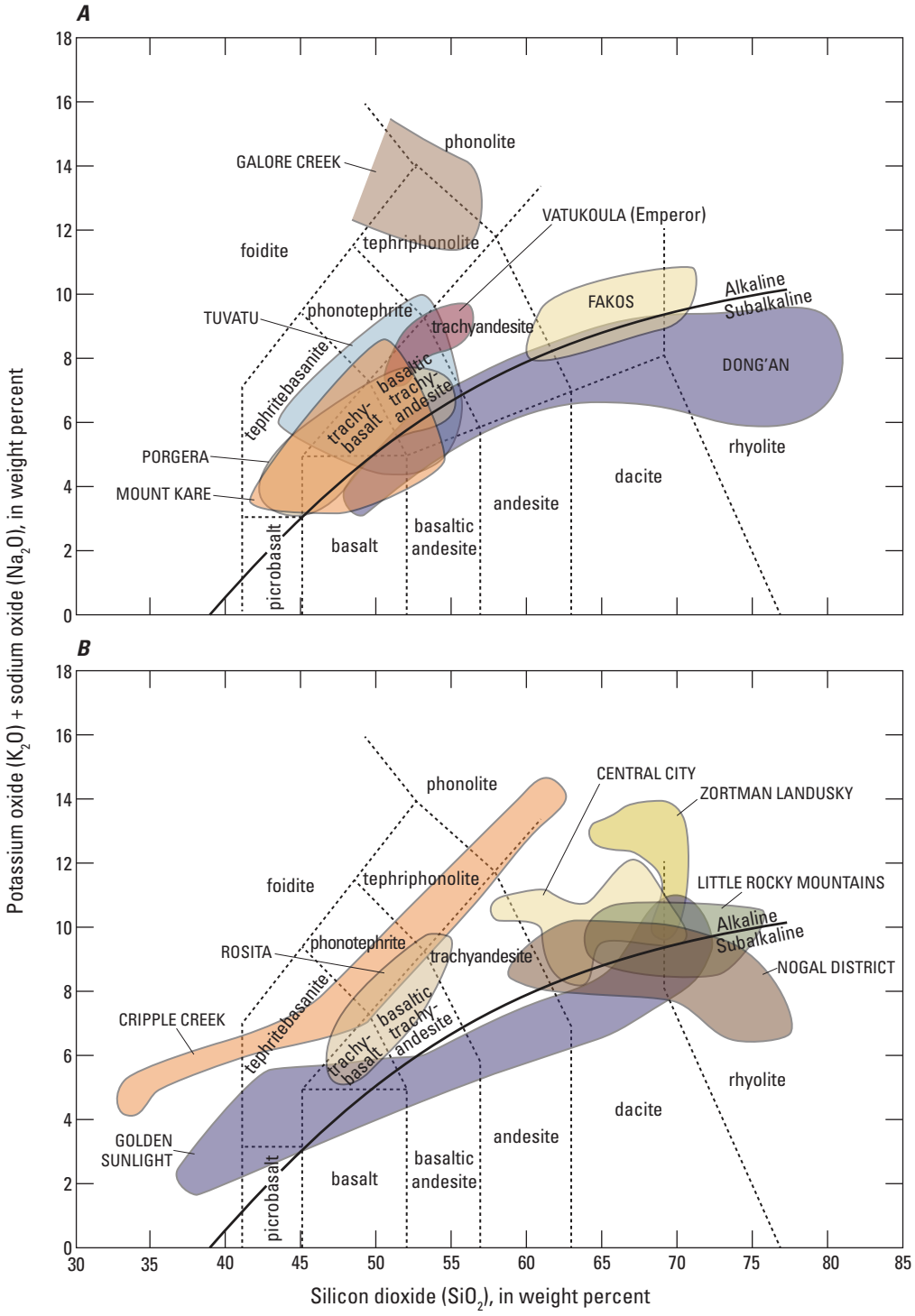

Figure 4. Total alkali versus silica diagrams (from Le Bas and others, 1986) showing compositions of igneous rocks spatially associated with alkalic-type epithermal gold deposits. *A*, Non-North American occurrences; and *B*, North American occurrences (see table 1 for references). The alkaline-subalkaline boundary is from Irvine and Baragar (1971).

Carbonatites are spatially associated with some alkalic-type epithermal gold deposits, although a genetic relation between them has not been established. Alkalic-type epithermal gold deposits in the Bear Lodge Mountains, Wyoming; at Laughlin Peak in the Chico Hills, New Mexico; and in eastern Mexico (McLemore, 2018) are spatially associated with Oligocene carbonatites. In the Gallinas Mountains, New Mexico, the presence of carbonatites at depth is inferred from the presence of fenitized and carbonatized breccias, elevated REE abundances, and similarity of the intrusive rocks and mineralization to those in areas that contain carbonatites (McLemore, 2010).

Relations to Sedimentary Rocks

Sedimentary rocks in districts that contain alkalic-type epithermal gold deposits may be important hosts to genetically-related deposits, including replacement and skarn deposits. For example, deposits at the Bessie G Mine in the La Plata district are hosted largely in Mesozoic clastic sedimentary rocks (Eckel, 1949; Saunders and May, 1986). The Kendall deposit in Montana is dominantly hosted in carbonate rocks adjacent to syenite. The gold mineralized zone at Kendall is characterized by a geochemical association (As, Hg, Sb) that suggests similarities between Kendall and Carlin-type deposits in Nevada (Lindsey, 1985). However, the presence of abundant disseminated fluorite and high concentrations of vanadium in the gold ore zones are characteristics of alkalic-type epithermal gold deposits.

Carbonate rocks adjacent to monzonite stocks, within a belt of alkalic-type epithermal gold deposits in New Mexico, host numerous copper and (or) lead-zinc and iron skarns (McLemore and North, 1987). In addition, as suggested by sulfur isotope data described in later sections of this document, sedimentary rocks may have been an important source of sulfur in some deposits.

Relations to Metamorphic Rocks

Metamorphic rocks are not genetically associated with alkalic-type epithermal gold deposits. Metamorphic rocks locally host epithermal deposits (for example, metabasalts and marbles partially host the Dashuigou and Majiagou deposits in southwest China), but regional metamorphism does not contribute to ore formation.

Physical Description of Deposit

Dimensions in Plan View

Alkalic-type epithermal gold deposits cover areas that range from <10 to >25 square kilometers (km^2). Many deposits are contained within calderas, breccia pipes, or diatremes (for example, Zortman-Landusky, Golden Sunlight, Cripple Creek, Ortiz Mountains) and these features control the ultimate dimensions of districts. Although most vein and disseminated mineralization at Cripple Creek is confined to a diatreme that covers at least 36 km^2, most of the ore is confined to structurally controlled zones that are <1 km wide (fig. 5*A*). In contrast, northeast trending veins in the Golden Sunlight deposit (fig. 5*B*) are in and well beyond a breccia pipe, in an area of at least 12 km^2. The currently mineable part of the deposit at Porgera is <0.5 km^2 in extent, but a regional aeromagnetic anomaly suggests other orebodies may exist within a larger 16 km^2 feature (fig. 5*C*).

Individual vein extents are highly variable. At Cripple Creek, veins form sheeted zones that consist of a number of narrow (<50 millimeters [mm]) subparallel fissures, which collectively may form a lode ranging from 0.5 to 3 m wide. Veins are widely distributed in the Jamestown district of Boulder County (fig. 5*D*) and the intersections of vein clusters constituted the principal production zones (Kelly and Goddard, 1969). Similarly, the Vatukoula deposit consists of fracture fillings and open cavities ranging up to 30 centimeters (cm) in width (Ahmad and others, 1987); the richest veins occur in a ~1-km-wide belt adjacent to the caldera (fig. 5*E*). At the Sandaowanzi deposit in China, vein orebodies are extensive and may be traced for >1.5 km along strike (Liu and others, 2011).

Vertical Extent

Many alkalic-type epithermal gold deposits have large vertical extents (fig. 6). For example, major veins in the Cripple Creek district exhibit remarkable continuity, extending to more than 1,000 m (fig. 6*A*) below the present-day surface (Loughlin and Koschmann, 1935; Thompson and others, 1985; Kelley and others, 2020), and those at Porgera exceed 700 m (Richards, 1995) where high-grade gold zones follow steeply dipping faults and structures (fig. 6*B*). At the Vatukoula deposit (fig. 6*C*), most lode deposits are vertically limited by declining gold content rather than at structural terminations (Ahmad and others, 1987). In longitudinal sections, most of the major deposits consist of steeply dipping veins with irregular outlines (fig. 6).

As previously noted, some deposits may grade downward into porphyry-type Cu(Au) or Mo deposits (Forsythe, 1971; Bonham and Giles, 1983; Mutschler and others, 1985; Spry and others, 1996; Jensen, 2003; Forsythe and others, 2019). In these cases, alteration assemblages characteristic of porphyry-style mineralization are overprinted by lower-temperature, epithermal assemblages. The transition between these two different hydrothermal systems may not be distinct. The total vertical extent of a mineralized system that includes both types of deposits may be significant, or in the case of Porgera and Ladolam (Richards, 1995; Jensen and Barton, 2000), the two types may overlap.

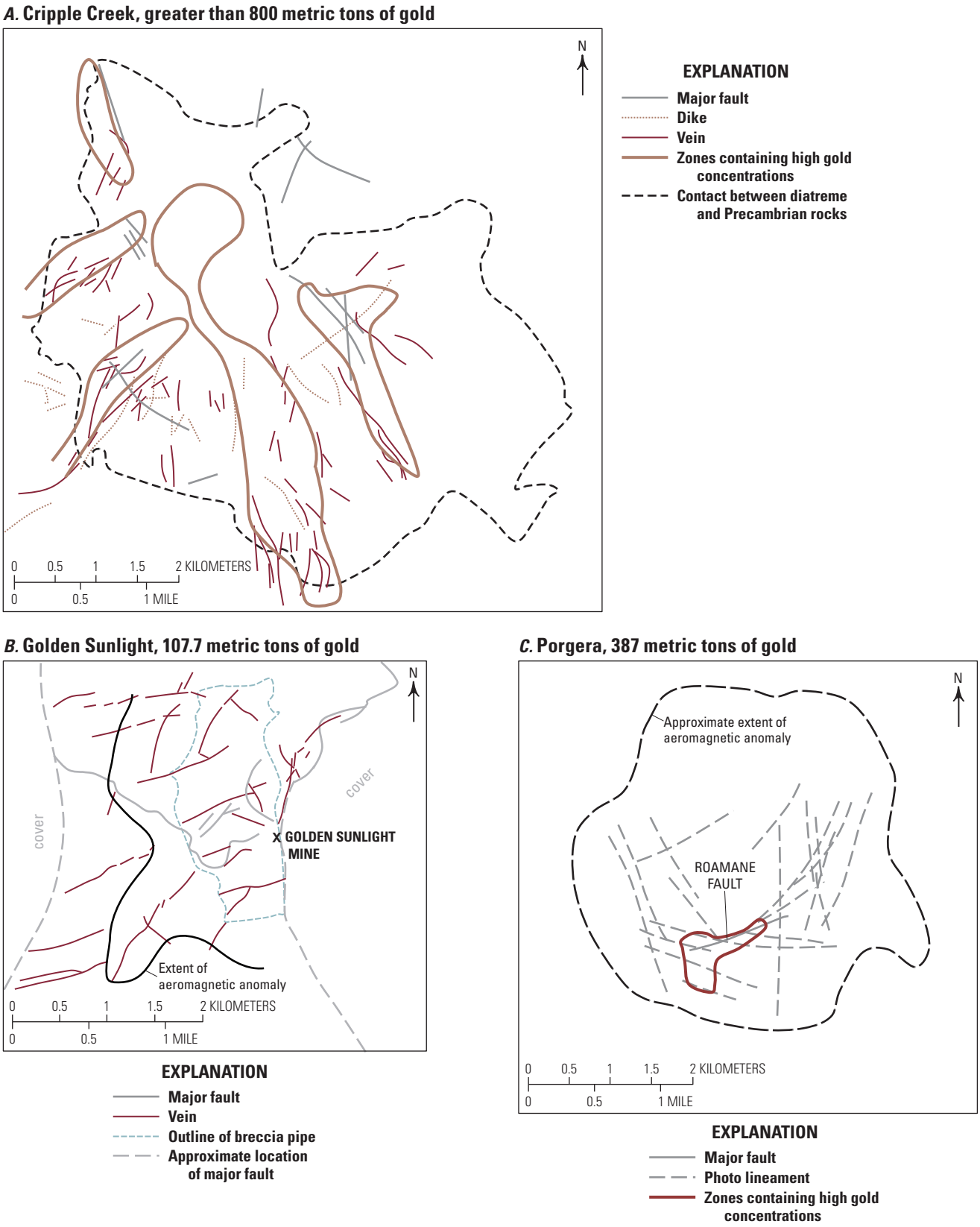

Figure 5. Sketch maps of alkalic-type epithermal gold deposits, showing orebody outlines. Note common scale for all maps. These illustrations show orebody variability with regard to size and shapes. *A*, Cripple Creek, Colorado (modified from Jensen and Barton, 2000). *B*, Golden Sunlight, Montana (modified from Spry and others, 1996). *C*, Porgera, PNG (modified from Richards, 1990; Jensen and Barton, 2000). *D*, Jamestown district, Colorado (modified from Kelly and Goddard, 1969). *E*, Vatukoula, Fiji (modified from Anderson and Eaton, 1990).

D. **Jamestown district**

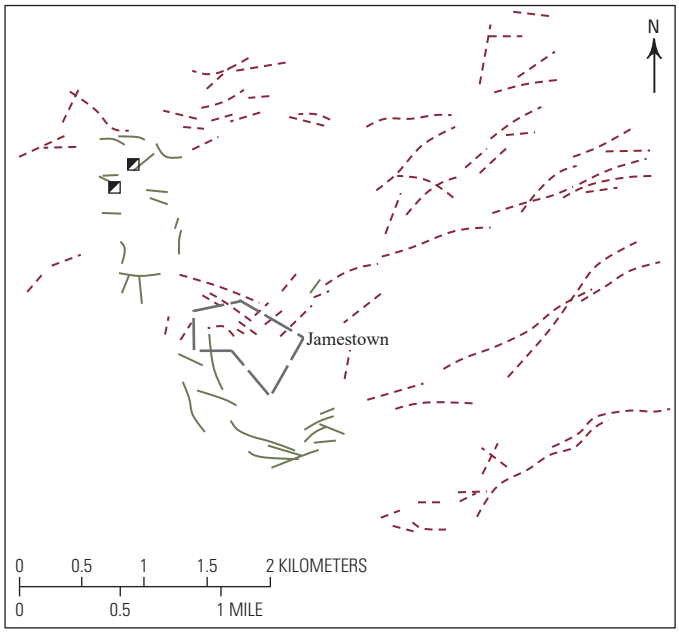

E. **Vatukoula, 280 metric tons of gold**

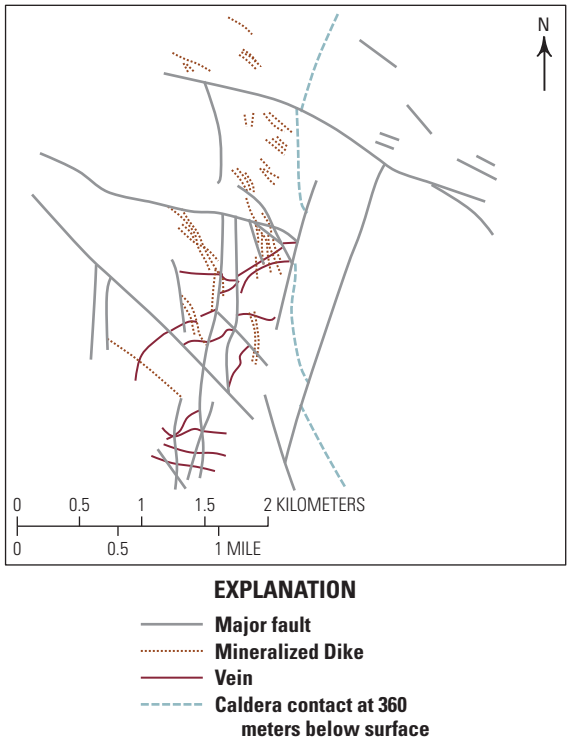

Figure 5. *D*, Jamestown district, Colorado (modified from Kelly and Goddard, 1969). *E*, Vatukoula, Fiji (modified from Anderson and Eaton, 1990).—Continued

Form/Shape

Structural and lithological controls influence orebody form and shape. Circular features may be prevalent for deposits associated with calderas and diatremes/breccia pipes, whereas linear trends are characteristic of fault-controlled deposits (fig. 5). Lithology is also important, especially where contrasts in permeability and porosity focus fluid flow through specific units, along rock contacts, or through permeable masses of brecciated rock. Most commonly, both lithology and structure play key roles in deposit localization, and therefore, affect the areal deposit distribution. Furthermore, because all of the alkalic-type epithermal gold deposits are associated with intrusions, whether exposed or buried, circular features may be present beyond the actual extent of mineralization, even if buried by younger rocks (see the "Geophysical Characteristics" section).

Most orebodies are in steeply-dipping veins, although many consist of disseminated ore in permeable strata within breccia pipes or diatremes. At Cripple Creek, a diatreme is filled with heterolithic breccias and multiple intrusions of alkaline igneous rock. In addition, veins cut Precambrian granodiorite, diatreme breccias, or are located along contacts with Tertiary dikes (Thompson and others, 1985). Vein form is also structurally controlled. Many of the relatively high-grade ore zones at Cripple Creek are in veins that trend northwest and northeast and are parallel to regional structures that originated during Mesoproterozoic deformation and reactivated during the Laramide orogeny or younger Rio Grande rifting events (Kelley and Ludington, 2002). Low-grade disseminated ore zones are in the diatreme and hydrothermal breccias but the highest-grade zones have trends similar to those of the dominant northwest and northeast trending faults (fig. 5*A*; Jensen and Barton, 2000).

The Porgera deposit, similar to the Cripple Creek deposit, contains low-grade disseminated gold and high-grade vein-hosted mineralization. Soft unconsolidated continental shelf sediments (that is, permeable) that host the mafic alkalic intrusive complex and associated deposits, and structurally associated faults (for example, the northeast-trending Roamane Fault) influenced ore localization (Richards, 1995). In addition, a 5-km-wide aeromagnetic anomaly centered over the complex delineates a large mid-crustal magma chamber beneath the deposit area (fig. 5*C*).

Host Rocks

Most deposits consist of veins that developed within the alkaline igneous rocks with which they are genetically related. Common igneous features include calderas (Vatukoula and Ladolam), diatremes (Golden Sunlight, Ortiz Mountains, and Cripple Creek), and hypabyssal intrusive stocks (Porgera, Boulder County, and the Montana alkali belt). Most districts were affected by multiple magmatic episodes and some contain satellite intrusive bodies (Jensen and Barton, 2000).

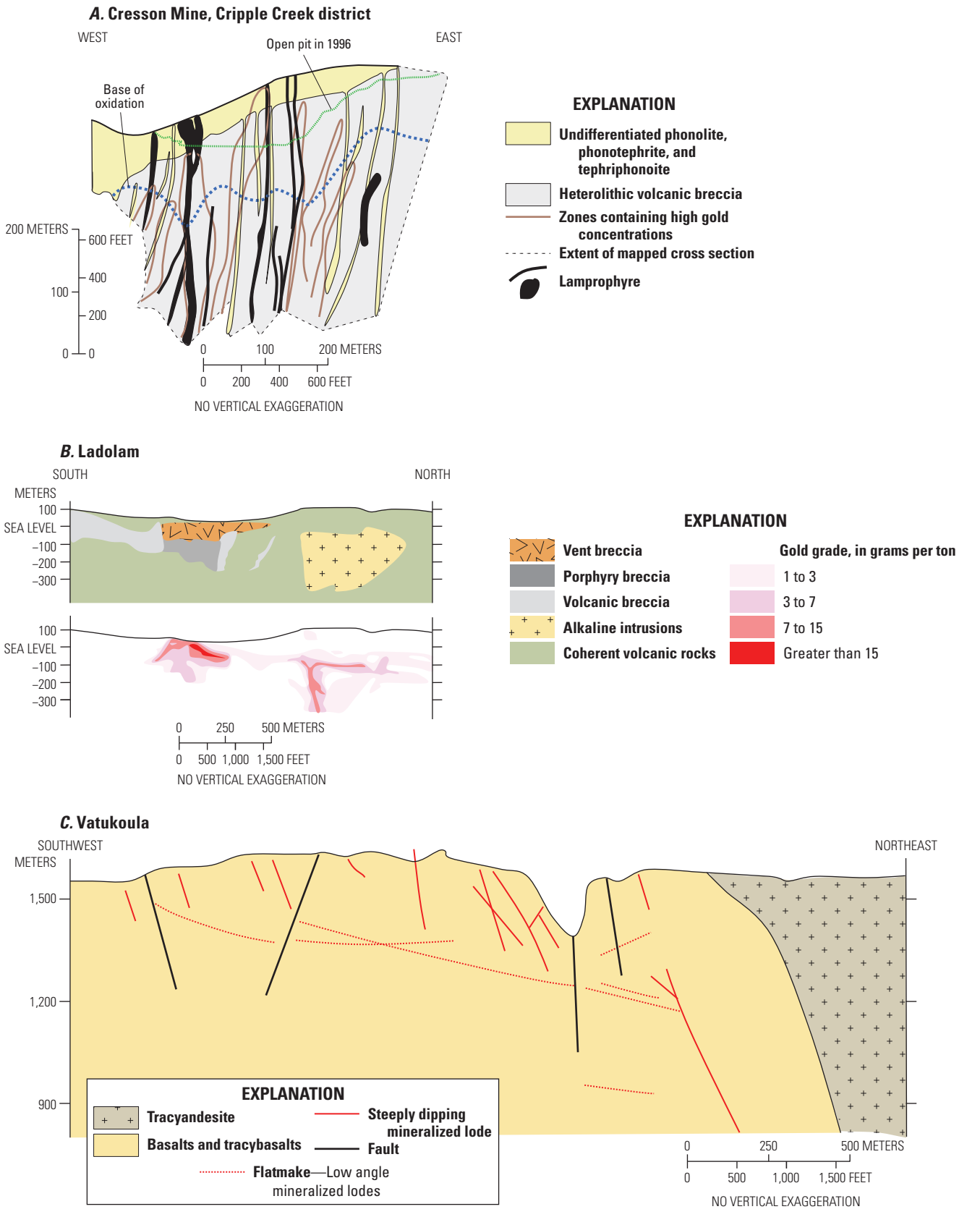

Figure 6. Vertical profiles of select deposits illustrating their large vertical extent. *A*, Cresson Mine, Cripple Creek district (modified from Jensen and Barton, 2000). *B*, Ladolam (modified from Carman, 2003 and Simmons and others, 2005). Vertical axis is distance related to sea level. *C*, Vatukoula (modified from Ahmad and others, 1987). Mine levels on y-axis are not related to sea level.

The alkaline rocks include mafic (for example, basalts in the Vatukoula deposit; alkali basalt/gabbro and trachybasalt in the Porgera and Ladolam deposits), and relatively more felsic compositions (for example, phonolite-syenite-trachyandesite in the Cripple Creek and Montana alkalic province deposits). Importantly, the host rock may not represent the magma directly linked to mineralization. For example, although mafic intrusive or volcanic rocks most commonly host ores at Porgera, radiogenic isotope data (Pb, strontium [Sr]) and geochemical data suggest that mineralization is linked to intrusive phases of intermediate compositions (Richards and others, 1991).

Many alkalic-type epithermal gold systems are spatially distal to the genetically associated intrusion. For example, most of the Boulder County veins are hosted in Precambrian basement rocks that were intruded by Tertiary alkaline rocks (Kelly and Goddard, 1969; Saunders, 1991; Geller, 1994), but the exact intrusion(s) responsible for mineralization have not yet been identified.

At Cripple Creek and Golden Sunlight, some ore is hosted in heterolithic breccias formed during diatreme emplacement, or hydrothermal events (Jensen and Barton, 2000; Kelley and others, 2020). These breccias were then intruded by alkaline igneous rocks, and the associated ores may be fine grained and disseminated or form coarse-grained accumulations within vugs and pockets (Lindgren and Ransome, 1906; Spry and others, 1996, 1997; Jensen and Barton, 2000). Carbonate or carbonaceous sedimentary rocks are the dominant host rocks at the Kendall deposit (Lindsey, 1985), and in some cases (for example, Porgera), both igneous and sedimentary rocks host mineralization.

Structural Setting(s) and Controls

Alkalic-type epithermal gold deposits most commonly form in continent-arc collision zones and back-arc or post-subduction rifts that are invariably characterized by the transition from convergent to extensional or transpressive tectonics (Richards, 1995; Begg and Gray, 2002; Scherbarth and Spry, 2006). Deep-seated regional-scale faults are typically spatially and genetically related to deposit formation (fig. 7).

Structural control on the localization of alkalic-type epithermal gold deposits is evident at both regional and local scales. In some cases, reactivated older structures may be the dominant control on ore trends, and in others, stress fields generated during emplacement of alkaline intrusions form radial or concentric structures that localized the ore. Some of the largest deposits (for example, Cripple Creek, Colorado; Golden Sunlight, Montana) in the western United States are spatially associated with regional lineaments, for example the Colorado Mineral Belt and Rio Grande Rift in Colorado (fig. 7*A*) and the Great Falls tectonic zone, Montana (fig. 7*B*). The two largest alkalic-type epithermal gold deposits in Fiji, Vatukoula and Tuvatu, are along the >250 km east-northeast-trending Viti-Levu lineament (fig. 7*C*) and are localized along local faults that parallel this orientation (for example, Begg and Gray, 2002; Scherbarth and Spry, 2006; Forsythe and others, 2019). According to Begg and Gray (2002), this lineament developed as the result of northeast-southeast extension caused by a reversal of subduction direction during initial formation of the Vanuatu trench.

The highest-grade ores typically occur at the intersection of regional scale structures and local faults that formed during emplacement of igneous rocks. For example, the Vatukoula deposit in Fiji is located at the intersection of the Tavua caldera boundary fault and a major shear zone (Anderson and Eaton, 1990). At the deposit scale, mineralization may occur at the intersection of major faults (for example, Vatukoula; Begg, 1996), in vertical or steeply dipping structures (for example, Mayflower, Montana [Cocker, 1993]; Gies, Montana [Zhang and Spry, 1994]), or shallowly dipping structures (for example, Tuvatu, Vatukoula). Zones of brecciation are commonly the locus of high-grade mineralization (for example, Gies, Vatukoula).

Geophysical Characteristics

Modern geophysical methods employed at multiple scales are useful in exploration for alkalic-type epithermal gold deposits. An up-to-date review on geophysical methods for mineral exploration is provided by Dentith and Mudge (2014) and is the basis for the method descriptions presented here. Several pertinent geophysical methods are discussed and examples of their utility in the exploration for alkalic-type epithermal gold deposits are highlighted.

Geophysical methods are successful only when the rocks, structures, and (or) ore bodies that are targets have physical properties that contrast with their surroundings. Thus, these methods are most sensitive to changes in the physical properties of rocks (or minerals). The physical properties include magnetism, density, electrical resistivity, radioactivity, and elasticity. Recent summaries of these methods are provided by Dentith and Mudge (2014) and Smith (2014). Optical remote sensing, another geophysical method, measures the way in which incident light from the sun reflects off surface material and can be helpful for mapping hydrothermal alteration (Sabins, 1999; Kruse and others, 2012; Pour and Hashim, 2012; van der Meer and others, 2012).

Magnetic and gravity methods, commonly referred to as "potential field methods," are commonly interpreted together. Magnetic susceptibility measurements greatly facilitate magnetic anomaly interpretation. These measurements can be made on both outcrop and drill core. Rocks with larger concentrations of magnetite have high magnetic susceptibilities and produce magnetic anomaly highs when compared to rocks with low magnetic susceptibilities. Magnetic susceptibilities are highly variable, spanning several orders of magnitude within a single rock type. Figure 8 shows magnetic susceptibility ranges (SI) for igneous rocks from Cripple Creek, Porgera, and Goonumbla compared to that for other common rock types (from Dentith and Mudge, 2014). Magnetic anomalies

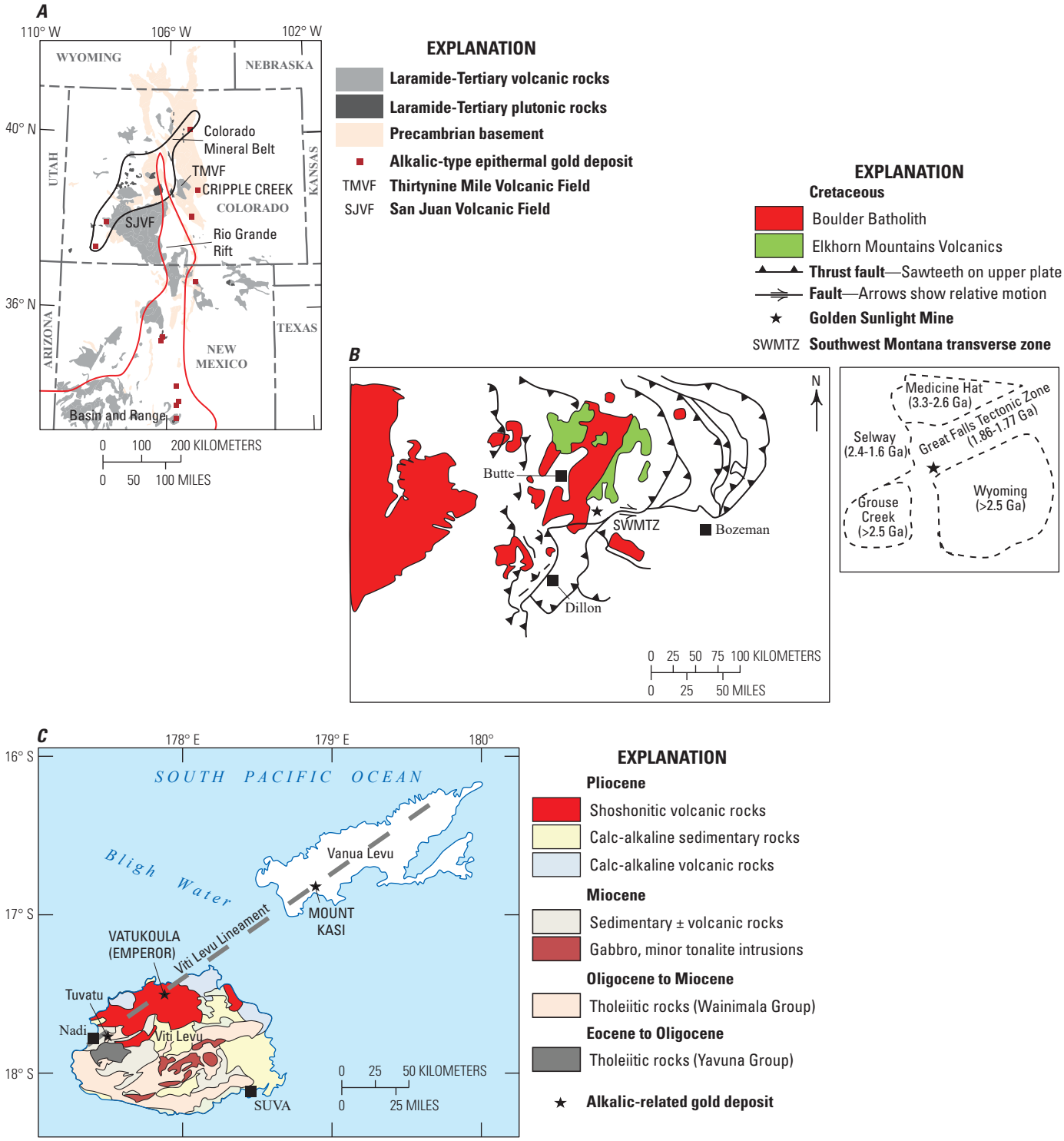

Figure 7. Regional maps showing structural control on some of the largest alkalic-type epithermal gold deposits. *A*, Cripple Creek and other alkalic-type epithermal gold deposits in Colorado and New Mexico, showing spatial association to Colorado Mineral Belt and Rio Grande Rift (modified from Kelley and Ludington, 2002). *B*, Golden Sunlight deposit showing relations to the Montana fold-and-thrust belt and Boulder Batholith (modified from Oyer and others, 2014). Inset shows mine location in relation to Archean cratons and Proterozoic basement terranes (from Foster and others, 2006). *C*, Tuvatu, Vatukoula (Emperor), and Mount Kasi deposits on the islands of Viti Levu and Vanua Levu, Fiji. Geology of Viti Levu and approximate location of proposed northeast-trending Viti-Levu lineament is modified from Begg (1996) and Scherbarth and Spry (2006). (>, greater than; Ga, billion years)

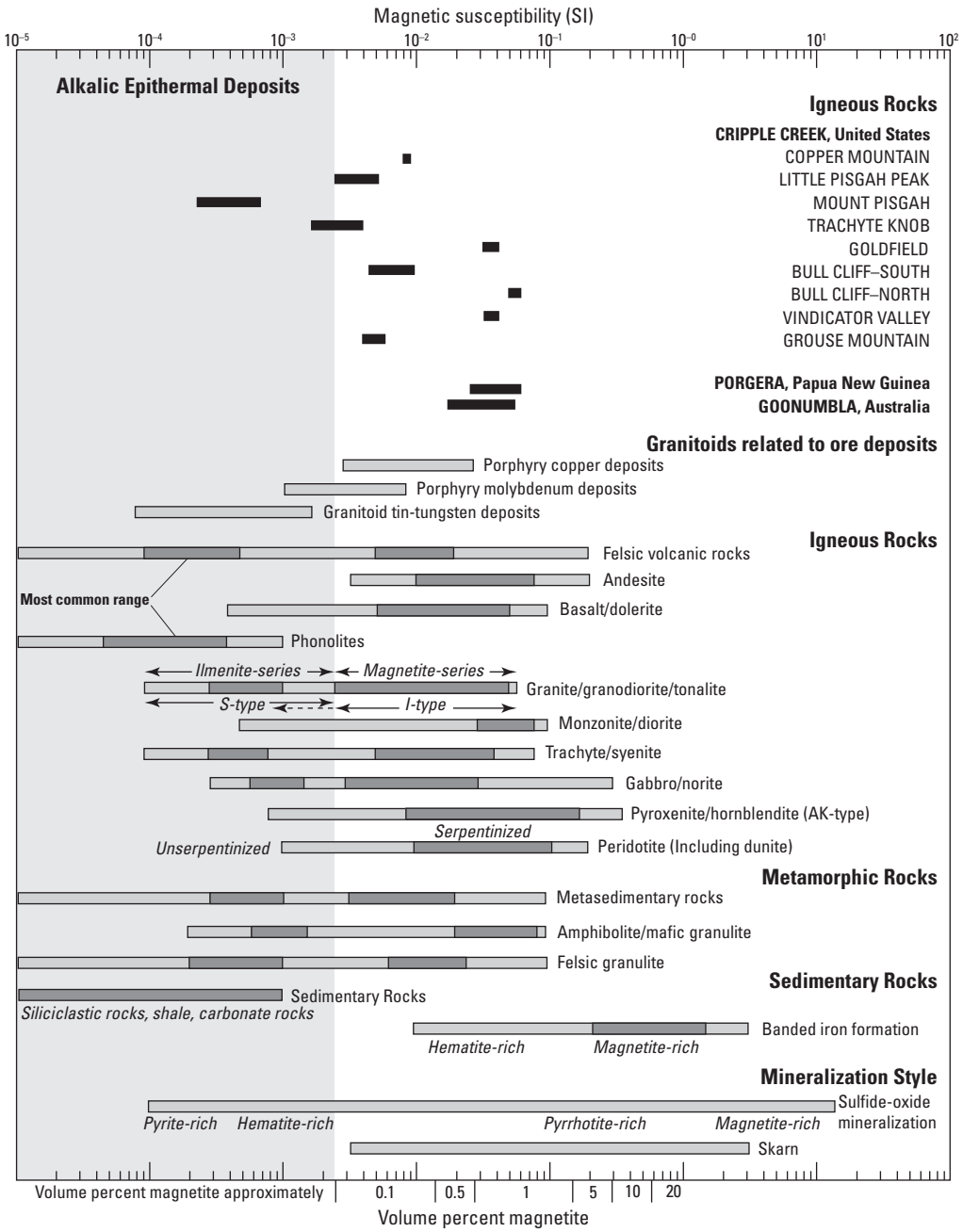

Figure 8. Magnetic susceptibility ranges (SI) for igneous rocks from Cripple Creek, Porgera, and Goonumbla compared to other common rock types (modified from Clark, 1997; Dentith and Mudge, 2014). The darker shading within horizontal bars indicates the most common ranges.

are caused by two different kinds of magnetism: induced and remanent. The induced component is mostly determined by the magnetic susceptibility of the rock. The remanent component depends on the thermal, mechanical, and magnetic history of the rock and is independent of the field in which it is measured. In general, the induced component is predominant, but the reverse can also be true. The ratio of remanent to induced magnetism in a rock is the Koenigsberger ratio and values less than unity indicate induced magnetism is dominant (fig. 9). Densities of common rock types are summarized in figure 10.

Several case studies demonstrating the application of these geophysical methods are available for the Cripple Creek district (Kleinkopf and others, 1970; Pitkin and Long, 1977; Taranik, 1990; Livo, 1994). The Cripple Creek district is localized within a Tertiary alkalic volcanic complex that intruded Precambrian granitic and gneissic rocks. The volcanic rocks have felsic to ultramafic compositions and form breccias, diatremes, dikes, and stocks. Both telluride-gold veins and disseminated gold and pyrite deposits are present. The veins cut both Precambrian and Tertiary rocks; the highest-grade ore is localized where

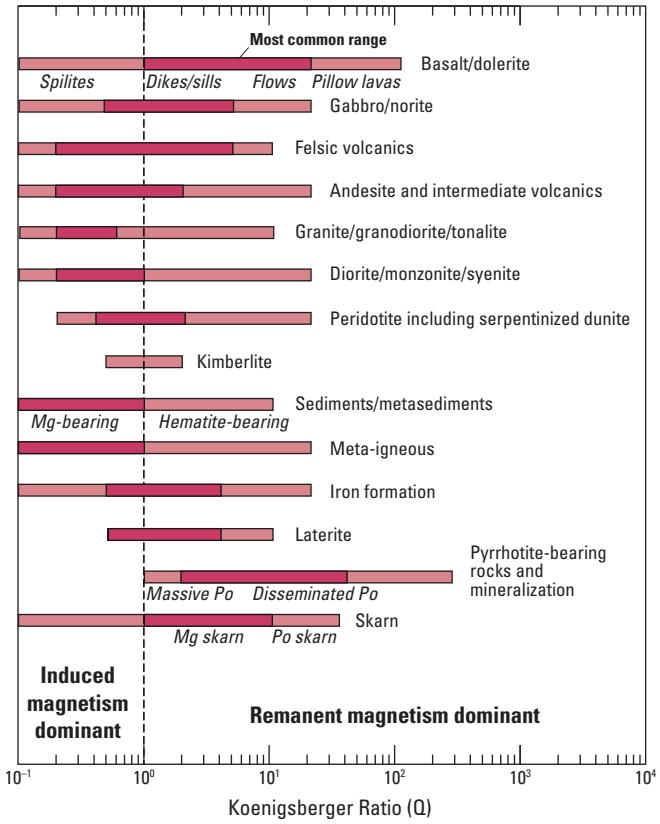

Figure 9. Koenigsberger ratios (Q) for common rock types. The darker shading within horizontal bars indicates the most common ranges. Modified from Clark (1997) and Dentith and Mudge (2014). (Mg, magnesium; Po, pyrrhotite)

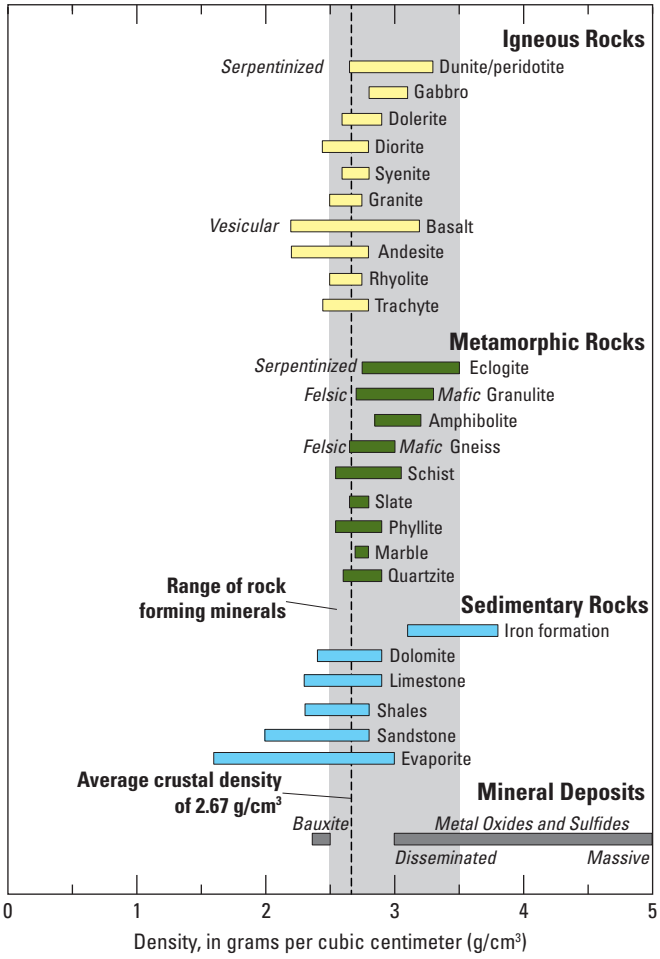

Figure 10. Density ranges for common rock types. Modified from Dentith and Mudge (2014).

northwest- and northeast-trending veins intersect. Aeromagnetic data were collected along northeast-southwest flight lines spaced 400 m apart. Owing to the rugged topography, a flight height was used that ranged from 150 to 450 m above the ground surface. A magnetic low is coincident with the volcanic complex and large amplitude magnetic highs correlate with Precambrian rocks beyond the limits of the volcanic complex (Kleinkopf and others, 1970).

Magnetic susceptibility measurements indicate that the altered volcanic rocks had relatively lower average susceptibilities than the Precambrian granites (Kleinkopf and others, 1970). Local magnetic lows within the volcanic complex that are unrelated to terrain effects may indicate locations of intense, magnetite-destructive hydrothermal alteration. The volcanic complex is also coincident with a bouguer gravity anomaly low of about 10 milligals (Kleinkopf and others, 1970). Northwest-trending linear gravity lows within the volcanic complex appear to reflect vein mineralization. Remote sensing studies using multispectral and hyperspectral data identify and delineate both primary and secondary minerals, including hematite, goethite, jarosite, kaolinite, and sericite, in spite of extensive soil development, vegetative cover, and poor outcrop exposure (Taranik, 1990; Livo, 1994).

Seismic geophysical data can be used to better understand the broad geologic and tectonic framework that is important for developing genetic models for alkalic-type epithermal gold deposits. For example, these data have been applied in the Lachlan Fold Belt of New South Wales, Australia (Finlayson and others, 2002; Glen and others, 2002), which hosts alkalic-type epithermal gold and porphyry systems in the Cadia and Northparkes districts (fig. 11). The alkalic igneous rocks of the Cadia and Northparkes districts are within a major basement structure, the Lachlan Transverse Zone (Scheibner and Stevens, 1974; Cooke and others, 2007). A wide-angle seismic profile conducted along a north-south line that extends from the Molong Volcanic Belt in the north across the Lachlan Transverse Zone suggests a compositional change in the upper and middle crustal rocks that straddle the southern boundary of the Lachlan Transverse Zone. In addition, the data indicate that the Lachlan Transverse Zone represents a zone of structural deformation and compositional difference in the region. The sheeted veins at Cadia Hill and Cadia Quarry alkalic porphyry deposits are parallel to the Lachlan Transverse Zone indicating a possible genetic relationship (Holliday and others, 2002; Wilson and others, 2004; Cooke and others, 2007).

The Cadia and Northparkes district deposits are spatially associated with shoshonitic volcanic rocks that occur within north-south-trending Early to Late Ordovician volcano-plutonic belts (Wyborn, 1992). Aeromagnetic and gravity data define the spatial distribution of these alkalic systems (Woods and Webster, 1985; Heithersay and Walshe, 1995; Walshe and others, 1995; Cooke and others, 2006; Holliday and Cooke, 2007). At a regional scale, the belts produce magnetic anomaly highs that contrast with the more subtle magnetic signature over the intervening Ordovician siltstones and Silurian to Devonian sediments, granites, and felsic volcanics rocks (fig. 11*A*). The Cadia district is coincident with one of many magnetic highs within the Molong Volcanic Belt. The Goonumbla Volcanic Complex hosts the Northparkes district in the Junee-Narromine Volcanic belt. The volcanic complex is imaged as an arcuate-shaped domain of variable magnetic intensity (fig. 11*A*), which has a corresponding gravity low (fig. 11*B*) that is likely because of the density contrast between monzonite and andesite rocks (Holliday and Cooke, 2007), and is similar to the gravity low observed in the Cripple Creek district (Kleinkopf and others, 1970). Similar gravity lows in the Lachlan Fold Belt have been considered a positive prospectivity indicator (Holliday and Cooke, 2007).

High resolution aeromagnetic data further assist deposit identification in the Cadia district (Holliday and Cooke, 2007). The outcropping Big and Little Cadia magnetite skarn deposits produce strong magnetic highs. The Cadia Ridgeway deposit is also located within a strong magnetic high, but the magnetic response is predominately due to shallow magnetic intrusions and magnetite-rich alteration of the volcanic rocks. The Cadia East deposit, although magnetic at depth, has a subdued magnetic response because of magnetite-destructive phyllic alteration that has affected shallow subsurface rocks. Thus, even with high resolution magnetic data, the signatures of individual deposits within a district can vary significantly.

Physical property measurements were obtained to help interpret gravity and magnetic characteristics of the Endeavour Cu-Au deposit in the Northparkes district (Clark and Schmidt, 2001). The deposit is associated with numerous porphyry stocks emplaced within coeval volcanic and intrusive rocks. The porphyry stocks extend downwards into underlying plutons. Alteration appears to be both magnetite constructive and destructive as shown by the physical property measurements that show a pattern of progressively decreasing susceptibility from early potassic (biotite + K-feldspar) to fresh rock to K-spar to phyllic. The mafic volcanic host rocks have consistently high magnetic susceptibilities. Magnetic susceptibilities of intrusive rocks decrease progressively from monzodiorite to monzonite to aplite to alkali feldspar granite. Mafic rocks also have higher densities than felsic rocks. At the prospect scale, a central magnetic low is surrounded by a ring of magnetic highs. The low magnetic core was attributed to the combined effects of felsic intrusions and late magnetite destructive alteration (Clark and Schmidt, 2001). Importantly, the magnetic signature of the deposits varies as a function of host rock composition. For example, volcanic hosts show a weak to moderate annular high and well-developed central low, whereas volcaniclastic hosts correspond to a weak to moderate central high.

The Porgera Intrusive Complex was emplaced into marine sedimentary rocks after arc-continent collision. The intrusive complex consists of hornblende and augite-hornblende diorite stocks and later, more differentiated andesite and feldspar porphyry stocks. Gold is in quartz veins that contain roscoellite, pyrite, galena, sphalerite, and chalcopyrite. The veins are commonly associated with a quartz-sericite alteration assemblage. Most mineralization is structurally controlled by the Romane Fault Zone along the margin of the Porgera Intrusive Complex.

Multiple geophysical methods were applied at Porgera (Schmidt and others, 1997; Levett and Logan, 1998). Physical property measurements indicate that the unaltered rocks of the Porgera Intrusive Complex have relatively high magnetic susceptibilities (Schmidt and others, 1997). Diorite intrusions have the highest susceptibilities, typically >0.025 magnetic susceptibility ranges (SI), whereas hydrothermally altered igneous rocks and sedimentary rocks generally have the lowest susceptibilities, with values <0.0013 SI. Hydrothermal alteration produced secondary magnetite through alteration of olivine, hornblende, and biotite. Magnetite was preserved in the propylitically altered rocks except where alteration was most intense. In contrast, phyllic alteration destroyed primary magnetite. Low Koenigsberger ratios indicate that induced magnetization is dominant in most intrusive rocks, with the exception of Yakatabari diorite (Schmidt and others, 1997). High-resolution aeromagnetic data delineate the Porgera Intrusive Complex and illustrate the importance of the reduction-to-the-pole transformation to better align causative magnetic sources at low magnetic latitudes (Levett and Logan, 1998). Magnetic modelling, constrained by physical property measurements, helped identify the diorite intrusive bodies at depth where contact geometries are important for high-grade ores (Schmidt and others, 1997; Levett and Logan, 1998). Radiometric data show an increase in potassium concentrations in the volcanic rocks and K/Th ratios constrain the extent of the sericitic alteration halo around the intrusive complex (Levett and Logan, 1998). Electromagnetic and resistivity methods were used to better delineate deep intrusive bodies (Schmidt and others, 1997; Levett and Logan, 1998). The igneous rocks are hosted in sedimentary rocks, resulting in significant electrical contrasts. Audio-frequency magnetotelluric (AMT) data identify several known intrusive bodies and suggest the presence of additional bodies at depth. An induced polarization survey helped characterize the Porgera Intrusive Complex and define chargeability highs associated with pyrite-rich alteration zones (Levett and Logan, 1998).

Alkalic-type epithermal gold deposits in northern Viti Levu, Fiji, are localized in caldera structures and are hosted in shoshonitic volcanic rocks intruded by monzonite intrusive complexes. Aeromagnetic and gravity data define regional-scale geologic trends associated with these deposits (Gunn and others, 2009a, b). A total magnetic intensity map

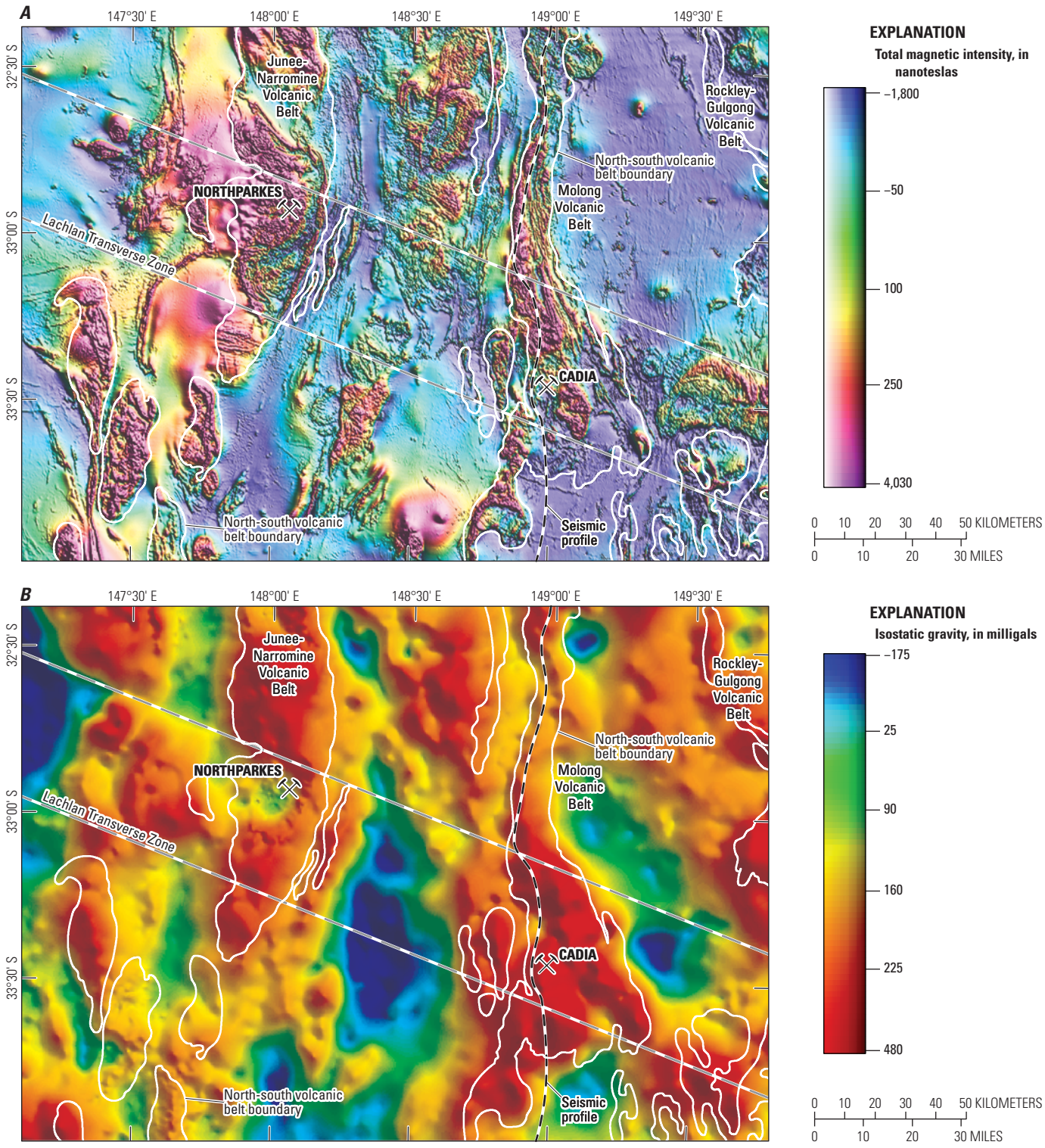

Figure 11. *A*, Total magnetic intensity map of the eastern Lachlan Fold Belt in New South Wales, Australia. The Cadia and Northparkes districts are within the north-south-trending volcanic belts that produce prominent magnetic anomalies. The Goonumbla volcanic complex hosts the Northparkes district and is coincident with an arcuate magnetic structure. Also shown is the location of the wide-angle seismic profile, which extends to the north and south of map area for 35 and 120 kilometers (km), respectively. Modified from Holliday and Cooke (2007). *B*, Isostatic gravity map of the eastern Lachlan Fold Belt in New South Wales, Australia. The Cadia and Northparkes districts are within the north-south-trending volcanic belts coincident with gravity anomaly highs. The Goonumbla volcanic complex hosts the Northparkes district and is coincident with a gravity low. Also shown is the location of the wide-angle seismic profile that extends to the north and south of map area for 35 and 120 km, respectively. The maps were developed based on data from Geoscience Australia, 2018.

reveals a pattern of highs and lows coincident with the caldera structures. The Tavua caldera, host to the Vatukoula deposit, is associated with a central magnetic low surrounded by highs near the caldera rim. The first vertical derivative of the total magnetic intensity map defines anomalous features that correlate with the mapped volcanic rocks. Magnetic data, upward continued to 500 m, were used to delineate the buried intrusive rocks. These deeper sourced magnetic anomalies align with gravity highs along a northeast trend and provide regional-scale targets for additional alkalic-type epithermal gold deposits. The Vatukoula and Tuvatu epithermal deposits are coincident with these magnetic and gravity highs. Increased potassium concentrations, likely the result of hydrothermal alteration, are associated with the volcanic rocks and vents of the Tuvato and Tavua calderas (Gunn and others, 2009a, b).

The Ladolam epithermal deposit is an active geothermal system. Aeromagnetic data indicate that hydrothermal alteration extends 1 to 2 km offshore. Magnetotelluric (MT) surveys define a shallow conductive layer interpreted as argillically altered rock. The conductive layer is truncated by the ground surface, which suggests some of the argillically altered rock has been removed (White and others, 2010).

The Mount Milligan porphyry/epithermal deposit in British Columbia was also the focus of geophysical investigations (Oldenburg and others, 1997; Ford and others, 2007; Yang and Oldenburg, 2012). The geophysical datasets include magnetic, direct-current resistivity, induced polarization, and airborne time-domain electromagnetic (EM) surveys. The Mount Milligan deposit is associated with a monzonite stock that intruded volcanic rocks. Mineralization is localized along the contact of the monzonite stock and within the trachytic units. Potassically altered rock surrounds the monzonite stock and contains chalcopyrite, bornite, and magnetite. Propylitically altered rock surrounds the potassic alteration zone and is coincident with an increase in pyrite content and minor amounts of magnetite. At a regional scale, the intrusive complex at Mount Milligan is associated with a broad magnetic high (Ford and others, 2007). Three-dimensional magnetic inversions centered on the monzonite stock define susceptibility lows related to the deposit (Oldenburg and others, 1997). In contrast, induced-polarization inversions indicate that the deposit is associated with a chargeability high (Oldenburg and others, 1997). Versatile time-domain EM (VTEM) data collected along a 200-m line spacing delineate plutonic rocks at depth (Yang and Oldenburg, 2012). The three-dimensional EM inversion results revealed a complex resistivity structure. The most conductive feature is a near-surface feature and is attributed to the younger sedimentary rocks. A central resistor at depth is interpreted as a pluton that is ringed by a conductor that has been interpreted as altered rock. This inferred overall structural setting agrees well with the results of direct-current resistivity inversions (Oldenburg and others, 1997). Radiometric data show an increase in potassium concentrations in the volcanic rocks with K/Th ratios indicating the extent of the mineralized rock (Ford and others, 2007).

Hypogene and Supergene Ore Characteristics

Mineralogy and Mineral Assemblages

Alkalic-type epithermal gold deposits contain a wide variety of mineral species, but most ore consists of a small number of mineral groups and species, including alkali feldspar, quartz, carbonates, fluorite, pyrite and base metal sulfides, and tellurides (table 2). Auriferous pyrite, native gold, and gold tellurides (with or without silver) are the principal economic minerals in alkalic-type epithermal gold deposits. In rare cases, native tellurium is present and tetradymite (Bi_2Te_2S) occurs with gold and is recovered as a primary or byproduct (fig. 12). Although these deposits contain many gold- or silver-tellurides, the most common of these are calaverite ($AuTe_2$), krennerite ($AuTe_2$), sylvanite ($AgAuTe_4$), hessite (Ag_2Te) and petzite (Ag_2AuTe_2) (table 2). Although tellurides are characteristic of many alkalic-type epithermal gold deposits, not all deposits, including the giant Ladolam deposit and many of the deposits in New Mexico (for example, Lincoln County and Elizabethtown-Baldy districts), contain these minerals (table 3). Importantly, several deposits, including Cripple Creek (Jensen, 2003; Dye, 2015) and Vatukoula, and Tuvatu (Pals and others, 2003; Scherbarth and Spry, 2006) contain significant quantities of invisible gold.

The number and variety of ore minerals among deposits is highly variable. For example, the Golden Sunlight deposit in Montana and deposits in Fiji (Vatukoula) have complex mineral assemblages that include at least six different tellurides in addition to native tellurium, as well as a large number of sulfide and gangue minerals (table 3). Gold deposits in Boulder County contain a complex sequence of 67 vein minerals including 13 different tellurides with various sulfides and sulfosalts (Kelly and Goddard, 1969). The relatively complex mineral assemblages of some deposits may be explained by (1) multiple overprinting stages of mineralization, for example, gold-rich telluride precipitation prior to silver-rich tellurides (Scherbarth and Spry, 2006); or (2) the presence of associated porphyry deposits, as exemplified by the Golden Sunlight and Fiji epithermal deposits (Ahmad and others, 1987; Spry and others, 1996, 1997; Pals and Spry, 2003; Spry and Scherbarth, 2006), that are spatially, temporarily, or genetically related to epithermal gold formation and which contain alteration and ore minerals unique to porphyry deposits that overprint epithermal minerals.

Mineral textures and associations including small amounts of sulfate minerals (for example, alunite and barite), and metal sulfide minerals (for example, covellite and chalcocite), indicate that some deposits have been overprinted by supergene processes (for example, Mount Milligan subepithermal deposit; LeFort and others, 2011). In general, however, the effects of supergene enrichment are minor in most of these systems.

Figure 12. Tellurium minerals found in alkalic-type epithermal gold deposits. *A*, Calaverite from the Cresson Mine, Cripple Creek, Colorado. The largest calaverite crystal is 9 millimeters (mm) long. Photograph courtesy of Rob Lavinsky (https://commons.wikimedia.org/wiki/File:Calaverite-255187.jpg). *B*, Sylvanite (silver) and calaverite (gold) from the Vatukoula Mine, Fiji. Photograph by Karen Kelley, USGS, 2017. *C*, Native tellurium from Boulder County, Colorado. Source: http://www.minclassics.com/colorado712.php. *D*, Tetradymite from Leshan, Sichuan, China. Source: https://www.mindat.org/locentries.php?p=693&m=3921.

Table 2. Mineralogy of alkalic-type epithermal gold deposits.

[—, indicates that the mineral has the same general formula as the higher category above]

Mineral	Formula
Native elements	
Amalgam	Ag-Au-Hg
Gold[1]	Au
Mercury	Hg
Tellurium	Te
Sulfides, sulfarsenides	
Acanthitie	Ag_2S
Arsenopyrite	FeAsS
Benleonardite	$Ag_8(Sb,As)Te_2S_3$
Bismuthinite	Bi_2S_3
Bravoite	$(Ni, Fe)S_2$
Chalcocite	Cu_2S
Chalcopyrite	$CuFeS_2$
Cinnabar	HgS
Covellite	CuS
Galena	PbS
Marcasite	FeS_2
Molybdenite	MoS_2
Pyrite[1]	FeS_2
Pyrrhotite	$Fe_{1-x}S$
Realgar	AsS
Sphalerite	ZnS
Stibnite	Sb_2S_3
Tellurides	
Altaite	PbTe
Buckhornite	$AuPb_2BiTe_2S_3$
Calaverite[1]	$AuTe_2$
Coloradoite	HgTe
Empressite	AgTe
Hessite[1]	Ag_2Te
Joséite	Bi_4TeS_2
Krennerite[1]	$AuTe_2$
Melonite	$NiTe_2$
Nagyagite	$Pb_5Au(Te,Sb)_4S_{5-8}$
Petzite[1]	Ag_3AuTe_2
Pilsenite	Bi_4Te_3
Stuetzite	Ag_5Te_3
Sylvanite[1]	$AgAuTe_4$
Tetradymite	Bi_2Te_2S
Tsumoite	BiTe

Table 2. Mineralogy of alkalic-type epithermal gold deposits.—Continued

[—, indicates that the mineral has the same general formula as the higher category above]

Mineral	Formula
Selenides	
Naumannite	Ag_2Se
Sulfosalts	
Aikinite[2]	$PbCuBiS_3$
Andorite	$PbAgSb_3S_6$
Jamesonite	$Pb_4FeSb_6S_{14}$
Proustite	Ag_3AsS_3
Pyrargyrite	Ag_3SbS_3
Stephanite	Ag_3SbS_4
Tetrahedrite	$(Cu,Fe)_{12}Sb_4S_{13}$
Tennantite	$(Cu,Fe)_{12}As_4S_{13}$
Lindstroemite[2]	—
Krupkaite[2]	—
Gladite[2]	—
Bismuthinite[2]	—
Benjaminite[2]	—
Oxides	
Brookite	TiO_2
Hematite	Fe_2O_3
Ilmenorutile	$(Ti,Nb,Fe)_3O_6$
Magnetite	Fe_3O_4
Pyrolusite	MnO_2
Rutile	TiO_2
Uraninite	UO_2
Halides	
Fluorite[1]	CaF_2
Carbonates	
Ankerite[1]	$Ca(Fe,Mg,Mn)(CO_3)_2$
Calcite[1]	$CaCO_3$
Dolomite[1]	$CaMg(CO_3)_2$
Rhodochrosite	$MnCO_3$
Sulfates	
Alunite	$KAl3(SO_4)_2(OH)_6$
Anhydrite	$CaSO_4$
Barite	$BaSO_4$
Celestite	$SrSO_4$
Tungstates	
Huebnerite	$(Mn,Fe)WO_4$
Ferberite	$FeWO_4$
Scheelite	$CaWO_4$
Wolfranite	$(Fe,Mn)WO_4$

Table 2. Mineralogy of alkalic-type epithermal gold deposits.—Continued

[—, indicates that the mineral has the same general formula as the higher category above]

Mineral	Formula
Phosphates	
Wavellite	$Al_3(PO_4)_2(OH,F)_3 \cdot 5H_2O$
Woodhouseite	$CaAl_3(PO_4)(SO_4)(OH)_6$
Silicates	
Dickite	$Al_2Si_2O_5(OH)_4$
Illite	$(K,H_3O)(Al,Mg,Fe)_2(Si,Al)_4O_{10}[(OH)_2,(H_2O)]$
Kaolinite	$Al_2Si_2O_5(OH)_4$
Alkali feldspars	$KAlSi_3O_8$
—Adularia[1]	—
—Orthoclase	—
—Sanidine[1]	—
Laumonite	$CaAl_2Si_4O_{12} \cdot 4H_2O$
Montmorillonite	$(Na,Ca)_{0.3}(Al,Mg)_2Si_4O_{10}(OH)_2 \cdot n(H_2O)$
Muscovite	$KAl_2Si_3O_{10}(OH)_2$
—Sericite	—
Quartz[1]	SiO_2
—Chalcedony[1]	—
Riebeckite	$Na_2(Fe,Mg)_3Fe_2Si_8O_{22}(OH)_2$
Roscoelite[1]	$K(V,Al,Mg)_2AlSi_3O_{10}(OH)$

[1]Common.

[2]Selenium-bearing sulfosalt minerals in the Golden Sunlight deposit.

Paragenesis

Mineral paragenesis is the sequence in which minerals are formed, and it varies from simple to complex among various alkalic-type epithermal gold deposits. As discussed earlier, the abundance and variety of ore and gangue minerals may be related to multiple ore-forming hydrothermal events, or to overprinting by cospatial epithermal and porphyry mineralizing events. Paragenetic complexity may also reflect other factors. For example, at least seven distinct stages of gangue and ore minerals have been identified at the Cripple Creek deposit (Dye, 2015), and at least five stages at the Tuvatu (Scherbarth and Spry, 2006) and Vatukoula deposits (Ahmad and others, 1987). At the large Porgera deposit, two main stages reflect early formation of porphyry and subsequent epithermal mineralization. The first stage consists of the formation/deposition (?) of relatively low-grade auriferous pyrite and various base metal sulfides in phyllic alteration zones. A variety of base metal sulfide minerals are associated with the pyrite. The second stage of mineralization is characterized by vuggy veins and hydrothermal breccias, locally containing bonanza concentrations of gold (Richards, 1995). The Ladolam deposit on Lihir Island is similar to Porgera because both involve weak porphyry-style mineralization followed by veining (Richards, 1995). Early precipitation of disseminated gold and sulfide minerals with subsequent vein formation is also characteristic of the Sandaowanzi deposit (Liu and others, 2013).

A highly generalized paragenesis that may apply to many deposits includes early deposition of base metal sulfide minerals (typically include sphalerite, galena, and less common chalcopyrite or molybdenite), followed by telluride deposition, and then native gold precipitation (fig. 13). Common iron sulfides include pyrite, marcasite, and pyrrhotite. Typically, telluride mineral compositions evolve from Au- to Ag-rich with time, a transition that has been documented for the Vatukoula and Tuvatu (Ahmad and others, 1987; Scherbarth and Spry, 2006), Golden Sunlight (Spry and others, 1996), and many of the Boulder County deposits (Nash and Cunningham, 1973; Saunders, 1986). However, the opposite sequence is reported for the Sandaowanzi deposit; although the general transition from

Table 3. Mineralogical and metal associations of select alkalic-type epithermal gold deposits and districts.

[act, acanthite; ad, adularia; Ag, silver; alt, altaite; an, anhydrite; ank, ankerite; As, arsenic; aspy, arsenopyrite; Au, gold; Ba, barium; bar, barite; Bi, bismuth; bis, bismuthinite; bl, benleonardite; bn, bornite; carb, carbonates; cc, chalcocite; co, coloradoite; cpy, chalcopyrite; cs, celestite; Cu, copper; cv, calaverite; cvt, covellite; do, dolomite; en, enargite; F, fluorine; fl, fluorite; gn, galena; Hg, mercury; hm, hematite; hs, hessite; jo, joséite; K, potassium; kr, krennerite; mc, marcasite; mo, molybdenite; Mo, molybdenum; ml, melonite; mt, magnetite; nm, naumannite; po, pyrrhotite; py, pyrite; pyl, pyrolusite; pyr, pyrargyrite/proustite; pz, petzite; qtz, quartz; rl, realgar; rt, rutile; Sb, antimony; sch, scheelite; Se, selenium; ser, sericite; sp, sphalerite; stb, stibnite; stn, stannite; sy, sylvanite; tb, tellurobismutite; TE, tellurium; tet, tetradymite; tn, tennantite; tour, tourmaline; ts, tsumoitett, tt, tetrahedrite; W, tungsten]

	Cripple Creek	Porgera	Ladolam	Vatukoula/Tuvatu	Fakos	Boulder County	Golden Sunlight	Ortiz Mountains	Jicarilla Mountains	Dashuigou
Major metals	Au	Au	Au, Cu	Au	Au	Au	Au	Au	Au	Te
Minor and trace metals	Ag, As, Ba, K, Hg, F, Mo, Te, V, W	Ag, Te	As	Ag, As, Bi, Sb, Se, Te	Ag	F, W, Te	Ag, Bi, Cu, Mo, Te	F, W	Ag, F	Au, Bi
Gold host	Native, py, tellurides	Electrum, native, py, tellurides	aspy, cpy, mc, native, py	Electrum, native, py, tellurides	Native	Electrum, native, py, tellurides	Native, tellurides	Native, py	Native, py	Native
Sulfide minerals	act, cpy, gn, mc, py, sp	aspy, cpy, gn, mc, py, pyr; sp, tt	aspy, cpy, cvt, en, gn, mc, mo; po, py, sp, tn, tt	aspy, cpy, gn, mc, po, py, pyr, rl, sp, stb, tt, tn	cpy, gn, en, py, sp, tt, tn	cpy, gn, py, sp,	act, aspy, bis[1], bn, cc, cpy, cvt, gn, mc, po, py, tn, sp, stn	cpy, gn, po, py	cpy, gn, py	po, py
Telluride minerals	alt, co, cv, kr, ml, pz, sy	alt, co, cv, hs, kr, pz	Rare sy	bl, co, cv, hs, kr, native, sy, ml, pz	alt, hs, pz	alt, co, cv, kr, native, pz, sy	cv, co, ml, native, pz, tb, tet	None	None	jo, tet, ts
Vanadium minerals	Roscoelite	Roscoelite	None	Karelianite, nolanite, roscoelite, V-silicate,	None	Roscoelite	None	None	None	None
Other	ad, cs, do, fl, hm, qtz, rt	bar, carb, qtz, ser	ad, an, bar, carb, mt, qtz, rt	ad, ank, bar, do, fl, hm, mt, nm, pyl, qtz, rt, ser, tour	qtz	fl, hm, qtz	bar, do, fl, hm, qtz, rt, ser	carb, mt, qtz, sch	carb, bar, qtz,	carb, do, qtz, ser
Reference(s)	Thompson and others, 1985; Saunders, 1986	Richards and others, 1991	Müller and others, 2001; Carman, 2003; White and others, 2010	Ahmad and others, 1987; Pals and Spry, 2003; Spry and Scherbarth, 2006	Fornadel and others, 2012	Kelly and Goddard, 1969; Saunders, 1986, Geller, 1994	Spry and others, 1997	Maynard, 1995	McLemore, 1996	Mao and others, 2002

base metal sulfide minerals to tellurides is consistent with other deposits, a general increase in the Au content during telluride deposition has been reported (Liu and others, 2013).

Zoning Patterns

High-density sampling is required to establish zoning patterns on a deposit scale, but only a few studies have focused on textural, mineralogical, or geochemical zoning across a deposit. At the Vatukoula deposit, Forsythe (1971) showed that Au-rich tellurides (krennerite, sylvanite, and calaverite) are relatively more abundant in upper parts of the deposit, whereas silver-rich tellurides, petzite and hessite, and native gold are more abundant in deeper parts of the deposit (that is, Au>Ag transitioning to Ag/Au with depth). However, it is unclear whether all minerals reported by Forsythe (1971) are from the same hydrothermal stage. Pals and Spry (2003) observed that the assemblage calaverite-sylvanite-krennerite consistently formed prior to petzite-hessite-native gold, which suggests that zoning is related to timing of deposition, rather than depth. Similar paragenetic relations characterize other deposits (Gies and Golden Sunlight in Montana; Zhang and Spry, 1994; Spry and Thieben, 2000).

Textures and Grain Size

Alkalic-type epithermal gold deposits form during hydrothermal brecciation, breccia pipe and diatreme development, and structurally controlled vein emplacement. Ore minerals are disseminated in wall rocks, resulting in highly variable ore textures. The ores can be extremely fine-grained and disseminated, or form coarse-grained aggregates in veins, vugs, or breccias (fig. 14).

The Cresson blowout is a breccia pipe within the Cripple Creek diatreme that contains vugs lined with ore minerals. The largest of these vugs, discovered in 1914, measures 4.3 m wide, 7 m long, and ~11 m high (Koschmann, 1949). Calaverite crystals in this vug were as long as 9 mm (fig. 12). Telluride mineral aggregates up to 1 cm in size are also present in Bessie G deposits (La Plata district in southwest Colorado) and the Black Rose deposits in Boulder County, Colorado (Saunders, 1986). However, more commonly, the ore mineral grains in veins or breccia pipes range from 10 to 600 microns. Krennerite in the Porgera deposit has average dimensions of about 200–300 microns (Richards and others, 1991), ore minerals including calaverite and other tellurides in the Golden Sunlight breccia pipe deposit average about 10–25 microns (Spry and others, 1997), and sylvanite and petzite grains in Sandaowanzi are as large as 200–600 microns (Liu and others, 2011). Disseminated free gold or auriferous pyrite grains are much finer grained, typically ≤10 microns (Richards and others, 1991; Pals and others, 2003; Dye, 2015).

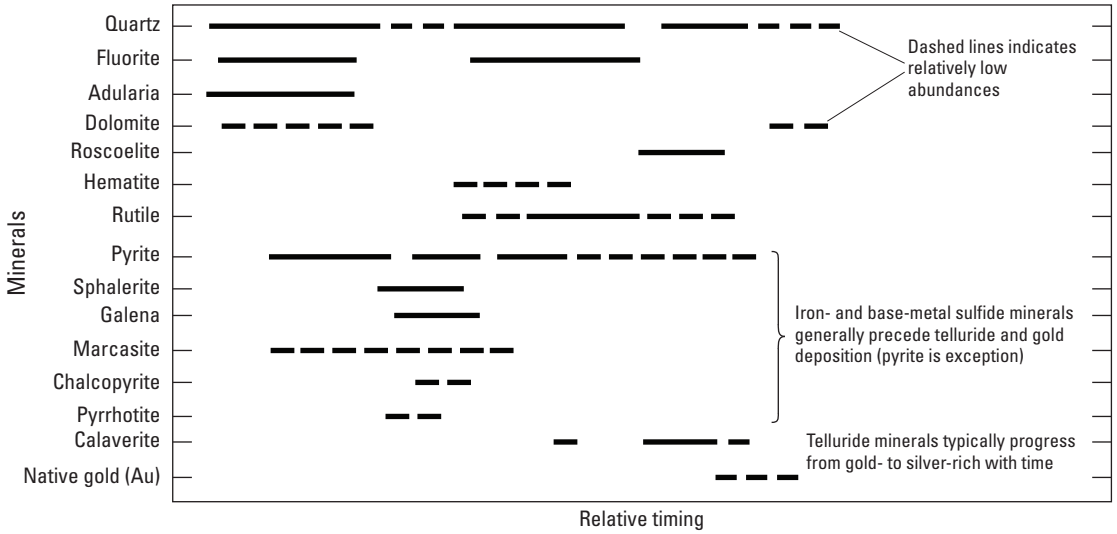

Figure 13. Highly generalized paragenetic diagram of alkalic-type epithermal gold deposits, showing relative timing of deposition of iron- and base-metal sulfide minerals, telluride minerals (where present), and native gold (based on Thompson and others [1985] for Cripple Creek; Ahmad and others [1987] for Vatukoula, Fiji; and Saunders [1986] for Boulder County deposits, Colorado). Dashed line indicates relatively low abundances. Although calaverite is listed as the sole telluride mineral, a large variety of gold-silver (Au-Ag) telluride minerals are typically present in ore associated with this deposit type.

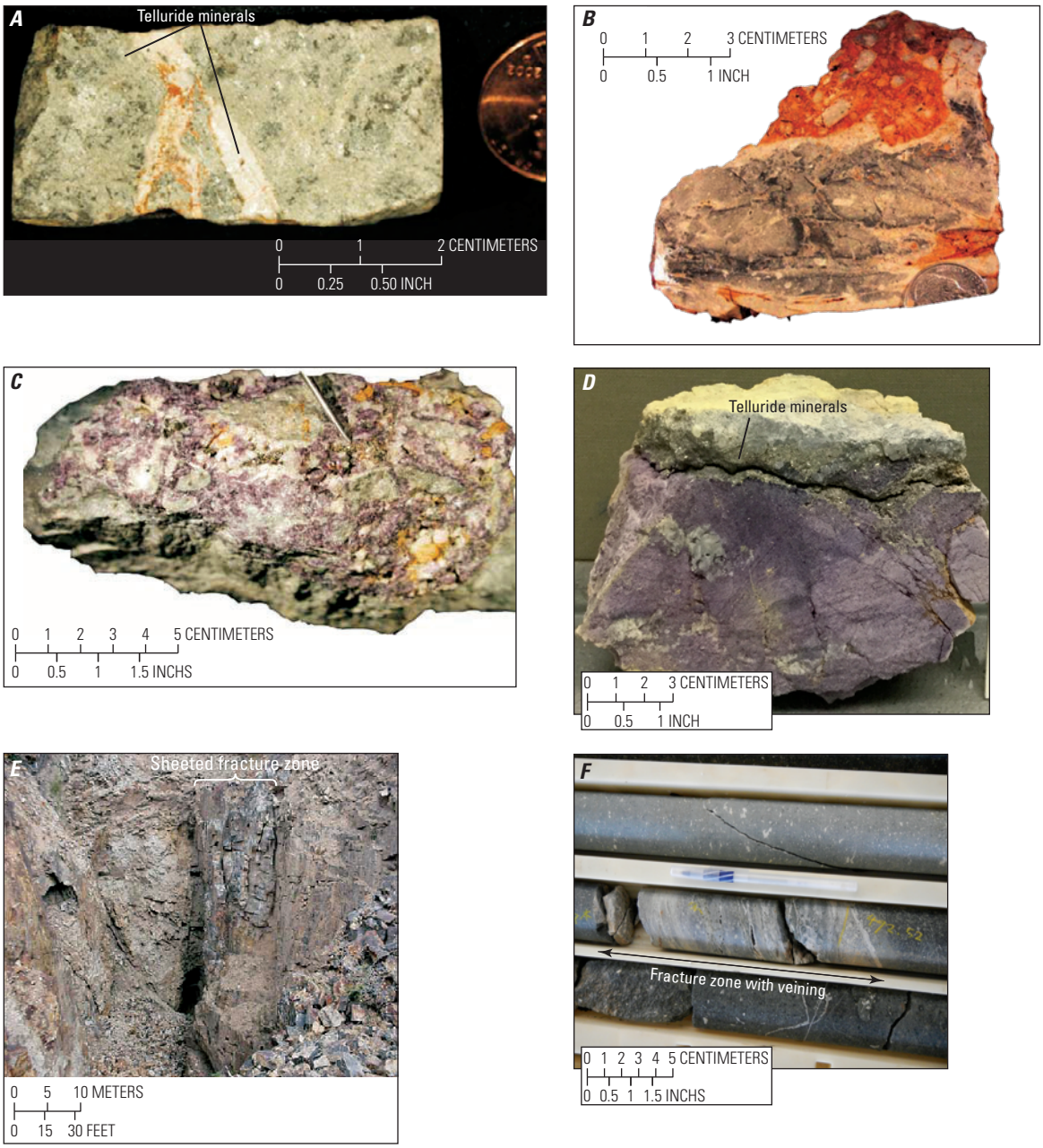

Figure 14. Mineralization styles and common ore and gangue mineral textures of alkalic-type gold deposits. *A*, Vein from the Cripple Creek district showing gold telluride minerals in thin seam of quartz cutting altered phonolite. Many high grade veins in the Cripple Creek district are characterized by thin seams of quartz that are only a few millimeters to centimeters wide. (Photograph from Jensen, 2003). *B*, Disseminated low-grade gold ore from the open-pit Cresson Mine. This type of ore is characteristic of that currently being exploited from the WHEX open-pit mine at Cripple Creek. The sample is laced with thin quartz-pyrite-telluride veinlets (dark streaks). Orange colors represent zones of oxidation, where limonite has replaced pyrite and ferroan carbonate. Native gold occurs in place of tellurides within the zones of oxidation. (Photograph from Jensen, 2003). *C*, Quartz-fluorite-carbonate matrix with accessory pyrite and gold tellurides from hydrothermal breccia at Cripple Creek. (Photograph from Jensen, 2003). *D*, Purple fluorite and telluride minerals in York vein from the Bueno Mine, Boulder County, Colorado. (Photograph by Karen Kelley, USGS, 2017). *E*, Example of a sheeted fracture zone exposed in open cut at Cripple Creek. Sheeted fracture zones consist of closely spaced joints/fractures developed over 1–10 meters in width; mineralization is best developed at the center of the fracture sets. (Photograph from Jensen, 2003). *F*, Core from Vatukoula deposit showing fractures in limited zone within alkaline basaltic rocks. (Photograph by Karen Kelley, USGS, 2017).

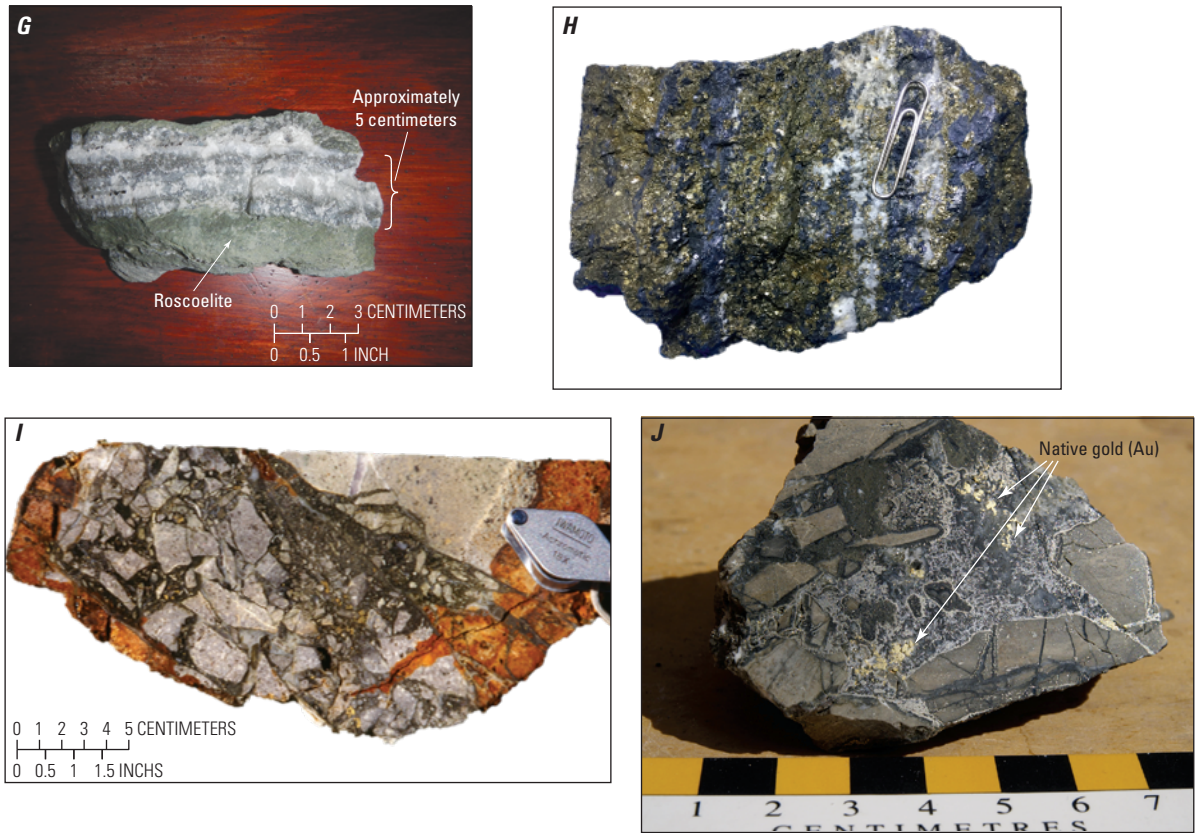

Figure 14. *G*, An atypically thick (about 5 centimeters) quartz vein with crustiform texture containing telluride minerals (dark) and adjacent selvage of roscoelite from the Vatukoula mine, Fiji. (Photograph by Karen Kelley, USGS, 2017). *H*, Stage 1 quartz-carbonate-base metal sulfide vein from the Porgera mine, Papua New Guinea. (Photograph by Antonio Arribas, University of Texas, El Paso, 2019, used with permission). *I*, Bonanza quartz-roscoelite veins and breccia from the Porgera deposit, Papua New Guinea (Photograph by Antonio Arribas, University of Texas, El Paso, 2019, used with permission). *J*, High-grade gold ore from the Porgera deposit showing native gold intergrown with gold-silver telluride minerals (silvery) and pyrite. (Photograph from Richards, 2013)—Continued.

Hypogene and Supergene Gangue Characteristics

Mineralogy, Mineral Assemblages, and Paragenesis

Quartz, adularia, carbonates (calcite, dolomite, ankerite), roscoelite [$K(V,Al,Mg)_2AlSi_3O_{10}(OH)$], and fluorite are the most common hypogene gangue minerals in alkalic rock-related epithermal gold deposits (tables 1 and 2). Barite, celestite, and rutile are less common gangue minerals. Roscoelite, a vanadium-rich, distinctly green mica (fig. 14*G*, *I*, and *J*) that forms fine-grained intergrowths with quartz and other gangue minerals (table 1) is a constituent of alkalic-type epithermal gold systems but not other types of epithermal deposits. In most cases, roscoelite is directly spatially associated with gold-bearing tellurides, particularly calaverite, and either native gold or electrum. This spatial association indicates a temporal relation with telluride deposition, and therefore, relatively late formation (that is, after base metal sulfides; fig. 13). Roscoelite has been identified in Colorado in the Cripple Creek deposit (Jensen and Barton, 2000) and Boulder County deposits (Kelly and Goddard, 1969; Saunders, 1991); in Fiji in the Vatukoula deposit (Ahmad and others, 1987; Pals and Spry, 2003); in Montana in deposits at the Spotted Horse, Maginnis, and Gies Mines and the Judith Mountains (Forrest, 1971; Zhang and Spry, 1994; Thieben and Spry, 1995), and in PNG in the Porgera deposit (Cameron and others, 1995) (table 3). It is not a constituent of epithermal deposits in New Mexico (McLemore, 1996, 2001, 2015). Other vanadium-rich minerals are rare among alkalic-type epithermal gold deposits, but the Tuvatu deposit in Fiji contains karelianite (V_2O_3), vanadian muscovite, Ti-free nolanite [$(V,Fe,Al)_{10}O_{14}(OH)_2$], vanadian rutile, schreyerite ($V_2Ti_3O_9$), and an unnamed vanadium silicate $VSiO_3(OH)$ (Spry and Scherbarth, 2006) (table 3).

Abundant gangue fluorite also distinguishes alkalic-type epithermal from other epithermal gold deposits (table 1; fig. 14*C*, *D*). Fluorite is most abundant in alkalic-type

epithermal gold deposits associated with felsic alkaline igneous rocks, particularly deposits at Cripple Creek and in Boulder County. It is much less abundant in deposits associated with mafic alkaline rocks owing to the low solubility of fluorite in calcium-rich environments. Where present, fluorite typically forms early during mineralization, prior to gold (± telluride) deposition (Kelly and Goddard, 1969; Nash and Cunningham, 1973; Thompson and others, 1985; Spry and Scherbarth, 2006) (fig. 13), and may be associated with base metal sulfide deposition (Kelly and Goddard, 1969). Exceptions include the Golden Sunlight and Dong'an deposits, in which fluorite precipitated late (Spry and others, 1997; Zhang and others, 2010). Two stages of fluorite deposition have been observed in the Boulder County deposits: an early purple fluorite and later green fluorite that followed Au-Te mineralization (Nash and Cunningham, 1973). Three stages of fluorite have been found in the Gallinas Mountains (McLemore, 2010).

Several hundred thousand metric tons of fluorspar (commercial name for fluorite) were produced from the Jamestown district in Boulder County, Colorado, between 1940 and 1973 (Kelly and Goddard, 1969; Nash and Cunningham, 1973). Most of this fluorite is associated with galena, sphalerite, chalcopyrite, pyrite, tennantite, and enargite (Kelly and Goddard, 1969). Gold and telluride mineralization occurs with and without fluorite in veins peripheral to the stock (Nash and Cunningham, 1973).

Supergene gangue minerals primarily include iron hydroxides (goethite, limonite, and hematite) formed by oxidation of pyrite and other sulfide minerals, clays, manganese oxide minerals, and silicates (Gott and others, 1969; Mutschler and others, 1985). Late hydrothermal activity produced a variety of sulfates including jarosite and anhydrite (Jensen and Barton, 2000).

Textures and Grain Size

Textures of gangue minerals in alkalic-type epithermal gold deposits, including quartz, carbonate, adularia, and sulfates (barite, celestite) are variable. In general, quartz is sparse in alkalic-type epithermal gold deposits associated with silica-undersaturated igneous rocks (for example, Cripple Creek), but is more abundant in deposits associated with quartz monzonite or granitic rocks (for example, Golden Sunlight). Banded quartz-bearing veins <5 mm wide are present but uncommon at the Porgera (Ronacher and others, 2004) and Vatukoula deposits (fig. 14*G*, *H*). Intersections of cross-cutting structures or within permeable breccias create open cavities that contain vein quartz crystals projecting from both sides, and (or) contain relatively banded quartz on outer margins of veins. For example, quartz crystals up to 1-cm long that lined vugs and cavities were found in the Cresson blowout breccia pipe (Carnein and Bartos, 2005).

In contrast to quartz in low- or high-sulfidation epithermal deposits related to calc-alkaline rocks, colloform or crustiform quartz textures are rare in alkalic-type epithermal gold deposits. Instead, quartz abundance is low and quartz-bearing veins form sheeted zones that consist of narrow (<50 mm) subparallel fissures, which collectively form lodes that range from 0.5 to 3 m wide (fig. 14*F*). These sheeted zones are well developed in deposits at Cripple Creek and the Vatukoula deposit (Thompson and others, 1985; Ahmad and others, 1987).

Most fluorite associated with alkalic-type epithermal gold deposits is purple, and it is typically massive, banded (fig. 14*D*), and intergrown with quartz. In the Jamestown district and Golden Sunlight deposits, coarse fluorite fragments cemented by fine-grained mixtures of fluorite and clays formed in breccia bodies (Kelley and Spry, 2016). At Golden Sunlight, some fluorite crystals are ~1 cm long (Spry and others, 1997).

Calcite commonly occurs with quartz in high-grade telluride veins (for example, Vatukoula, Fiji), sometimes forming closely spaced anastomosing veinlets. It also occurs with roscoelite in inner halos surrounding veins. Lattice textures consisting of platy calcite are common in association with other epithermal gold deposits (Simmons and others, 2005), but rare in alkalic-type epithermal gold deposits. Some veins contain adularia with quartz, carbonates, and sulfates, or as alteration haloes around veins.

Geochemical Characteristics

Trace Elements and Element Associations

In addition to Au, most alkalic-type epithermal gold deposits have elevated abundances of Ag, Ba, Te, K, F, and V, and less commonly Mo and Hg (table 3). Enrichments in As, Sb, Th, and base metals (Cu, Zn, Pb) are locally evident and a few deposits contain elevated PGE contents (Mutschler and others, 1985), REE, Se, and tungsten contents (Mutschler and others, 1985; Kelley and Spry, 2016). High Au/Ag ratios are typical of vein mineralization associated with alkalic-type epithermal gold deposits (Mutschler and Mooney, 1995; Jensen and Barton, 2000); exceptions include Zortman-Landusky in the Little Rocky Mountains, Montana; Ortiz Mountains, New Mexico; and the Republic deposit in Washington (in the Boundary area on the United States and Canadian border) (Mutschler and others, 1985). The suite of enriched elements for alkalic-type epithermal gold deposits is similar to that for the other epithermal deposit types, particularly other low-sulfidation deposits (Simmons and others, 2005; John and others, 2018), except for elevated concentrations of F and V.

Few geochemical studies of alkalic-type epithermal gold deposits have been made, so that geochemical characteristics are inferred primarily from ore and gangue mineralogy (table 3). For example, deposits that contain roscoelite are assumed to have elevated concentrations of vanadium. Because

geochemical data are sparse, the distribution of elements around alkalic-type epithermal gold deposits is poorly characterized, both within and among deposits. Available geochemical data for some alkalic-type epithermal gold deposits indicate large ranges of element concentrations, and controls on their distributions are poorly understood. Geochemical data across the Cripple Creek district (72 samples of vein and disseminated ore) show an average Te concentration of 38 parts per million (ppm), but some vein samples contain as much as 300 to 690 ppm Te (Dye, 2015). Vein samples from Boulder County (39 samples) contain average Te concentrations of 53 ppm, but two samples have >1,000 ppm Te (Kelley and Spry, 2016). Abundances of F and tungsten in mineralized samples are similarly variable and reflect the distribution of the minerals that host these elements. Large variations in element concentrations are attributable to host rock and (or) basement rock composition, degree of interaction between ore fluids and host rocks, and transport and ore deposition mechanisms.

Zoning Patterns

As stated earlier, vertical geochemical zoning is well documented in few alkalic-type epithermal deposits. Some deposits (Vatukoula, Gies, and Golden Sunlight) display a trend from Au>Ag in relatively shallow parts to Ag>Au in deeper deposit levels, an observation entirely inferred from mineralogical variations. Relatively Au-rich tellurides (krennerite, sylvanite, and calaverite) are present in shallow parts of the Vatukoula deposit, whereas silver-rich telluride minerals, such as petzite and hessite, and native gold, are prevalent in deeper parts of the deposit (Forsythe, 1971). Similar zoning has also been described for other deposits (for example, Gies and Golden Sunlight in Montana [Zhang and Spry, 1994; Spry and Thieben, 2000]). Detailed paragenetic studies of the Vatakoula deposit reveal that the calaverite-sylvanite-krennerite assemblage consistently formed earlier than Ag-rich telluride minerals (Pals and Spry, 2003), which suggests that the timing of deposition, rather than depth of formation, is responsible for the zoning patterns. Similar paragenetic relations also characterize other deposits (for example, Gies and Golden Sunlight in Montana [Zhang and Spry, 1994; Spry and Thieben, 2000]).

Fluid-Inclusion Microthermometry

Fluid-inclusion characteristics constrain the physical and chemical properties of hydrothermal fluids responsible for the formation of alkalic-type epithermal gold deposits. Studies of these deposits have focused primarily on gangue minerals, such as quartz, fluorite, and barite, in veins because of their relatively coarse grain size. In many of these studies, documentation is lacking about what was measured (for example, primary versus secondary inclusions), and the spatial and temporal relationships between gangue and ore minerals are not well described. Consequently, evaluating whether the reported results reflect ore-stage fluids, or fluids that pre- or post-date ore deposition is challenging.

Homogenization temperatures of inclusions in quartz, fluorite, and barite vary significantly, from ~80 to 350 °C, and most reported salinities range from 0.5 to 10 wt. percent NaCl. Evolution of ore fluid compositions are consistent among some alkalic-type epithermal gold deposits. As has been documented for Porgera (Ronacher and others, 2004), Cripple Creek (Thompson and others, 1985), many of the Boulder County deposits (Nash and Cunningham, 1973; Saunders, 1991), and the Judith Mountains deposits (Zhang and Spry, 1994), early vein fluids were hot (>200 °C) and saline (>5 equivalent weight [equiv. wt.] percent with some >20 equiv. wt. percent NaCl); later fluids had progressively lower homogenization temperatures and salinities.

High salinity (as much as 80 percent equivalent NaCl) fluid inclusions with homogenization temperatures of 500–600 °C (Phillips, 1990; Phillips and others, 1991; Banks and others, 1994; Campbell and others, 1995) suggest that elevated rare earth element abundances and trace gold contents in alkalic-type epithermal gold deposits of the Capitan Mountains region, New Mexico, probably formed from magmatic fluids. Crush-leached samples of quartz and fluorite contain anomalous concentrations of Na, K, Ca, Cl, S, Fe, Mn, Zn, and light REE (Banks and others, 1994; Campbell and others, 1995). Similar fluid inclusions are characteristic of the Capitan Mountains pluton granitic rocks (Ratajeski and Campbell, 1994).

Some deposits, such as Cripple Creek, have been observed to contain liquid carbon dioxide (CO_2) in fluid inclusions, which would require a deep level of formation (many kilometers of lithostatic load). However, the CO_2-rich nature of the fluids implied by other lines of evidence are consistent with a much shallower level of formation (epithermal) with likely effervescence of CO_2 during vein formation. Along with mineralogic and chemical evidence, these characteristics suggest that ore was deposited by relatively cool (<225 °C), CO_2-rich, low-salinity fluids that circulated in a relatively shallow environment (Jensen, 2003).

In many cases, including at Tuvatu, Fiji (Scherbarth and Spry, 2006), Fakos, Greece (Fornadel and others, 2012), Mount Milligan (LeFort and others, 2011), Galore Creek (Enns and others, 1995; Lang and others, 1995), Golden Sunlight (Spry and others, 1996, 1997), Jamestown district, Boulder County (Nash and Cunningham, 1973; Saunders, 1991), and La Plata (Werle and others, 1984), fluid inclusion compositions and temperatures have been used to associate the near-surface epithermal deposit to known or suspected contemporaneous subjacent porphyry systems.

Stable Isotope Geochemistry

Oxygen and Hydrogen

Stable isotope compositions ($\delta^{18}O$ and δD, in one part per thousand or per mil, ‰) are commonly used to constrain the origin of ore-forming fluids. Stable isotope data for gangue minerals from many alkalic-type epithermal gold deposits are available. Reported fluid compositions in equilibrium with gangue minerals indicate significant enrichment in ^{18}O and depletion in deuterium that are inconsistent with compositions indicated by the present-day meteoric water line (PDMWL, fig. 15). Ore fluids associated with most alkalic-type epithermal gold deposits at least partly overlap the field for volcanic vapor produced by magmatic boiling and (or) the arc magmatic water field (Taylor, 1997) (fig. 15). The range in values for the Porgera (Richards and Kerrich, 1993), Vatukoula (Ahmad and others, 1987), Dashuigou (Mao and others, 2002; Zhang and others, 2018), Tuvatu (Scherbarth and Spry, 2006), Golden Sunlight (Spry and others, 1996), Cripple Creek (Kelley and others, 1998), northern Black Hills (Annie Creek and Gilt Edge) (Paterson and others, 1989), Central City (Rice and others, 1985), and the Pingyi area in eastern China (Hu and others, 2006) are similar, and are adjacent to or overlap the arc magmatic water field (fig. 15). Consequently, these alkalic-type epithermal gold deposits may have formed largely from magmatic fluids.

However, significant excursions in $\delta^{18}O$ and δD suggest minor to major contributions from external fluids. The Mount Milligan and Dusty Mac deposits are depleted in either δD or $\delta^{18}O$, or both, compared to magmatic fluids and fluids associated with most other alkalic-type epithermal gold deposits (fig. 15). Mount Milligan is an alkali porphyry deposit overprinted by late-stage Au-Te hydrothermal veins. Porphyry- and epithermal-style veins at Mount Milligan have similar stable isotope systematics, and the δD depletion in fluids are typical of other porphyry systems in British Columbia (LeFort and others, 2011). This shift in δD is attributed to mixing or contamination of magmas or magmatic fluids with evolved groundwater (meteoric water modified by extensive water rock reaction or deeply convected meteoric water), or assimilation of deuterium-depleted country rocks. Zhang and others (1989) similarly concluded that the large shift in δD and $\delta^{18}O$ for ore-forming fluids responsible for vein formation in the Dusty Mac deposit (fig. 15) indicates a large component of meteoric water, with calculated water-rock ratios between 1.1 and 1.7.

In general, the oxygen and hydrogen isotopic characteristics of alkalic-type epithermal gold deposits indicate a dominant magmatic component. This contrasts with other types of epithermal systems that are characterized by meteoric fluids with much lighter $\delta^{18}O$ values (fig. 6.6 in Taylor, 1997).

Sulfur and Carbon

Many of the rocks associated with alkalic-type epithermal gold deposits have light sulfur isotopes, which has been attributed to the oxidation state of sulfur in alkaline systems or the progressive oxidation of hydrothermal fluids through boiling, or to leaching of sedimentary sulfur (Jensen and Barton, 2000). Sulfur isotope compositions of sulfides from the Fakos porphyry-epithermal gold deposit have $\delta^{34}S$ values that range from −6.82 to −0.82 in one part per thousand (per mil, ‰). The isotopically light sulfur isotope values were attributed to changes in oxidation state during sulfide deposition (that is, boiling) and (or) disproportionation of sulfur-rich magmatic volatiles upon cooling. Derivation of sulfur by reduction of seawater sulfate and leaching of sulfides from sedimentary rocks were discounted because of the absence of primary sulfides in sedimentary rocks proximal to the deposit (Fornadel and others, 2012).

Comparison of sulfur isotope compositions of sulfide minerals between epithermal- and porphyry-style mineralization/alteration zones within the Golden Sunlight (Spry and others, 1996) and Porgera deposits (Richards and Kerrich, 1993) show overlap, suggesting that porphyry and epithermal deposit types at each locality are linked temporally and spatially. Sulfides from the breccia pipe and other mineralized rocks at Golden Sunlight have $\delta^{34}S$ values from −12.2 to 9.5‰; the large range and relatively higher isotopic values suggest a mixed magmatic-sedimentary source (Spry and others, 1996). The $\delta^{34}S$ values from the Porgera deposit range from 1.4 to 5.2‰. These values are interpreted to reflect a magmatic source, with the large range most likely resulting from fluctuations in $f0_2$ during sulfide deposition, which can cause significant changes in fluid $\delta^{34}S_{H2S}$ values under pyrite-stable conditions (Richards and Kerrich, 1993). Isotopically light sulfur isotope values (−4.2 to −15.3‰) for pyrite and galena separates from the Vatukoula deposit suggest a dominantly sedimentary source for sulfur (Ahmad and others, 1987).

Stable isotope ratios of carbon among gangue minerals in veins from alkalic-type epithermal gold deposits range from ~−10 to 1‰. These values overlap magmatic values, but are sufficiently variable to allow for derivation, in part, from sedimentary sources (Ahmad and others, 1987; Richards, 1995; Spry and others, 1996; Jensen and Barton, 2000).

Tellurium

In naturally occurring minerals, tellurium has eight stable isotopes, ^{120}Te (0.09 percent abundance), ^{122}Te (2.55 percent), ^{123}Te (0.89 percent), ^{124}Te (4.74 percent), ^{125}Te (7.07 percent), ^{126}Te (18.84 percent), ^{128}Te (31.74 percent), and ^{130}Te (34.08 percent); and four oxidation states, −II, 0, +IV, and +VI. Accordingly, tellurium should exhibit isotopic fractionation among diverse geologic materials. The first investigations of stable tellurium isotope compositions in

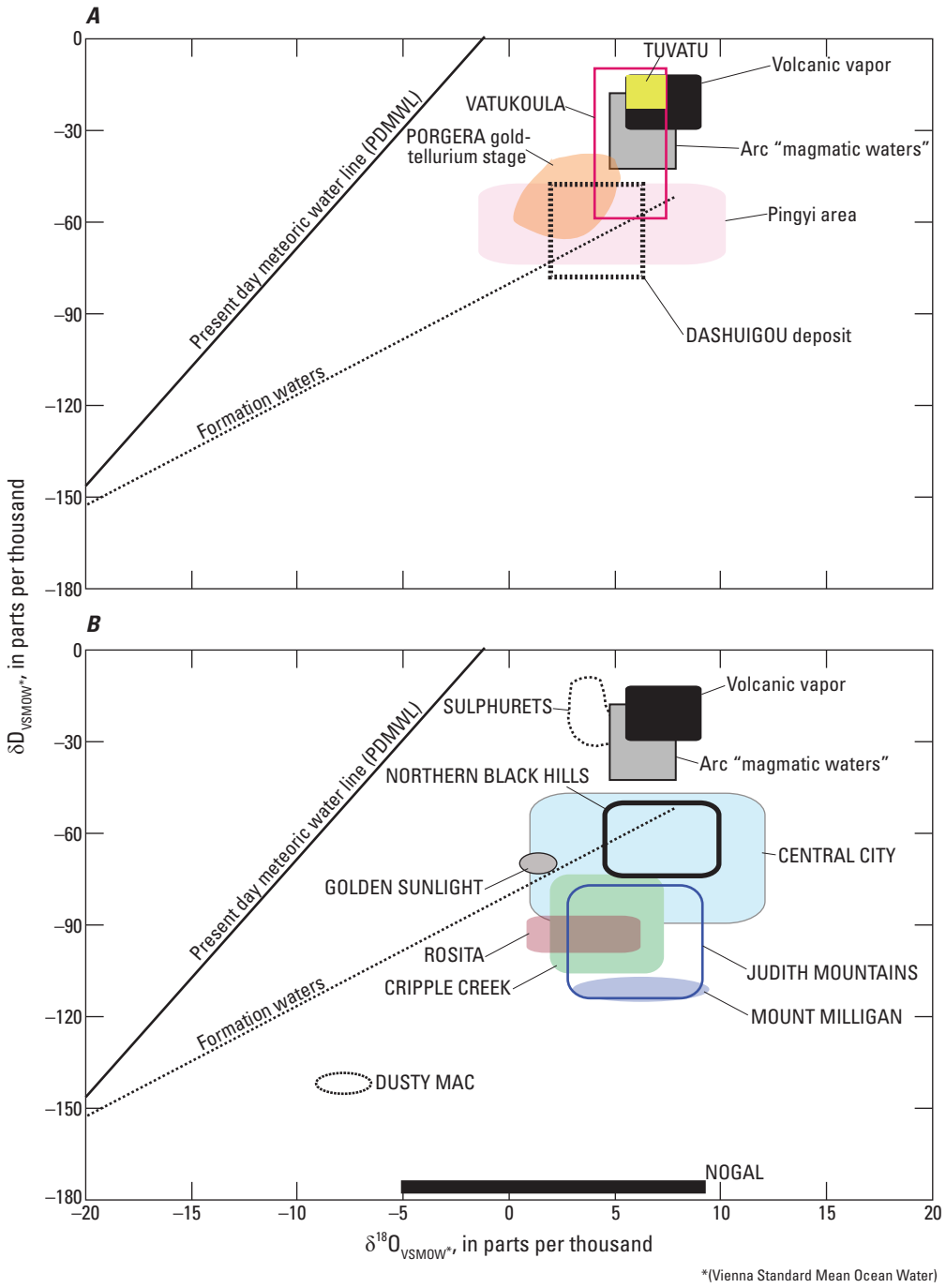

Figure 15. Oxygen and hydrogen isotopic compositions (in parts per thousand or per mil, ‰) for fluids from select alkalic-type epithermal gold deposits. *A*, Non-North American deposits. *B*, North American deposits. The present day meteoric water line (PDMWL) and field of compositions for formation waters (from Craig, 1961, 1963) are shown, along with the field for volcanic vapor (solid black) produced by magmatic boiling (from Hedenquist and others, 1998) and arc magma field (shaded gray; from Taylor, 1997). Data are from the following references: Central City (Rice and others, 1985); Cripple Creek (Kelley and others, 1998); Dashuigou deposit (Mao and others, 2002); Dusty Mac (Zhang and others, 1989); Golden Sunlight (Spry and others, 1996); Judith Mountains (Gies deposit) (Zhang and Spry, 1994); Mount Milligan—data for subepithermal veins only (LeFort and others, 2011); Northern Black Hills (Gilt Edge, Annie Creek) (Paterson and others, 1989); Porgera Au-Te stage (Richards and Kerrich, 1993); Pingyi area (Hu and others, 2006); Rosita (McEwan and others, 1996); Sulphurets (Margolis, 1993); Tuvatu (Scherbarth and Spry, 2006); Vatukoula (Ahmad and others, 1987). Fluids associated with other types of epithermal deposits are characterized by much lighter $\delta^{18}O$ values (see Taylor, 1997, fig. 6.6). Calculated $\delta^{18}O$ fluid compositions (in equilibrium with quartz) for Nogal gold deposits (which lack corresponding hydrogen isotope compositions) are shown along x-axis of diagram (from Douglass and Campbell, 1994).

tellurium-bearing minerals were conducted by Smithers and Krouse (1968) on six samples of sylvanite, native tellurium, and tetradymite (Bi_2Te_3) from four mineral deposits. Values of $\delta^{130/122}$ define as much as a 4‰ variation relative to an internal standard (refined tellurium). Smith and others (1978) analyzed the tellurium isotope composition of krennerite, coloradoite (HgTe), tetradymite, and native tellurium in six samples of tellurides from various hydrothermal ore deposits. Although large fractionations (up to 14.0‰ for $^{130}Te/^{120}Te$, 10.4‰ for $^{130}Te/^{122}Te$, 10.0‰ for $^{130}Te/^{123}Te$, 10.3‰ for $^{130}Te/^{124}Te$, 9.4 for $^{130}Te/^{125}Te$, 6.8‰ for $^{130}Te/^{126}Te$, 3.0‰ for $^{130}Te/^{128}Te$) were determined relative to spectroscopically pure tellurium metal, associated analytical uncertainty was as much as several per mil; consequently, no significant isotopic compositional variations were apparent from the study. These data were obtained using a thermal ionization mass spectrometer equipped with an electron multiplier. However, Lee and Halliday (1995) have questioned the accuracy of the data because the electron multiplier used by Smith and others (1978) produced mass discrimination problems that yielded poor results.

Using a multicollector-inductively coupled plasma-mass spectrometer, Fornadel and others (2014, 2017) analyzed natural hypogene tellurides and native tellurium in the system Au-Ag-Te and obtained an isotopic range for $^{130}Te/^{125}Te$ of 1.54 to 0.44‰ (relative to spectroscopically pure tellurium metal) with a precision as low as ±0.08‰. Tellurites (TeO^{2-}_3), which form mostly from the oxidation and weathering of tellurides and native tellurium, have $\delta^{130Te/125Te}$ values that range from 1.54 to 0.44‰ and demonstrate that the isotopic range of oxidized and reduced Te species are similar. The isotopic compositions of naturally occurring samples are consistent with those determined from thermodynamic calculations (Fornadel and others, 2017) and suggest that mass-dependent processes are responsible for fractionation (Fornadel and others, 2014, 2017). Tellurium is most efficiently transported as a reduced vapor phase or an oxidized aqueous phase under hydrothermal conditions (Grundler and others, 2013). As such, reduction of oxidized Te in hydrothermal fluids or reduction of Te directly from the vapor phase is required to form tellurides and native tellurium in various hydrothermal ore deposits. Preliminary studies suggest that Te isotope compositional variations among telluride minerals in alkalic-type epithermal gold deposits are less pronounced than that in orogenic gold deposits and volcanogenic massive sulfide deposits (Fornadel and others, 2017). The underlying causes for these isotopic compositional variations in hydrothermal ore deposits remain speculative but will be better understood when the Te isotope composition of common rocks and additional precious and nonprecious metal tellurides have been determined. Fortunately, recent studies (Fehr and others, 2018) provide some of this information. Nine terrestrial samples collected from manganese nodules, shale, marine mud, stream sediment, jasperoid, soil, and mill heads from a porphyry Cu deposit have $\delta^{130/125}Te$ values that range from −0.15 ± 0.07 to 0.74 ± 0.05‰. Two samples of jasperoid from the Drum Mountains, Utah, have the lightest values ($\delta^{130/125}Te$ = −0.18 and −0.13 ± 0.07‰), and a manganese nodule from the Atlantic Ocean has the heaviest value ($\delta^{130/125}Te$ = 0.74 ± 0.05‰). A recent Te isotope study of the Vatukoula deposit by Fornadel and others (2019) showed isotopic variation ($\delta^{130/125}Te$ = 0.66 ± 0.13 to −0.47 ± 0.13‰) with distance from the causative intrusion, which they interpreted as largely being the result of Rayleigh fractionation of the ore fluids.

Hydrothermal Alteration

Mineralogy and Mineral Assemblages

Almost all alkalic-type epithermal gold deposits include potassically altered rocks, either as broad zones of K-feldspathized wall rocks (Cripple Creek) to narrow zones of sericitic alteration (Porgera). The type of alteration varies as a function of host rock composition. Potassic alteration is interpreted as having preceded the main phase of gold mineralization at Cripple Creek and Vatukoula (Kwak, 1990; Dye, 2015).

During alteration associated with most alkalic-type epithermal gold deposits, significant amounts of potassium were added, whereas sodium and calcium were removed by leaching (Jensen and Barton, 2000). Among alkalic-type epithermal gold deposits, alteration style varies with magma type and host rock compositions. Potassic alteration, commonly forming broad alteration zones, is dominant in deposits associated with felsic rocks (for example, Cripple Creek, Zortman-Landusky), whereas narrow zones of sericite + carbonate + K feldspar assemblages predominate in deposits associated with mafic-intermediate rocks (for example, Porgera, Mount Kare, Vatukoula). During potassic alteration, K-silicate phases replace nepheline, plagioclase, or Na-rich alkali feldspar. Mafic minerals are typically replaced by sulfides (pyrite with or without arsenopyrite, pyrrhotite, marcasite, and base metals), Fe-Mg carbonates, leucoxene, and clays (illite-montmorillonite), which impart a bleached appearance (Jensen and Barton, 2000).

Several pervasive alteration assemblages, including phyllic (argillization and sericitization) and carbonate alteration, form prior to ore deposition in alkalic-type epithermal gold deposits (Mutschler and others, 1985). Regional peripheral propylitic alteration assemblages are variably developed near some deposits; these assemblages likely formed prior to epithermal mineralization, sometimes in association with deeper porphyry-style mineralization (Choquelimpie [Gröpper and others, 1991], Ladolam [Moyle and others, 1990], Vatukoula [Pals and Spry, 2003]).

In contrast to high-sulfidation epithermal gold deposits, most alkalic-type epithermal gold deposits are deficient in hydrothermal quartz and acidic styles of alteration assemblages are poorly developed (Jensen and Barton, 2000).

However, the Dong'an deposit (Zhang and others, 2010), Choquelimpie deposit (Gröpper and others, 1991), Lifanggou deposit in the Pingyi area (Hu and others, 2006), and the Sandaowanzi deposit in northeast China (Liu and others, 2011) have silica-rich alteration zones, particularly adjacent to veins. In addition, several deposits, including the Ladolam (Moyle and others, 1990; Richards, 1995), Fakos (Fornadel and others, 2012), Vatukoula (Eaton and Setterfield, 1993), and Rosita (Mutschler and others, 1998), include zones of advanced argillic alteration. These deposits are characterized by kaolinite (with or without pyrophyllite or dickite), alunite, and quartz alteration superimposed upon earlier potassic alteration (Jensen and Barton, 2000). The acidic alteration zones are typically located in the upper levels of deposits, generally near or conformable with the surface. Restricted zones of acid alteration (quartz-dickite), that form narrow, late-stage veins that cut across all other assemblages, are also associated with some deposits, including Cripple Creek (Jensen and Barton, 2000), Choquelimpie (Gröpper and others, 1991), and Golden Sunlight (Spry and others, 1996), and the Bessie G Mine in the La Plata Mountains (Saunders and May, 1986).

Lateral and Vertical Dimensions

The lateral and vertical extent of alteration associated with alkalic-type epithermal gold deposits varies greatly. Wall-rock compositions (mafic or felsic, quartz-poor or quartz-rich, pelitic or carbonate) probably exert the most influence on the size of alteration halos. The Mayflower deposit in Montana consists of ore-bearing silicified dolomitic limestones up to 7 m wide that are surrounded by adularia, quartz, pyrite, and sericite (with or without roscoelite) alteration halos that are up to 10 m wide (Cocker, 1993). At the Cripple Creek deposit, nearly the entire diatreme (>30 km^2) has been altered to some extent, despite the much more spatially restricted distribution of high-grade mineralized zones (fig. 5). Weakly altered rocks are also located beyond the diatreme, in areas surrounding satellite intrusions (Rahfeld, 2013).

At Ladolam, sedimentary rocks within about 2 km of major ore bodies are altered (Jensen and Barton, 2000). Alteration zones at Porgera are generally much more restricted (~300 m) (Richards and Kerrich, 1993). In some cases, such as at Vatukoula, zones of intense potassic alteration spatially coincide with areas of gold mineralization (Kwak, 1990), but the relative timing of alteration and gold mineralization are poorly constrained.

Rock Matrix Alteration and Alteration Intensity

Potassic alteration associated with alkalic-type epithermal gold deposits may be very intense, resulting in replacement of the entire rock by low-temperature K feldspar (adularia). These rocks may also contain small amounts of widely distributed but volumetrically minor (a few percent of rock volume) quartz and sericite (Jensen and Barton, 2000). In these adularia alteration halos, gold is commonly present as discrete grains of native gold or is a constituent of electrum (usually with a high Au:Ag ratio), tellurides, or as auriferous pyrite (Pals and others, 2003; Dye, 2015). Disseminated gold in these potassic halos are commonly sufficient to constitute economic resources, as is true at several deposits, including Landusky-Zortman (Hastings, 1988), Cripple Creek (Dye, 2015), and stage I mineralization at Porgera (Richards and others, 2006). Other alkalic-type epithermal gold deposits affected by extreme potassic alteration include Galore Creek, British Columbia (Allen and others, 1976), the Allard Stock, Colorado (Werle and others, 1984), and Vatukoula, Fiji (Kwak, 1990).

Although some rock volumes affected by potassic alteration are large, this alteration is not always demonstrably spatially or temporally associated with gold mineralization. In these cases, potassic alteration may reflect conditions appropriate for gold transport but not for gold deposition, which may require somewhat different physiochemical conditions that prevail elsewhere along the fluid flow paths (Jensen and Barton, 2000).

Textures

Most commonly, partially altered rocks are characterized by heterogeneous replacement of igneous textures. Potassium silicate phases replace nepheline, plagioclase, or Na-rich alkali feldspar, resulting in a net addition of potassium (Jensen and Barton, 2000). For example, at Cripple Creek, weakly to moderately altered rocks contain phenocrysts of sanidine, pyroxene, and amphibole that were partially or wholly replaced by potassium feldspar (Rahfeld, 2013). At this site, increasingly intense potassic alteration caused complete destruction of primary igneous textures.

Petrology of Associated Igneous Rocks

Rock Names

Alkaline igneous rock nomenclature includes a plethora of terms (Sorensen, 1974) that is partly a result of the unusual chemistry and mineralogy of the rocks, and partly from disagreements among petrologists concerning their classification. The compositions of alkaline rocks associated with epithermal gold deposits range from ultrapotassic lamprophyres (<40 wt. percent SiO_2) to fractionated, high-K phonolites. Whether the compositions of igneous rocks are alkaline or subalkaline depends on the relative abundances of $Na_2O + K_2O$ versus SiO_2 (fig. 4), and many alkaline igneous rocks are peralkaline (molar $Na_2O + K_2O$ > molar Al_2O_3). Igneous rocks commonly associated with epithermal gold deposits include syenite, monzonite, alkali basalt or alkali gabbro, diorite, latite, phonolite (and more

mafic tephriphonolite and phonotephrite), vogesite, banakite, hawaiite to mugearite, monchiquite, trachyte, bostonite, absarokite, and shoshonite (Mutschler and others, 1985).

Compositions of the igneous rocks associated with alkalic-type epithermal gold deposits may also range widely within a single district. For example, at Cripple Creek, compositions of intrusive and extrusive rocks range from phonolite to trachyandesite to silica-deficient phonotephrite and lamprophyre. Many alkaline igneous complexes associated with alkalic-type epithermal gold deposits contain coeval alkaline and subalkaline rock types, which is in accord with the large range in compositions with single deposits or districts (fig. 4). However, in any given district, not all of the compositionally distinct igneous intrusions are genetically associated with gold mineralization; determination of the intrusion actually responsible for gold mineralization is rarely demonstrable.

Forms of Igneous Rocks and Rock Associations

The forms of igneous rocks associated with alkalic-type epithermal gold deposits are as diverse as their compositions (table 1). Rocks associated with these deposits form calderas, breccia pipes, or diatremes (for example, Zortman-Landusky, Golden Sunlight, Cripple Creek, Ortiz Mountains), dikes, composite flows, sills, laccoliths, and dome shaped volcanic features (for example, La Plata; Moccasin Mountains, Montana; Dashuigou). In addition, many forms of igneous rocks are commonly present in a single district or deposit as a result of multiple episodes of intrusion. For example, at Cripple Creek, early phonolitic intrusions are characterized by stocks and voluminous tabular-shaped subhorizontal bodies that commonly exhibit brecciated margins, and irregular geometries suggestive of intrusion into loosely consolidated and (or) wet diatreme breccias (Jensen, 2003). Subsequent intrusions were manifested as stock-like geometries with a greater prevalence of tabular-shaped and dike-like features, culminating with emplacement of relatively more mafic tep hriphonolite-phonotephrite-lamprophyre dikes (Kelley and others, 1998). In such cases, the form of igneous rocks may be linked to composition (relatively higher silica contents have higher viscosity). Alternatively, the timing of emplacement may control form, because permeability and porosity of country rocks decreases with time, or early intrusions may form barriers that serve to funnel later magmatic and hydrothermal fluids into local structures.

Mineralogy and Textures

The mineralogy and textures of igneous rock types associated with alkalic-type epithermal gold deposits varies significantly (table 1). Textures range from aphanitic to porphyritic; most associated volcanic rocks are porphyritic. In some flows, phenocrysts are common and may be trachytically aligned. The mineralogy is dependent on rock composition. Felsic rocks such as phonolite and slightly more mafic alkaline rocks contain abundant alkali feldspar (sanidine), clinopyroxene (typically aegirine-augite), magnetite, amphibole, plagioclase, and feldspathoid minerals, most commonly nosean, analcime, and sodalite (Jensen and Barton, 2000). Some relatively felsic igneous rocks contain fluorite (for example, Cripple Creek, Jamestown district in Boulder County). Mafic and ultramafic rocks typically consist of olivine, clinopyroxene, amphibole, and phlogopite (Jensen, 2003; Richards and others, 1991).

The Vatukoula deposit is hosted by flat-lying basalt flows that contain phenocrysts of augite, plagioclase, and olivine up to 5 mm in diameter. These flows are intruded by trachyandesite dikes consisting of pyroxene and plagioclase phenocrysts (Ahmad and others, 1987). Monzodiorite and syenite stocks that host many alkalic-type epithermal gold deposits (La Plata, Fakos, Montana, and New Mexico deposits) are typically porphyritic and contain abundant hornblende and augite.

The presence of hydrous phases (for example, hornblende, biotite) as phenocrysts in igneous rocks is evidence for high dissolved solids content in water, and Fe^{3+}-bearing phases such as magnetite and aegirine indicate high oxidation states (Jensen and Barton, 2000). Oxidized magmas favor precipitation of large quantities of gold because sulfide saturation is suppressed, and therefore sulfur is mostly present in the melt as sulfate, not sulfide, and the loss of precious metals through partitioning into sulfide phases is minimized (Richards, 1995). Another effective variable for increasing mineralization potential of a magma may be halogen content (Müller and others, 2001), which is reflected in minerals such as fluorite and sodalite. The increased chloride solubility results in an increase in ore metals (including gold) that are complexed with chloride.

Grain Size

The grain size characteristics of individual volcanic or intrusive rocks associated with alkalic-type epithermal gold deposits primarily reflect physicochemical conditions prevailing during magma solidification and consequently are highly variable. For example, in the Cripple Creek district alone, host rocks range from aphanitic dikes and sills to porphyritic dikes, and phonolite intrusions may be aphanitic to porphyritic rocks containing sanidine or plagioclase phenocrysts up to 2 mm long (Kelley and others, 1998). The dominant host rocks at the Vatukoula Mine are olivine basalt flows that contain phenocrysts of augite, plagioclase, and olivine up to 5 mm in diameter (Ahmad and others, 1987). The ore at Porgera is hosted in the Porgera Intrusive Complex, which consists of numerous small stocks, most of which are porphyritic and contain phenocrysts about 1 mm long (Richards, 1990).

Petrochemistry

The petrogenesis of alkaline magmas has long been debated but the general consensus is that they are derived by partial melting of metasomatically modified mantle rocks (for example, Gast, 1968). Pilet and others (2008) proposed that mantle metasomatism and small degrees of partial melting may generate amphibole-, volatile- and alkali-rich magmas, including syenite, monzonite, alkali basalt, diorite, latite, phonolite, vogesite, banakite, hawaiite, monchiquite, andesite, trachyte, bostonite, absarokite, and shoshonite. An association to mantle-derived alkaline magmas is suggested by He and Ar isotope compositions of ore-forming fluids responsible for alkalic-type epithermal gold deposits along the Red River-Jinshajiang fault belt, China (Hu and others, 2006).

Major oxide and trace element characteristics of igneous rocks associated with alkalic-type epithermal gold deposits are largely consistent with a genesis involving partial melting of metasomatically modified rocks. The SiO_2 contents of unaltered rocks range from <40 wt. percent to about 77 wt. percent, and $K_2O + Na_2O$ contents range from <2 to ~16 wt. percent. Although many rocks fall within the compositional alkaline field, some straddle the alkaline-subalkaline boundary (fig. 4). The Na_2O and K_2O compositions of alkaline igneous rocks within a single district can be highly variable (see Jensen and Barton, 2000, fig. 3C, p. 286), and overlap the ultrapotassic, shoshonitic, and calc-alkaline fields of Peccerillo and Taylor (1976).

Trace element contents further constrain possible sources of magmas. Alkaline igneous rocks associated with alkalic-type epithermal gold deposits, including unaltered rocks spatially associated with the Porgera, Mount Kare, Ladolam, Vatukoula, and Tuvatu deposits (Richards and Ledlie, 1993; Müller and others, 2001; Scherbarth and Spry, 2006; Forsythe and others, 2019) are typically light rare earth element enriched, heavy rare earth element depleted, and characterized by large ion lithophile element enrichments. Abundances of some high field strength elements, including Nb, Th, Ta, and U, are depleted at Vatukoula and Tuvatu (Scherbarth and Spry, 2006), whereas Nb, Th, and U abundances are enriched at Porgera and Mount Kare (Richards and Ledlie, 1993). These differences may reflect an intraplate setting for deposits in the PNG highlands versus an oceanic setting for the ocean floor basalts associated with the Fijian deposits. High field strength element abundances are also depleted in alkaline igneous rocks associated with the Ladolam deposit (Müller and others, 2001) and may reflect the oceanic, island arc setting of Lihir Island. The compositions of igneous rocks associated with some alkalic-type epithermal gold deposits may transition to those that are calc-alkaline.

Radiogenic Isotope Geochemistry

Radiogenic isotopes are commonly used to constrain the origin and tectonic environment in which alkaline magmas associated with alkalic-type epithermal gold deposits were generated. Magma source composition and tectonic setting are factors that likely influence the location and nature of mineralization. The presence of mantle xenoliths and the common occurrence of gold deposits in regions underlain by thin crust suggest that some gold deposits are associated with mantle-derived magmas (Jensen and Barton, 2000), an observation that is supported by radiogenic isotope data. At Ladolam, peridotite xenoliths and osmium isotopic evidence suggests the magmas were derived from a mantle source effected by extreme noble metal enrichment (McInnes and others, 1998). Similarly, mantle sources for alkaline magmas associated with the Porgera deposit are suggested by depleted neodymium (Nd; $^{143}Nd/^{144}Nd$~0.512950; ε_{Nd}~+6) and Sr ($^{87}Sr/^{86}Sr$~0.7035) isotopic signatures (Richards and others, 1991). The ratio of the Nd isotopes $^{143}Nd/^{144}Nd$ in a sample is expressed as a deviation from the same ratio in the "chondritic uniform reservoir," which is assumed to be representative of the bulk Earth. Because samarium (Sm; the parent of radiogenic ^{143}Nd) is more incompatible than neodymium, the ratio Sm/Nd (and hence $^{143}Nd/^{144}Nd$) is enriched in the solid residue and depleted in the melt during partial melting. Negative εNd values are consequently indicative of crustal sources whereas positive values indicate a mantle source component. Major, trace, and radiogenic isotope data (Sr, Pb, and Nd) for alkaline lavas associated with mineralization at the Vatukoula deposit, Fiji, suggest high degrees of mantle melting associated with subduction (Rogers and Setterfield, 1994; Pals and Spry, 2003). Monzosyenite associated with gold deposits in the Pingyi area of China have Sm-Nd characteristics consistent with derivation from the lithospheric mantle in an extensional regime (Hu and others, 2006).

In contrast, isotopic data for intrusive phases related to some alkalic-type epithermal gold deposits show evidence of crustal involvement. Strontium and lead isotope compositions of Cretaceous and Tertiary alkaline rocks associated with gold deposits in the southern Cordillera of the United States, including Cripple Creek, and deposits in Boulder County and in New Mexico, reflect mantle sources affected by crustal contamination. These deposits generally have low initial Sr isotopic ratios of <0.706 (Simmons and Hedge, 1978; Stein and Crock, 1990; Kelley and others, 1998) that are consistent with mantle sources, but ε_{Nd} values ranging from −9.8 to −1.9 (Stein and Crock, 1990) require significant contributions from the lower crust. The Sr and Pb isotope ratios of alkaline igneous rocks associated with Au deposits at Cripple Creek and elsewhere in the southern Cordillera suggest that the associated magmas were derived from subduction-modified subcontinental lithosphere during a transition to an extensional regime (Kelley and Ludington, 2002). However, isotopic compositional variations, primarily higher $^{208}Pb/^{204}Pb$ (>38.2) ratios in alkaline rocks associated

with Cripple Creek and Boulder County deposits relative to those farther south in the Cordillera reflect differences in the composition of underlying Proterozoic crust and (or) a relatively greater degree of assimilation of lower crust by Cripple Creek and Boulder County magmas. This crustal component may have contributed to higher dissolved H_2O (and CO_2, F, Cl, and other volatiles) and may be responsible for differences in deposit sizes and compositions. Cripple Creek and Boulder County deposits are many times larger than those further south (table 1; fig. 1), and they contain fluorite, roscoelite, and tellurides that are absent in the more southerly deposits (Kelley and Ludington, 2002).

Numerous studies have similarly used radiogenic isotopes to constrain crustal rock contributions. High $^{87}Sr/^{86}Sr$ ratios (>0.707253) and negative ε_{Nd} values for alkaline intrusions associated with the Dong'an deposit in northeast China indicate magma derivation from differentiates of parental andesitic magmas generated during partial melting of mafic lower crust, immediately preceding extension (Zhang and others, 2010).

Although radiogenic isotopic data are useful in constraining relative contributions by crustal and mantle sources, these are neither unique nor definitive (Jensen and Barton, 2000). For example, some mantle materials have isotopic characteristics (mantle nodules with ε_{Nd} <–20 and $^{87}Sr/^{86}Sr$ >0.830) that are identical to those characteristic of crustal magma reservoirs.

Depth of Emplacement

Like all types of epithermal deposits, alkalic-type epithermal gold deposits form in the shallow parts of near-surface hydrothermal systems (Simmons and others, 2005; John and others, 2018) at paleodepths of <~1,500 m. Fluid inclusion analyses are typically used to constrain the depth at which these deposits form, but those analyses must be interpreted with caution. For example, Dye (2015) has shown that precipitation of fluorite and early generations of quartz commonly preceded gold mineralization, and therefore, fluid compositions and temperatures measured for inclusions in those minerals do not directly correspond to those pertinent to ore formation. Fluid inclusion data for quartz and fluorite in veins cutting Precambrian rocks from the Cripple Creek district indicate homogenization temperatures of 206–510 °C and high salinities of 33 to >40 equiv. wt. percent NaCl (Thompson and others, 1985). However, these high temperature fluid inclusions pertain only to veins that cut older Precambrian rocks (not Tertiary rocks), and thus may be unrelated to the Tertiary gold system (Jensen, 2003). The inclusions in minerals that are paragenetically related to the telluride ore deposition were deposited by fluids below 175 °C with salinities of <8.3 equiv. wt. percent NaCl (Saunders, 1986; Jensen, 2003). This relationship of early high-temperature, highly saline fluids and later lower-temperature, lower salinity fluids has also been documented for the Boulder County deposits (Nash and Cunningham, 1973; Saunders, 1991), Bessie G vein in the La Plata Mountains (Saunders and May, 1986), Vatukoula deposit (Ahmad and others, 1987), Porgera (Ronacher and others, 2004), and Judith Mountains deposits (Zhang and Spry, 1994).

Fluids associated with some alkalic-type epithermal gold deposits are characterized by high CO_2 abundances, which have important implications for the conditions prevailing during gold formation. The solubility of CO_2 in magma-hydrothermal systems increases with pressure (Lowenstern, 2001), and therefore has commonly been interpreted as an indication of deep levels of formation (many kilometers). Jensen (2003), however, showed that the CO_2 rich nature of fluids responsible for gold deposition at Cripple Creek could be produced by CO_2 effervescence during vein formation, and in combination with other lines of evidence at Cripple Creek, is consistent with a shallower level of formation. Alternatively, the high CO_2 (and also methane) contents in fluid inclusions could have been sourced by thermal degradation of lignitized wood that commonly occurs in Cripple Creek diatreme volcaniclastic rocks (Saunders, 1986). Data from other alkalic-type epithermal gold deposit systems indicates deposition of gold at relatively cool (<225 °C) temperatures involving CO_2-rich, low-salinity fluids that circulated ≤~1,500 m below the paleosurface (Thompson and others, 1985; Saunders, 1986; Ahmad and others, 1987; Jensen, 2003).

Theory of Deposit Formation

A genetic model for alkalic-type epithermal gold deposits must account for numerous shared and distinct characteristics among these deposits (table 1); importantly, the shared characteristics suggest relatively consistent ore formation controls. Features common to these deposits include their spatial association with alkaline igneous rocks; the presence of Au-telluride, F, or V-rich minerals; the role of early magmatic-hydrothermal fluids and involvement of externally derived groundwater during later stages of deposit formation, as indicated by fluid inclusion and stable isotope studies; clear relationships with alkalic porpyhyry-type activity; and large-scale structural control on intrusion emplacement and deposit formation (Richards, 1995; Mutschler and others, 1998; Jensen and Barton, 2000) (table 1). Differences among deposits include the styles and superficial characteristics of these deposits as well as minor differences in alteration and ore mineral assemblages. These differences may reflect host rock and (or) magmatic source rock compositional variation, or depth of erosion of the deposit.

Ore Deposit System Affiliation(s)

The genetic link between alkalic-type epithermal gold deposits and porphyry-style Mo or Cu deposits has long been known (for example, Richards, 1995; Jensen and Barton, 2000). The ore-forming process for porphyry and epithermal deposit types is part of a continuum between early, magmatic

high temperature conditions and later lower temperature hydrothermal conditions. The spatial and genetic relationship between low-grade porphyry Mo and gold telluride deposits has been documented at Golden Sunlight (Spry and others, 1996) and Central City (Rice and others, 1985). Some alkalic-type epithermal deposits are spatially and genetically associated with porphyry Cu deposits; examples include Vatukoula (for example, Eaton and Setterfield, 1993; Begg, 1996), LaPlata (Werle and others, 1984), Tuvatu (Scherbarth and Spry, 2006; Forsythe and others, 2019), Fakos (Fornadel and others, 2012), Ladolam (Carman, 2003), and Porgera (Ronacher and others, 2004; Cooke and others, 2006).

A number of other deposit types are either spatially, temporally, or genetically related to alkalic-type epithermal gold deposits. The most common types of associated deposits include (1) copper, iron, gold, and zinc-rich skarns, such as those in New Mexico (McLemore, 1996), deposits near Galore Creek (Enns and others, 1995), and many in Montana (Woodward and Giles, 1993); (2) polymetallic replacement deposits (Ag, Pb, Zn, Cu, Au), the best example of which is the Kendall deposit in Montana (Lindsey, 1985); (3) fluorspar vein and breccia deposits and tungsten-bearing veins, exemplified by deposits in Boulder County (Kelly and Goddard, 1969; Nash and Cunningham, 1973); and (4) local carbonatites (REE, Nb), for example in New Mexico (McLemore, 2010). The presence of these deposits does not necessarily indicate the existence of nearby alkalic-type epithermal deposits, nor does their absence preclude the occurrence of nearby alkalic-type epithermal gold deposits.

Sources of Metals and Fluids

Strontium and lead isotope compositions of ore and gangue minerals (apatite, carbonates, roscoelite, and galena) from veins in the Porgera alkalic-type epithermal gold deposit are intermediate between those characteristic of the Porgera intrusions and their host sedimentary rocks (Richards and others, 1991), which suggests a mixed magmatic-sedimentary source for both Pb and Sr. Gold may also have been derived from one or both of these sources (Richards and others, 1991), but the bulk of the gold was likely magmatic (Richards, 1995). Lead isotope compositions of galena in veins from the Cripple Creek deposit almost entirely overlap those of potassium feldspar in the associated alkaline igneous rocks, which suggests a genetic relationship between alkaline magmatism and mineralizing processes. However, higher $^{207}Pb/^{204}Pb$ and $^{208}Pb/^{204}Pb$ ratios of some galena samples suggest a contribution to the ore fluid from surrounding early Proterozoic rocks, probably through leaching by mineralizing fluids (Kelley and others, 1998).

Stable isotope compositions ($\delta^{18}O$ and δD) suggest that ore fluids responsible for the genesis of some alkalic-type epithermal gold deposits are dominated by magmatic fluid input, although contributions from meteoric or other external fluids (seawater, evolved groundwater) were also variably important to deposit genesis. Many alkalic-type epithermal gold deposits have light sulfur isotope compositions that reflect the oxidation state of sulfur in the associated alkaline magmas or progressive boiling-related oxidation of hydrothermal fluids, or leaching of sedimentary sulfur (Richards and Kerrich, 1993; Jensen and Barton, 2000). Sulfur isotope compositions of sulfides from the porphyry and epithermal deposits suggest a common sulfur source.

Chemical Transport and Transfer Processes, and Precipitation Mechanisms

The close association between alkalic-type epithermal gold deposits and alkaline magmas suggest that gold is partitioned from magmas to associated hydrothermal fluids (Richards, 1995). The presence of Fe^{3+}-bearing phases, such as magnetite and aegirine, and light sulfur isotope values (Jensen and Barton, 2000) reflect the association of this deposit type with oxidized, alkaline magmas with low to moderate sulfidation states. Oxidizing and low to moderate sulfidation states favor retention of copper and gold in silicate melts (Sillitoe, 1979) because sulfur saturation is suppressed, and sulfur is present in the melt mostly as SO_2 rather than H_2S; therefore, metals are only minimally partitioned into sulfide phases (Richards, 1995). Cooling eventually results in disproportionation of SO_2 to sulfate and sulfide species, which promotes precipitation of Cu-bearing sulfide minerals. Some gold may also be deposited with these sulfides; however, much of it may remain in solution as bisulfide complexes after conversion from chloride to bisulfide (Hayashi and Ohmoto, 1991). Typically, early deposition of copper (in porphyry deposits) and later gold deposition at shallower levels in epithermal environments, as observed at La Plata, Ladolam, and Vatuoula, may reflect these processes (Richards, 1995; 2009).

The common presence of fluorite and roscoelite in alkalic-type epithermal gold deposits may reflect high volatile contents (for example, H_2O, F, CO_2) in associated alkaline magmas. Increased dissolved H_2O (and CO_2, F, Cl) contents may result in larger and (or) higher-grade gold deposits due to more efficient magmatic-hydrothermal systems. It is unclear how tellurium is enriched in magmatic-hydrothermal solutions. However, thermodynamic modeling by Cooke and McPhail (2001) predicts that tellurium species, $Te_2(g)$ and $H_2Te(g)$, are carried in the vapor phase and then condense to react with aqueous gold-bearing species $Au(HS)^{-2}$ or $Au(HS)$.

Isotopic evidence suggests that sulfur and select ore metals in some alkalic-type epithermal gold deposits were derived in part by leaching sulfide-bearing sedimentary rocks (Paterson and others, 1989; Richards and others, 1991; Spry and others, 1996). At Porgera, isotopic similarities between sulfides in sedimentary rocks and those in spatially associated alkalic-type epithermal gold deposits suggest that the sulfides in sedimentary rocks were likely deposited by early magmatic-hydrothermal fluids, and then

dissolved and redeposited in the epithermal environment (Richards and others, 1991). However, this two-stage precipitation-redissolution mechanism may not be necessary and instead, direct transfer of ore components to circulating groundwater may reflect mixing with late-stage magmatic fluids, as has been suggested for many alkalic-type epithermal gold deposits (Richards, 1995; Jensen and Barton, 2000).

The transfer of gold from alkaline magmas to hydrothermal fluid phases is suggested by the close association of alkalic-type epithermal gold and porphyry deposits, but there remains uncertainty on the melt-fluid partitioning of gold. Gold may behave in an analogous manner to copper (Candela, 1989) and thus should preferentially partition into the volatile phase during devolatilization; both gold and copper would dissolve in that phase as chloride complexes (Seward, 1973). Fluid inclusion data from many alkalic-type epithermal gold deposits show high (>30 equiv. wt. percent NaCl) chloride contents (Thompson and others, 1985; Richards and others, 1991), at least for the early, relatively high temperature fluids; these high salinities, together with oxidized conditions, favor chloride transport of gold.

Some authors have suggested that tellurium complexing of gold may play an important role in alkalic-type epithermal gold systems (for example, Seward, 1973; Saunders and May, 1986; Jensen and Barton, 2000; Cooke and McPhail, 2001). McPhail (1995) recognized that tellurium complexes partition to the vapor phase, a concept that has been supported by the presence of tellurium-bearing particulate matter, tellurides in vesicles, and tellurium-rich sublimates of recently active volcanoes (for example, Greenland and Aruscavage, 1986; Fulignati and Sbrana, 1998). Experimental studies have demonstrated that more oxidized Te(IV) is better solubilized than reduced species, such as Te(0) and Te (-II), and that the oxidized species more effectively complex with chlorides, both of which enhance transport of gold and tellurium in hydrothermal systems. Since Te is found as tellurides in hypogene ores, Grundler and others (2013) proposed that a change in redox conditions is a possible trigger for the deposition of precious-metal tellurides. However, other studies (Seward, 1973; Cooke and Simmons, 2000) have suggested that gold is more strongly complexed with $Au(HS)_2^-$ or $Au(HS)_{(aq)}$ than with tellurium complexes.

Elevated vanadium contents in alkaline igneous rocks (for example, Mutschler and others, 1985; Eaton and Setterfield, 1993; Zhang and Spry, 1994; Scherbarth and Spry, 2006) suggest that vanadium in hydrothermal fluids may be derived directly from the alkaline magmas, particularly relatively more mafic compositions (Mutschler and others, 1985; Afifi and others, 1988; Scherbarth and Spry, 2006). In many cases, however, such assertions about vanadium source are circumstantial and without definitive proof (Richards, 1995). Nevertheless, the Navilawa Monzonite, host to the Tuvatu deposit, contains as much as 0.69 and 0.49 wt. percent V_2O_3 in magnetite and phlogopite, respectively, which suggests that alkaline rocks may indeed be the source of elevated vanadium abundances in alkalic-type epithermal gold deposits. Alternatively, the spatial association among gold tellurides, roscoelite, and other V-minerals (for example, nolanite) in alkalic-type epithermal gold deposits may be a simple consequence of the stability fields of these minerals overlapping with regard to oxygen fugacity (fO_2) and pH conditions associated with epithermal mineralization (Spry and Scherbarth, 2006).

The processes responsible for gold precipitation in alkalic-type epithermal gold deposits, including boiling with loss of H_2S to a vapor phase (Ahmad and others, 1987; Richards and Kerrich, 1993), fluid mixing resulting in reduction, oxidation, or dilution (Kwak, 1990; Spry and others, 1996; Zhang and Spry, 1994), and cooling (Thompson and others, 1985), are diverse and not unique to this deposit type. In most systems, several of these processes may occur contemporaneously, which hinders identification of the dominant mechanism. Evidence of any one of these processes may be lacking, but such an absence of evidence does not necessarily preclude involvement of that process. For example, the lack of fluid inclusions and (or) inclusions that show evidence of boiling do not preclude boiling as a precipitation mechanism (Richards, 1995).

In addition, mafic-ultramafic and other Fe-rich rocks constitute ideal reactive sulfidation traps for hydrothermal fluids and may be another mechanism for gold deposition. Wall rock sulfidation promotes H_2S reduction, which in turn destabilizes gold bisulfide complexes. For example, at Cripple Creek, lamprophyre and late-stage mafic dikes host a disproportionate amount of total gold in the district (Jensen and Barton, 2000). Reduced sediments may constitute similar traps.

The Importance of Magma Composition and Tectonic Environment

The alkaline rocks that are associated with epithermal gold deposits vary widely in composition, from alkali basalts and related lamprophyres, through intermediate compositions, to evolved rocks (table 1). The presence of hydrous phenocryst phases (hornblende, biotite) in the rocks suggest high water contents. Furthermore, the presence of Fe^{3+}-bearing phases, such as magnetite and aegirine that are so common in alkaline rocks, suggests high oxidation states (Jensen and Barton, 2000), which suppress sulfur saturation and prevent the loss of precious metals into sulfide phases (Richards, 1995). Another effective variable for increasing mineralization potential of a magma may be halogen contents (Müller and Groves, 2019). Both F and Cl are enriched in alkaline magmas, particularly potassic ones (Müller and others, 2001). Most fluid inclusion studies of alkaline-related epithermal Au deposits show that fluids contain high F concentrations (as fluorite) and are CO_2-rich, suggesting high volatile contents.

Assuming there is a direct relationship between epithermal Au deposits and hydrous alkaline magmatism, the tectonic environment in which the magmas are generated

is a critical factor. Alkaline rocks are commonly associated with crustal-scale rifting, convergent margins, and intraplate environments (Jensen and Barton, 2000). Alkaline rock provinces are typically characterized by low volumes of magma; therefore, these systems occur in isolation or as clusters of magmatic centers, but generally not as regionally extensive provinces (Richards, 1995).

In nearly all examples of alkalic-type epithermal gold deposits described in this report (table 1), there is some association between alkaline magmatism and subduction-zone activity (Richards, 1995). Trachyandesites and trachybasalts (including shoshonites) are commonly erupted in arcs with complex subduction geometries, or where arcs have undergone tectonic reconfiguration (Jensen and Barton, 2000). Examples of deposits with a clear relationship to arc magmatism include the young belts in PNG and Fiji, as well as the Stikinia and Quesnellia terranes in Canada (table 1). The Ordovician shoshonite belt (Goonumbla deposit) may represent a paleoarc environment (Müller and others, 2001), although a rift-related origin is possible (Jensen and Barton, 2000). Other arc-related and subduction-related deposits include those in the Colorado Mineral Belt (La Plata and Boulder Counties), Montana, South Dakota, and Wyoming that formed during early, middle, or late stages of the Laramide orogeny (table 1).

Some gold systems show displacement either in space or time from the active magmatic arc. In these settings, the driving force responsible for voluminous arc magmatism is not present or has ceased, and melting that does occur in the mantle is usually small in extent and volume and occurs in response to distal effects or post-subduction readjustments (Richards, 1995). The mechanisms and triggers for mantle melting in such settings are diverse and poorly understood, but may explain the heterogeneity and compositionally diverse range of magmas (Richards, 1995). Possible examples of such deposits include Cripple Creek and other deposits to the south in New Mexico, deposits in the Pingyi area in China and Eastern Mongolia, and the Fakos deposit in Greece (table 1).

Deep-seated and regionally extensive structures serve an important role in localizing alkaline magmas and associated gold deposits as discussed previously. Some of these predate arc activity and may be at an angle to the orogeny, suggesting tensional reactivation of older lithospheric features (Montana alkalic province; Boulder County and La Plata in the Colorado Mineral Belt; Porgera-Mount Kare, and the Tavua deposit, Fiji; table 1) (Richards, 1995). The deep structures allow mantle- or lower crust-derived magmas to ascend to high levels in the crust (Jensen and Barton, 2000). On the deposit scale, economic mineralization is restricted to areas where hydrothermal activity was focused, typically structurally controlled faults, fissures, and veins. Nearly all epithermal Au deposits exhibit such localization, whether the deposits are along contacts between intrusive and host sedimentary rock sequences (central Montana deposits), grabens or extensional faults (Boundary area, Washington and British Columbia), or on the edge of rifts (Colorado, New Mexico deposits).

Exploration/Resource Assessment Guides

Geological, Geophysical, and Geochemical Data

Alkalic-type epithermal gold deposits generally form at shallow crustal depths in a variety of tectonic settings, including island arc environments (Porgera, Vatukoula, and Ladolam) and regions of thickened continental crust (Cripple Creek and deposits in Montana). Most magmas associated with these deposits have high total concentrations of Na_2O and K_2O but can have a wide range of silica contents. The spatial extent of mineralized systems (including alteration zones) varies from narrow zones less than a few tens of meters wide and adjacent to faults to areas that range over tens of square kilometers.

Crucial to any assessment of alkalic-type epithermal gold deposits is understanding the geologic framework in the study area, including the age and chemical character of intrusive and extrusive rocks. Therefore, geologic maps are critical in the early phases of site examinations. Geologic features useful in exploration and assessment activities include the presence of (1) known alkalic-type epithermal gold deposits and prospects, (2) rock units that are commonly associated with this deposit type, (3) hydrothermal alteration similar to that characteristic of this deposit type, (4) breccia pipes or diatremes that indicate explosive volcanism, and (5) structures and structural zones of types known to localize mineralization. Some of the largest deposits (for example, Cripple Creek, Colorado; Golden Sunlight, Montana; Vatukoula, Fiji) are spatially associated with regional lineaments, the Colorado Mineral Belt/Rio Grande Rift, Great Falls tectonic zone (Montana), and Viti-Levu lineament, which reflect first-order structural control on localization of not only alkaline magmas but also related epithermal and other hydrothermal deposit types (fig. 7).

Understanding the broad tectonic settings and identification of major basement structures in permissive areas may be enhanced by the use of seismic data. Aeromagnetic and gravity data may also be used to delineate regional-scale trends (fig. 11). For example, the northeast-trending regional-scale Viti-Levu lineament, delineated by deep sourced magnetic anomalies and aligned gravity high, includes the Vatukoula, Tuvatu, and Mt. Kasi epithermal deposits (fig. 7*C*).

Geophysical data can also be employed to delineate large areas of altered rocks associated with alkalic-type epithermal gold deposits. Aeromagnetic and magnetic susceptibility data were used to identify large areas of altered rocks at Cripple Creek in Colorado, Porgera, and Ladolam, PNG. In some cases, given adequate magnetic contrasts, aeromagnetic data allow direct delineation of alkaline intrusions themselves. Similarly, distinguishing alkaline rocks with different compositions on the basis of gravity data may be possible, provided sufficient density contrasts are present (Cripple Creek, Lachlan Fold Belt). In spite of extensive soil development at the Cripple Creek deposit, vegetative

cover, and lack of outcrops, remote sensing studies using multispectral and hyperspectral data can help identify both primary and secondary minerals, including hematite, goethite, jarosite, kaolinite, and sericite (Taranik, 1990; Livo, 1994; Kadel-Harder and Price, 2017). Radiometric data may identify elevated potassium concentrations that are characteristic of volcanic rocks associated with alkalic-type epithermal gold deposits (Porgera, PNG; Tuvato, Fiji). At Porgera, K/Th values define the extent of the sericitic alteration halo around the intrusive complex (Levett and Logan, 1998).

Most alkalic-type epithermal gold deposits lack extensive lithogeochemical halos because vein extent is minor; however, deposits with extensive alteration zones may be identifiable using rock geochemical data. Shoshonitic (potassium-rich) rocks have been suggested as a potential guide for alkalic-type epithermal gold deposits but shoshonitic compositions alone do not uniquely or reliably identify igneous systems that are prospective for associated alkalic-type gold deposits because host rock compositions are demonstrably variable and some of these potassium-rich rocks may, in fact, have acquired that characteristic by potassic alteration (Jensen and Barton, 2000). For example, in a district such as Cripple Creek, unaltered rocks are rich in sodium compared to their potassium content. Altered phonolites typically show >14 wt. percent K_2O, whereas unaltered phonolites contain <6 wt. percent K_2O (Jensen, 2003). Therefore, macroscopically unaltered rocks with very low Na/K values likely reflect potassic alteration. This style of metasomatism is notable for its extensive nature, subtle or cryptic appearance (preserving original rock textures and not recognizable with petrographic microscopes but instead requiring staining to identify potassium), and intimate association with gold mineralization (Jensen, 2003).

Soils and stream sediments proximal to alkalic-type epithermal gold deposits may be enriched in Ag, As, Au, Bi, Cu, F, Hg, K, Mo, Sb, Pb, Te, V, and Zn that reflect the ore, gangue, and alteration minerals typically associated with these deposits. Several elements including Au, Ag, Te, K, and V are found in anomalous concentrations in soil samples from Cripple Creek deposits (Gott and others, 1969), similar to samples of soils collected over the Gold Hill deposit in Boulder County (Jenkins and Carter, 1997). Jensen and Barton (2000) suggest that gold itself may be the best indicator element, because other elements, such as, Sb, Cu, Pb, and Zn, may be variably enriched depending on variations in ore and gangue mineralogy among deposits within a single district. However, the coincidence of multiple element anomalies (Te and V in addition to Au) rather than a single element reinforces the likelihood that the geochemical signature reflects alkalic-type epithermal gold deposits.

Attributes Required for Inclusion in Permissive Tract at Various Scales

Within the broad array of epithermal deposits, permissive tracts can be extremely large because nearly all rock types, as well as poorly consolidated sediments, can host these deposits (John and others, 2018). The characteristics of tracks permissive for alkalic-type epithermal gold deposits are geologically similar to those of the broader array of epithermal deposits. However, alkalic-type epithermal gold deposits form only in spatial and genetic association with alkaline igneous rocks, which further constrains their permissive tracts. Permissive tract delineation may be further limited to geologic provinces that include calderas, breccia pipes, or diatremes (for example, Zortman-Landusky, Golden Sunlight, Cripple Creek, Ortiz Mountains) because of the association of many of these deposits with those types of magmatic centers. Two principal criteria that can be used to exclude areas from permissive tracts are (1) evidence (that is, fluid inclusion pressure estimates) that suggests that genetically associated alkaline igneous rocks formed at depths greater than that at which epithermal gold deposits form (>1.5 km), and (2) exposed rocks that reflect erosion to depths beneath those favorable for epithermal deposit formation.

Geoenvironmental Features and Anthropogenic Mining Effects

Soil and Sediment Signatures Prior to Mining

According to Plumlee (1999), soil and sediment signatures associated with alkalic-type epithermal gold deposits are influenced by several factors, including primary host rock mineralogy, hypogene hydrothermal ore mineralogy, and secondary mineralogy (supergene minerals and minerals resulting from weathering in the vadose zone). The signatures are also influenced by climate, topography, and permeability/porosity of the deposit (Plumlee, 1999).

Partitioning of elements into soil and sediment occurs both by physical processes, such as weathering and mass wasting, and by hydromorphic processes, including mineral decomposition resulting from the weathering and subsequent elemental transport in water as dissolved species or as elements sorbed onto iron or manganese oxide colloids. The acid-base characteristic of the deposit, which is the balance between acid-forming and acid-neutralizing processes, influences the rate at which minerals break down, although climate also affects mineral weathering and elemental transport. The porosity and permeability of a deposit affect access of minerals to oxygen and water, and the rate at which metal-laden, acidic water can flow from the deposit and transport elements through surface and groundwater flow, which is also influenced by topography.

The ore minerals characteristic of alkalic-type epithermal gold deposits yield Au, Cu, Ag, As, S, Sb, Mo, Hg, Zn, Pb, Te, and Bi that may be enriched in both soil and stream sediments proximal to these deposits. As stated earlier, these elements may be good indicators of areas with potential for these deposits (Gott and others, 1969; Jenkins and Carter, 1997).

Secondary Minerals

Secondary minerals include supergene minerals, those that form in the vadose (unsaturated oxidized) zone at or near the surface, and minerals that form on waste piles, tailings material, and on material affected by mine drainage waters; some constituents of the secondary mineral assemblages may be present in several of these environments. Significant supergene zone development in association with alkalic-type epithermal gold deposits is not common, owing to the typically low pyrite content of these deposits (Kelley and Spry, 2016).

Gold telluride minerals are easily altered in the weathering environment (Kelley and others, 1995); for example, emmonsite ($Fe_2(TeO_3)_3{\cdot}2H_2O$), also known as durdenite, is a secondary iron-tellurium phase in which tellurium has been oxidized to tellurite and the precious metals have been solubilized. Weathering of calaverite typically results in formation of a fine-grained, dull, mustard-colored secondary gold that is released as telluride grains decompose (Cook, 2010). Other secondary tellurium minerals reported in association with alkalic-type epithermal gold deposits include various tellurates and tellurites, paratellurite (TeO_2), deddingite ($(Mn,Ca,Zn)Te_2O_5$), moctezumite ($Pb(UO_2)(TeO_3)_2$), montanite ($Bi_2(TeO_6).2H_2O$), and poughite ($Fe_2(TeO_3)(SO_4)(H_2O).H_2O$) (for example, Fornadel and others, 2014), as well as weissite ($Cu_{2-x}Te$) (Shackleton and others, 2003), and bilibinskite ($Au_3Cu_2PbTe_2$) (Webminerals, 2014).

Although alkalic-type epithermal gold deposits typically have low base metal contents, secondary associated base metal minerals have been identified in these deposits. These include secondary copper minerals, such as chalcocite and covellite (Shackleton and others, 2003), secondary zinc minerals, such as goslarite (zinc sulfate) or smithsonite (zinc carbonate), and secondary lead minerals, such as anglesite (lead sulfate) or cerrusite (lead carbonate), as reported at the Dongping Au-Te deposit, China (Mindat, 2014). Various iron and manganese oxide minerals may also form in the weathering environment (Kelley and others, 1995).

Metal Mobility from Solid Mine Waste

Acid-Base Accounting

Acid-base accounting is used to assess the potential for mine waste or tailings to produce acidic mine drainage or for altered or mineralized rock in its natural setting to produce acidic rock drainage. Most commonly, iron sulfides in the presence of water and oxygen weather to produce sulfuric acid. Numerous chemical reactions describe the processes. The typical first reaction involving pyrite (FeS_2) oxidation (O_2 and H_2O) and acid (SO_4^{2-}. H^+) production (Seal, 2010) is shown in equation 1:

$$FeS_2 + 7/2\ O_2 + H_2O \rightarrow Fe^{2+} + 2\ SO_4^{2-} + 2\ H^+. \quad (1)$$

Once oxidation of pyrite has begun, some ferrous iron (Fe^{2+}) is converted to ferric iron (Fe^{3+}) by oxygen (O_2) (Seal, 2010) according to equation 2:

$$2\ Fe^{2+} + 1/2\ O_2 + 2\ H^+ \rightarrow 2\ Fe^{3+} + H_2O. \quad (2)$$

In the presence of the bacterium *Acidithiobacillus ferrooxidans,* the rate of this reaction is increased by a factor of 100,000. When the pH of the solution decreases to about 4, oxidation of pyrite by ferric iron (eq. 3) produced in the reaction represented in equation 2 becomes more important (Nordstrom and Alpers, 1997). Ferric iron is a much more effective oxidizer of pyrite, according to equation 3 (Seal, 2010):

$$FeS_2 + 14\ Fe^{3+} + 8\ H_2O \rightarrow 15\ Fe^{2+} + 2\ SO_4^{2-} + 16\ H^+. \quad (3)$$

An overall simplification of acid production by oxidation of pyrite, which involves up to 15 separate reactions involving both oxygen and ferric iron, each with different rates, is shown in equation 4 (Nordstrom and Alpers, 1997):

$$FeS_2 + 15/4\ O_2 + 7/2\ H_2O \rightarrow Fe(OH)_3 + 2\ H_2SO_4. \quad (4)$$

Equation 4 implies that, overall, one mole of pyrite will produce two moles of sulfuric acid or four moles of hydronium ion (sulfuric acid is diprotic) for a total of four moles of acid per mole of pyrite. Carbonates, most notably calcite, are the most effective acid neutralizers. The neutralization reaction at pH below 6.4 (White and others, 1999), which is the acidity condition of most interest, is given by equation 5:

$$CaCO_3 + 2H^+ \rightarrow H_2CO_3 + Ca^{2+}. \quad (5)$$

Equation 5 indicates that one mole of calcite will neutralize two moles of acid, and equations 4 and 5 together clarify that two moles of calcite are required to neutralize the acid produced from one mole of pyrite. Because pyrite has a formula weight of 120 grams/mole and calcite has a formula weight of 100 grams/mole, about 1.7 weight percent calcite is required to neutralize 1.0 weight percent pyrite. Sulfosalts and other sulfides can also produce acid, both by reaction with oxygen (for example, pyrrhotite, arsenopyrite, enargite, and tennantite/tetrahedrite), or by oxidation by ferric iron (for example, the previously mentioned minerals plus chalcopyrite, covellite, and cinnabar) (Plumlee, 1999).

Dissolution of acid-storing salts (formed during wet-dry cycles from primary iron sulfides), such as melanterite or copiapite, also releases acid. In addition, hydrolysis of metal ions other than iron can produce acid. Carbonates (most effectively, calcite and dolomite) react to neutralize acid; some acid neutralization is possible through reactions involving silicate minerals, such as biotite, feldspars, and chlorite, although the amount and rates of neutralization are minor relative to reactions involving carbonates. Different geologic materials (for example, ore or waste from different deposit types, different degrees of alteration, or waste reflecting within-deposit variations) have different acid-producing and (or) acid-neutralizing capability.

Various laboratory approaches have been used to predict acid-production potential. Total sulfur analyses can be used to estimate acidity, provided that the sulfur is present entirely as sulfide; sulfate phases such as barite or gypsum do not produce acid because the sulfur is already oxidized. Multiplying the appropriate sulfide sulfur value (in weight percent) by 31.25 gives an acid potential (AP) in kilograms per ton $CaCO_3$ equivalent (Sobek and others, 1978). Similarly, net acid production (NAP) can be measured directly by oxidizing sample powder with hydrogen peroxide; the acid produced from sulfides, or released from soluble acid salts, then reacts with whatever neutralizing minerals are present in the sample. After sufficient time for the acid-producing and acid-consuming minerals to react, the resulting solution is titrated to a pH of 7 (Lapakko and Lawrence, 1993). Neutralization potential (NP) is measured either by adding acid to a sample and back titrating, or by direct titration of a sample slurry (U.S. Environmental Protection Agency, 1994).

Alkalic-type epithermal gold deposits contain variable amounts of total sulfides and pyrite (2–10 percent), but commonly also contain abundant carbonate gangue (Kelley and others, 1995). The Vatukoula deposit contains ~0.5 to 1 percent pyrite (Pals and Spry, 2003), whereas the Cripple Creek deposit contains between 0.5 and 3.2 percent sulfide sulfur and from 1.1 to 16.8 percent carbonate (Denny and others, 1930).

The pH values of drainage resulting from the weathering of mine waste, tailings, or rock is primarily determined by the balance between acid-generating and alkalinity-generating reactions (Price and others, 1997). The net NP (NNP) is defined as NNP = NP – AP, that is, the difference between neutralization and AP. Another parameter, the NP ratio (NPR) is defined as NPR = NP/AP. If NNP is <−20 kilograms/ton (kg/ton) $CaCO_3$, the acid-producing potential is significant, whereas values >20 kg/ton $CaCO_3$ indicate minimal acid-producing potential. Similarly, if the NPR is less than 1:1, acid production is likely, but if it is more than 3:1, acid production is unlikely (Price and others, 1997). The interpretation of the NAP value is similar to that for NNP, but with the opposite sign: a NAP value >20 kg/ton indicates significant acid producing potential, whereas a NAP of <−20 kg/ton suggests no acid-producing potential (Fey and others, 2000). These tests are termed static tests, and do not measure or predict the rates at which acid drainage will be generated.

Mine waste or tailings material that returns a low AP value (low sulfide content) may yet produce significant acid drainage if neutralizing mineral contents are also low. For example, at the Zortman-Landusky mines in Montana, waste rock with low sulfide content (approximately 1 percent) and an AP of typically <20 kg/ton $CaCO_3$ was not expected to generate acid drainage. However, NP values were also typically <10 kg/ton $CaCO_3$; correspondingly, NPR was ≤0.5, and significant acid drainage with high dissolved metal content developed (Williams and others, 2009). Most alkalic-type epithermal gold deposit waste material, because of low sulfide content and sufficient carbonate content, should be non-acid generating, with <20 kg/ton $CaCO_3$ NAP or >20 kg/ton $CaCO_3$ NNP, or a NPR of more than 3:1. Tailings from the cyanide leach process used to remove precious metals have been subjected to alkaline cyanide leach conditions, and so would rarely be acid producing.

Drainage Signatures

The drainage associated with many mineral deposits and mining operations pose environmental hazards. Physical, mineralogical, chemical, climatic, and topographic characteristics influence the behavior and impact of that drainage (Plumlee, 1999).

The abundance of elements of environmental concern (sum of the concentrations of Zn + Cu + Cd + Pb + Co + Ni, in micrograms per liter) plotted against the pH of deposit drainage water (fig. 16, modified to include data for As in the sum of elemental abundances) yields a Ficklin plot (Plumlee and others, 1999). Published drainage data for alkalic-type epithermal gold deposits are limited, but Plumlee and others (1999) published three analyses for alkalic-type epithermal Au-Te deposits and stated, “as a result of their generally low sulfide contents and high carbonate contents, these deposits tend to generate near-neutral pH waters with low dissolved base-metal concentrations” (Plumlee and others, 1999, p. 402). However, as described previously, the Zortman-Landusky mines are an exception. Three data points each for samples from the Zortman and Landusky mines that represent predictions of water quality from high, moderate, and low acid-generating materials (Shaw, 2000) illustrate the wide range of drainage composition possible from a single mineralizing system. The data for the Carlton drainage tunnel at Cripple Creek and from Eldora, Colorado, reflect high pH and low summed metal abundances (Plumlee and others, 1999). A sample of river water downstream from the Porgera deposit, PNG, (where much of the waste is directly deposited into the river system) illustrates that high pH does not necessarily result in low summed-metal abundances (International Institute for Environment and Development, 2002). The high metal sum abundance for Porgera is

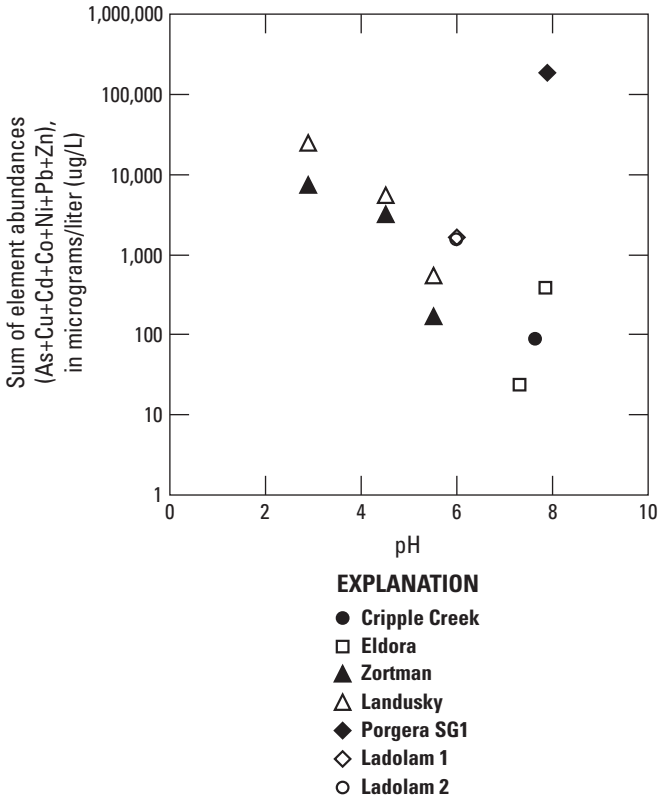

Figure 16. Modified Ficklin plot showing the composition of drainage water for numerous samples from six alkalic-type epithermal gold deposits (modified from Plumlee and others, 1999). The pH values for the two Ladolam samples are estimated.

dominated by zinc (93 percent of the total). The data for two samples from the Ladolam Mine, PNG, are almost identical, but one sample is dominated by zinc and the other by arsenic (Lihir Gold Limited, 2006). In summary, possible pH versus summed metal abundances are highly variable among alkalic-type epithermal gold deposits (fig. 16).

Past and Present Mining Methods and Ore Treatment

High ore grades and the accompanying economic feasibility caused underground mining methods to dominate gold ore extract operations before the 1980s. After the 1970s, gold prices increased, which enabled the mining of lower-grade deposits by open-pit methods. Regardless of deposit type, the grade of ore mined worldwide has declined progressively with time (Mudd, 2007); today, recovered ore contains an average of about 3–4 g/t gold. Accordingly, open-pit operations, which are easier, less expensive, and quicker to develop, are currently the predominant mine type (Norgate and Haque, 2012). Open-pit mines yield lower unit value ore, but with much greater ore volumes, greater amounts of gold, silver, copper, and other commodities are recovered.

In historical mining operations (pre-1900s), gold was recovered by mercury amalgamation, and the mercury subsequently removed by roasting. This recovery method is rarely (?) used at a large scale today, as issues relating to the cost of mercury, attendant human health risks, and environmental hazards associated with lost mercury, make the technique unattractive, though it is still used on a small scale in some low-technology, artisanal mining operations.

Today, industrial scale mining operations recover gold from crushed ore using a sodium cyanide leach process through the reaction known as the Elsner equation: $4\ Au + 8\ NaCN + O_2 + H_2O = 4\ NaAu(CN)_2 + 2\ NaOH$ (Smith and Mudder, 1997). In the Elsner equation, the cyanide solution has a typical strength in the range of 0.01 and 0.05 percent (Logsdon and others, 1999). Leaching is conducted either in tanks, or for lower-grade ores, coarsely ground ore is leached on pads (“heaps”) for weeks or months, and the “pregnant” solution is then processed. The leachate from either tank or heap leaching is further processed in one of two ways. In one process, activated carbon is added to the leach solution, whereby the gold-cyanide complex is sorbed (two variants are carbon-in-leach and carbon-in-pulp) and removed from the solution by filtration. The gold is then released from the carbon by reverse stripping with a hot caustic cyanide solution. The other method of recovering gold from the leachate (the Merrill-Crowe process; Adams, 2005) involves adding finely powdered zinc to the solution that, through a replacement reaction, precipitates gold from solution and dissolves the zinc. Further processing steps include electrowinning and smelting (Norgate and Haque, 2012). Alternative lixiviants, such as thiourea and thiosulfate, are not currently used because of chemical management issues and environmental concerns (Zanbak, 2012).

Some ores are relatively refractory because the gold is bound more tightly in sulfide phases or is encapsulated in quartz. Gold in alkalic-type epithermal deposits is contained within arsenian pyrite, arsenian marcasite, and arsenopyrite, as well as in gold and silver-gold tellurides (Spry and others, 2004), or it forms native gold inclusions in petzite, calavarite, buckhornite, and krennerite, encapsulated in grains of pyrite, chalcopyrite, and tennantite (Spry and Thieben, 2000). The principal gold telluride, calaverite, is itself fairly refractive to cyanidation. Gold contained in these ores requires additional processing before extraction. These processes include chemical oxidation, roasting, pressure oxidation, and bio-oxidation (Spry and others, 2004). These additional treatment steps precede cyanidation, and oxidize and decompose sulfide components, which causes gold to become more leachable (Norgate and Haque, 2012).

Volume and Footprint of Mine Waste and Tailings

The volume of waste and tailings associated with mineral deposits is related to the size of the deposit, the depth to the deposit, and the competency of the country rock; the latter two influence the stripping ratio (Seal, 2010). Underground mines tend to have smaller footprints than open-pit mines. In addition to the area occupied by mine pits, adits, or shafts themselves, mine operations include mill tailings, waste piles, cyanide heap leach pads, cyanide tank leaching operations, and other facilities that support the actual mining activity, all of which increase the "disturbed ground" footprint.

An approximation of the volume of waste rock and tailings can be made from initial estimates of reserves, which can change over time due to exploration activities that add additional reserves, changes in mining technology, or economic condition, or from production records. If a deposit has been mined out and operations have ceased, total production records can be used to estimate the mass of waste rock and tailings produced. The estimated volume can then be calculated by dividing the mass by density and applying an approximate expansion factor. For example, a density of 2.7 metric tons per cubic meter (t/m^3) and an expansion factor of 1.2 were used to estimate the volume of waste rock and tailings material at the McLaughlin Mine (a quartz-adularia epithermal deposit) in California (Diggles and others, 1996). The stripping ratio is defined as the ratio of the mass of waste rock to the mass of ore removed and is generally between 2 and 10 for open-pit mines (Mudd, 2007). In contrast, a stripping ratio of 11 has been quoted for the Porgera Mine in PNG (International Institute for Environment and Development, 2002). Both underground and open pit mining techniques have been used at Porgera but the waste ratio associated with underground operations is not known. Given that far more ore has been recovered by open-pit mining, the mass/volume estimate of waste was calculated based on open-pit mining. Production from underground mining began in 1990 and was supplanted by open-pit operations in 1993; estimated total production at Porgera by both mining methods is more than 16 million ounces of gold (MiningLink, 2014). Using an estimated gold content of 4 g/t and the 11:1 stripping ratio, an estimate for the total amount of material removed (waste and ore) is 1.6 billion tons. Using a density estimate of 2.7 t/m^3 and an expansion factor value of 1.2 (Diggles and others, 1996), the calculated volume is about 600 million cubic meters of waste material.

Many open-pit mines are visible in aerial imagery, which allows the size of the pits and total operational footprints to be estimated (table 4). These area estimates do not necessarily reflect official mine property descriptions, but depict all disturbances from mining operations, at a particular mine, as deduced from aerial imagery.

Analysis of imagery for six open-pit alkalic-type epithermal gold mines suggests that median pit size is 85 hectares (ha); the smallest pit is 5.5 ha (Cunningham Hill, New Mexico) and the largest single pits are 125 ha (Cripple Creek, Colorado) and 110 ha (Porgera, PNG). The associated median footprint for 14 deposits is about 190 ha; the smallest size is 3 ha at the Spotted Horse Mine (a small underground operation) in the Judith Mountains, Montana, and the largest total disturbed area footprint is associated with operations at Cripple Creek, Colorado, Golden Sunlight, Montana, and Porgera, PNG, which each cover about 1,000 ha. The fraction of area occupied by the pit relative to total mine footprint ranges from 3 percent at Northparkes and Goonumbla, Australia, to about 10 percent at Cripple Creek, Colorado, Porgera, PNG, and Golden Sunlight, Montana. The median pit area is about 9 percent.

Smelter Signatures

Data for these deposits are lacking.

Climate Effects on Geoenvironmental Signatures

The climatic setting of sulfide-bearing mineral deposits can affect chemical reaction rates and the composition of waters that are in contact with ore, waste material, or tailings. Temperature, total precipitation, and evaporation are important climatic factors (Seal and Ayuso, 2011). The overall impact of sulfide deposits is likely to be greater in wet climates, because of the increased availability of water to interact with sulfidic material (Seal, 2010). In arid and semiarid climates, less drainage is generated (Plumlee and others 1999), but it is likely to be more acidic and metal rich because of evaporation effects and the creation of acid-storing soluble metal-sulfate salts (Seal, 2010). In addition, in arid climates, windblown transport of metal-laden dust from waste and tailings may be significant.

The secondary mineralogy suite formed on tailings surfaces associated with mineral deposits that have similar primary mineralogy varies substantially in different climatic settings (Dold, 1999). Dold and Fontbote (2001) studied these effects in three different climatic settings that were (1) precipitation dominant (alpine climate) at 2,150 m elevation where annual precipitation (700 mm) exceeds evaporation (70 mm), (2) evaporation dominant (Mediterranean climate) at 725 m elevation with 540 mm annual precipitation and high summer evaporation, or (3) hyperarid at an elevation of 2,270 m with only 20 mm annual precipitation and very high evaporation. Although the study by Dold and Fontbote (2001) pertains to porphyry Cu deposits, not alkalic-type epithermal gold deposits, and processed tailings, not ore or waste, their observations provide useful general concepts relative to varying climatic effects on the environmental signatures of sulfide deposits.

In the precipitation-dominant climate, bivalent cations, such as copper and zinc, were leached from upper oxidation zones; below this zone, increasing pH values controlled the sorption of these cations onto secondary manganese (II) and

Table 4. Total disturbed area footprints and pit areas, in hectares, and ratio of pit area to total area for selected alkalic-type epithermal gold deposits. Surface mining operations where obvious pits are lacking, or pit dimensions are otherwise difficult to discern, have "not determined" (n.d.) entered for pit area.

Deposit	Mining operation type (past or current)	Disturbed area (hectares)	Pit area (hectares)	Area ratio
Cripple Creek, Colorado, U.S.A.	Open pit and underground	1,330	125	0.1
Vatukoula (Emperor), Fiji	Underground	23	n.d.	n.d.
Golden Sunlight, Montana, U.S.A.	Open pit	1,000	93	0.1
Northparkes/Goonumbla, Australia	Open pit and underground	831	24	0.03
Judith Mountains Spotted Horse, Montana, U.S.A.	Underground	3	n.d.	n.d.
Ladolam, Papua New Guinea	Open pit	390	78	0.2
Kendall, Montana, U.S.A.	Open pit	190	n.d.	n.d.
Annie Creek, South Dakota, U.S.A.	Open pit	460	n.d.	n.d.
Gilt Edge, South Dakota, U.S.A.	Open pit	93	n.d.	n.d.
Richmond, South Dakota, U.S.A.	Underground	80	n.d.	n.d.
Cunningham Hill, New Mexico, U.S.A.	Open pit and underground	80	5.5	0.07
Porgera, Papua New Guinea	Open pit and underground	1,000	110	0.11
Sandaowanzi, China	Underground	37	n.d.	n.d.
Zortman-Landusky, Montana, U.S.A.	Open pit	470	n.d.	n.d.
	Minimum	3	5.5	0.03
	Maximum	1,330	125	0.11
	Median	188	85	0.093
	Average	400	72	0.079

iron (III) hydroxides and clay minerals. Below the water table, with somewhat more reducing conditions (relative to the vadose zone), replacement processes, including the transformation of chalcopyrite to covellite, were dominant. In contrast, where evaporation exceeded precipitation, capillary forces caused upward migration of water in the vadose zone and transportation of mobilized elements toward the top of the tailings. Further evaporation near the surface leads to supersaturation of some mineral salts, resulting in the precipitation of water-soluble secondary sulfates (for example, chalcanthite, a secondary copper sulfate). Low temperatures and low precipitation, as in arctic environments, would likely reduce the rates of mineral decomposition, element leaching, and subsequent transport of either soluble or sorbed elements.

Potential Ecosystem Impacts

The mining and processing of alkalic-type epithermal gold deposits may affect the environment. For example, acid mine drainage and its attendant metal loads can affect surface and groundwater resources, and sediment can end up in surface drainages, especially in deposit settings with humid or wet climates and high topographic relief. Zinc, copper, lead, and arsenic are the elements most likely to affect water quality. Low pH waters produced by the interaction of iron sulfides, oxygen, and water can also introduce dissolved or colloidal iron and aluminum, although water hardness can have a partial ameliorating effect (Seal, 2010). Relative to that in acid waters that drain non-carbonate sulfide deposits, aquatic life in environments that host alkalic-type epithermal gold deposits may be afforded some protection because these deposits typically contain carbonates, yielding relatively high pH water that also contain calcium and magnesium ions that increase water hardness.

Drainage from abandoned mines and waste and tailing piles associated with deposits that contain arsenic-bearing minerals (for example, enargite) can affect ecosystem health. Pit lakes that form after the cessation of mining and pumping are likely to intersect the water table. In dry climates, evaporation from pit lakes can result in increased water acidity and higher dissolved metal contents. In settings favorable for wetting/drying cycles, waste or tailings piles will generate easily soluble efflorescent sulfate salts that store both acid and metals (Plumlee and others, 1999; Seal, 2010). These salts can then be released during rainstorms or spring snowmelt events and cause metal concentration spikes and increased loadings in the receiving streams (for example, Wirt and others, 1999; Fey and others, 2002).

In addition to the effects on aquatic systems, the mining of gold deposits requires large volumes of water and energy for metal production. The trend toward mining and processing of progressively lower grade gold ore necessitates greater water and energy usage per ton of ore processed or mass of gold produced. Life-cycle assessments for all gold deposit types (Norgate and Haque, 2012), indicate that a decrease in ore grade from 3.5 g/t to 2 g/t requires approximately 1.8 times as much water per ounce of gold produced (from 7,750 liter per ounce [L/oz] to 14,000 L/oz) and increases energy requirements by a factor of approximately 1.6 (from 6,200 Megajoule per ounce [MJ/oz] to 10,200 MJ/oz).

Although sodium cyanide usage in ore processing is carefully controlled and attendant techniques are well developed and regulated, accidental releases of cyanide have occurred. For example, a tailings impoundment failure at Baia Mare, Romania, a quartz-adularia epithermal deposit, that released 20,000 tons of sediment containing 120 tons of cyanide in 2000 (Baia Mare Task Force, 2000); an accident involving a truck delivering cyanide to the Kumtor Mine site in Kyrgyzstan in 1998 that resulted in the release of 1,760 kilograms of sodium cyanide into the Barskaun River (Hynes and others, 1998); and a cyanide release at the Summitville Mine (quartz-alunite epithermal deposit) in Colorado (U.S. Environmental Protection Agency, 2004); are high-profile examples of accidental cyanide releases into the environment.

Total cyanide, weak-acid-dissociable cyanide, and free cyanide constitute distinct forms of cyanide. Free cyanide is the most toxic, and is stable in low-pH solutions as CN^- or hydrogen cyanide gas (HCN). HCN is the predominant form of cyanide at pH <8. These conditions favor cyanide gas volatilization and dispersion into the air. Weak-acid-dissociable cyanide includes weak and moderately strong metal-cyanide complexes, including those of Ag, Cd, Cu, Ni, and Zn (Logsdon and others, 1999; Botz, 2001). These weak-acid-dissociable complexes can be toxicologically hazardous because, during dissociation, they form free cyanide and release the complexed metals; these processes are mostly dependent on (low) pH (Logsdon and others, 1999; Mudder and others, 2001). Metals, especially gold and iron, form strong complexes with cyanide that do not easily dissociate in the environment.

Until the late 1970s, natural cyanide degradation in tailings ponds was the only process used for effluent detoxification. Since then, mining operations have added chemical treatment technologies to supplement or replace the natural processes (Demopoulos and Cheng, 2004). These treatments include chemical oxidation by sulfur dioxide and air (INCO process) to create cyanate ([OCN^-]), oxidation by hydrogen peroxide, oxidation by peroxymonosulfuric acid (H_2SO_5, also known as Caro's acid), alkaline chlorination (formerly widely used but mostly replaced by other processes), iron-cyanide precipitation, and biodegradation. Cyanide can also be stripped and recovered from solution by acidifying solutions to a pH of <8. This process creates aqueous HCN, which is air-stripped and volatilized as HCN gas, and then absorbed into an alkaline solution of sodium hydroxide (the Cyanisorb and AVR processes; Botz, 2001). Other recovery processes include the SART process (sulfidize, acidify, recycle, thicken), the Hannah process (strong base resin extraction of free cyanide and metal cyanides), and the AuGMENT process (strong base resin extraction of copper and cyanide) (SGS Mineral Services, 2013). Demopoulos and Cheng's studies (2004) of the relative costs of cyanide recovery versus destruction suggest that destruction is more effective, especially because recovery techniques alone cannot meet environmental standards. However, recovery followed by secondary treatment and destruction could be effective, and may ameliorate concerns relative to cyanide use and management in some parts of the world; if so, cyanide recovery and destruction may constitute an attractive future alternative.

Processes operating naturally in the environment also attenuate cyanide. These processes include metal chelation (complexation), predominantly with iron, which can immobilize cyanide through sorption onto organic or inorganic surfaces. Iron cyanide-metal complexes also precipitate over a broad pH range (Mudder and others, 2001). Oxidation of cyanide produces cyanate, which is significantly less toxic. This reaction requires a strong oxidizer, and consequently is not particularly active on a large scale in natural systems; however, in engineered processes, oxidation can be applied to degrade cyanide. Bioattenuation by soil bacteria, a process that is most effective under aerobic conditions, can convert cyanide compounds to ammonia and then to nitrates. Formation of thiocyanate from free cyanide by reaction with forms of sulfur, mostly polysulfides and thiosulfate, also attenuates cyanide in the environment; importantly, thiocyanate is less toxic than free cyanide (Mudder and others, 2001). Thorough overviews of cyanide chemistry and geochemistry are provided in Logsdon and others (1999), Botz (2001), Mudder and others (2001), and Demopoulos and Cheng (2004).

Other ecosystem concerns include the effects, on soil and surface water systems, of windblown dust that contains sulfide or sulfate salts, and the effect of smelter emissions on air and soil quality. Mercury associated with some alkalic-type epithermal gold deposits may be released into the environment by mining and milling operations. This potential is a serious environmental concern in warm, humid climates where methylated compounds may form. Most alkalic-type epithermal gold deposits do not contain high mercury concentrations, but at historical sites and at modern-day artisanal operations, mercury has been or is used to amalgamate gold; the attendant releases of mercury pose significant environmental risks. Tailings and waste piles need to be properly engineered in arctic or tundra settings to prevent drainage seepage into permafrost and to prevent impoundment dam failure associated with basal permafrost saturation.

References Cited

Adams, M.D., ed., 2005, Advances in gold ore processing: Amsterdam, Elsevier, 1,076 p.

Afifi, A.M., Kelly, W.C., and Essene, E.J., 1988, Phase relations among tellurides, sulfides, and oxides—Pt. II, Application to telluride-bearing ore deposits: Economic Geology and the Bulletin of the Society of Economic Geologists, v. 83, no. 2, p. 395–404. [Also available at https://doi.org/10.2113/gsecongeo.83.2.395.]

Ahmad, M., Solomon, M., and Walshe, J.L., 1987, Mineralogical and geochemical studies of the Emperor gold telluride deposit, Fiji: Economic Geology and the Bulletin of the Society of Economic Geologists, v. 82, no. 2, p. 345–370. [Also available at https://doi.org/10.2113/gsecongeo.82.2.345.]

Alderton, D.H.M., and Fallick, A.E., 2000, The nature and genesis of gold-silver-tellurium mineralization in the Metaliferi Mountains of western Romania: Economic Geology and the Bulletin of the Society of Economic Geologists, v. 95, no. 3, p. 495–516. [Also available at https://doi.org/10.2113/gsecongeo.95.3.495.]

Allen, D.G., Panteleyev, A., and Armstrong, A.T., 1976, Galore Creek, *in* Sutherland Brown, A., ed., Porphyry deposits of the Canadian Cordillera—A volume dedicated to Charles S. Ney: [Montreal, Canada], Canadian Institute of Mining and Metallurgy, Special Volume 15, p. 402–414.

Anderson, W.B., and Eaton, P.C., 1990, Gold mineralisation at the Emperor Mine, Vatukoula, Fiji: Journal of Geochemical Exploration, v. 36, no. 1–3, p. 267–296. [Also available at https://doi.org/10.1016/0375-6742(90)90058-I.]

Baia Mare Task Force, 2000, Report of the international task force for assessing the Baia Mare accident, Reliefweb web page, accessed June 16, 2014, at https://reliefweb.int/report/hungary/report-international-task-force-assessing-baia-mare-accident.

Banks, D.A., Yardley, B.W.D., Campbell, A.R., and Jarvis, K.E., 1994, REE composition of an aqueous magmatic fluid—A fluid inclusion study from the Capitan pluton, New Mexico, USA: Chemical Geology, v. 113, no. 3–4, p. 259–272. [Also available at https://doi.org/10.1016/0009-2541(94)90070-1.]

Barton, P.B., Jr., and Skinner, B.J., 1967, Sulfide mineral stabilities, *in* Barnes, H.L., ed., Geochemistry of hydrothermal ore deposits: New York, Holt, Rinehart and Winston, p. 236–333.

Begg, G., 1996, Genesis of the Vatukoula gold deposit, Fiji: Melbourne, Australia, Monash University, Ph.D. thesis, 466 p.

Begg, G., and Gray, D.R., 2002, Arc dynamics and tectonic history of Fiji based on stress and kinematic analysis of dikes and faults of the Tavua Volcano, Viti Levu Island, Fiji: Tectonics, v. 21, no. 4, p. 5(1)–5(14). [Also available at https://doi.org/10.1029/2000TC001259.]

Begg, G., Loucks, R., Gray, D., Foster, D., Kent, A., and Cooke, D.R., 2007, Gold and tectonics—A dynamic link [abs.], *in* Ores and Orogenesis—A Symposium Honoring the Career of William R. Dickinson, 2007, Programs with Abstracts: Tucson, Ariz., Arizona Geological Society, p. 90–91.

Bissig, T., Lee, J.K.W., Clark, A.H., and Heather, K.B., 2001, The Cenozoic history of volcanism and hydrothermal alteration in the central Andean flat-slab region—New ^{40}Ar–^{39}Ar constraints from the El Indio–Pascua Au (-Ag, Cu) Belt, 29°20′–30°30′S: International Geology Review, v. 43, no. 4, p. 312–340. [Also available at https://doi.org/10.1080/00206810109465016.]

Bonham, H.F., 1984, Three major types of epithermal precious-metal deposits: Geological Society of America Abstracts with Programs, v. 16, p. 449.

Bonham, H.F., 1986, Models for volcanic-hosted epithermal precious metal deposits—A review, *in* Proceedings of Symposium 5, Volcanism, Hydrothermal Systems and Related Mineralization, 1986: New Zealand, University of Auckland, International Volcanology Congress, p. 13–17.

Bonham, H.F., and Giles, D.L., 1983, Epithermal gold/silver deposits—The geothermal connection: Geothermal Resources Council Special Report, v. 13, p. 257–262.

Botz, M.M., 2001, Overview of cyanide treatment methods: London, Mining Environmental Management, Mining Journal Ltd., p. 28–30. [Also available at https://chemistry.mdma.ch/hiveboard/rhodium/pdf/cyanide.destruction.overview.pdf.]

Buret, Y., von Quadt, A., Heinrich, C., Selby, D., Wälle, M., and Peytcheva, I., 2016, From a long-lived upper-crustal magma chamber to rapid porphyry copper emplacement—Reading the geochemistry of zircon crystals at Bajo de la Alumbrera (NW Argentina): Earth and Planetary Science Letters, v. 450, p. 120–131. [Also available at https://doi.org/10.1016/j.epsl.2016.06.017.]

Cameron, G.H., Wall, V.J., Walshe, J.L., and Heinrich, C.A., 1995, Gold mineralization at the Porgera gold mine, Papua New Guinea, in response to fluid mixing, *in* Pacific Rim Congress ‘95, Auckland, New Zealand, 1995: Carlton, Australia, Australasian Institute of Mining and Metallurgy, no. 9, p. 99–100.

Campbell, A.R., Banks, D.A., Phillips, R.S., and Yardley, B.W.D., 1995, Geochemistry of Th-U-REE mineralizing magmatic fluids, Capitan Mountains, New Mexico: Economic Geology, v. 90, no. 5, p. 1271–1287. [Also available at https://doi.org/10.2113/gsecongeo.90.5.1271.]

Candela, P.A., 1989, Felsic magmas, volatiles, and metallogenesis, chap. 13 *of* Whitney, J.A., and Naldrett, A.J., eds., Reviews in economic geology, v. 4: Littleton, Colo., Society of Economic Geologists, p. 223–233.

Carman, G.D., 2003, Geology, mineralization, and hydrothermal evolution of the Ladolam gold deposit, Lihir Island, Papua New Guinea: Society of Economic Geologists, Special Publication, v. 10, p. 247–283. [Also available at https://doi.org/10.5382/SP.10.14.]

Carnein, C.R., and Bartos, P.J., 2005, The Cripple Creek mining district: The Mineralogical Record, v. 36, p. 143–185.

Chapin, C.E., 2012, Origin of the Colorado mineral belt: Geosphere, v. 8, no. 1, p. 28–43. [Also available at https://doi.org/10.1130/GES00694.1.]

Chiaradia, M., Schaltegger, U., Spikings, R., Wotzlaw, J., and Ovtcharova, M., 2013, How accurately can we date the duration of magmatic-hydrothermal events in porphyry systems?—An invited paper: Economic Geology and the Bulletin of the Society of Economic Geologists, v. 108, no. 4, p. 565–584. [Also available at https://doi.org/10.2113/econgeo.108.4.565.]

Clark, D.A., 1997, Magnetic petrophysics and magnetic petrology—Aids to geological interpretation of magnetic surveys: AGSO Journal of Australian Geology and Geophysics, v. 17, p. 83–103.

Clark, D.A., and Schmidt, P.W., 2001, Petrophysical properties of the Goonumbla Volcanic Complex, NSW—Implications for magnetic and gravity signatures of porphyry Cu-Au mineralisation: Exploration Geophysics, v. 32, no. 3–4, p. 171–175. [Also available at https://doi.org/10.1071/EG01171.]

Cocker, M.D., 1993, Primary element dispersion patterns in a carbonate-hosted, epithermal, high-grade Au-Ag telluride system—Mayflower Mine, Madison County, Montana, USA: Journal of Geochemical Exploration, v. 47, no. 1–3, p. 377–390. [Also available at https://doi.org/10.1016/0375-6742(93)90077-Y.]

Cook, N.J., Ciobanu, C.L., Damian, C.L., and Damian, F., 2004, Tellurides and sulphosalts from deposits in the Golden Quadrilateral, *in* Cook, N.J., and Ciobanu, C.L., eds., Gold-silver-telluride deposits of the Golden Quadrilateral, South Apuseni Mts: Romania, International Association on the Genesis of Ore Deposits Guidebook Series, v. 12, p. 111–144.

Cook, N.J., Ciobanu, C.L., Spry, P.G., and Voudouris, P., 2009, Understanding gold-(silver)-telluride-(selenide) mineral deposits: Journal of International Geoscience—Episodes, v. 32, no. 4, p. 249–263. [Also available at https://doi.org/10.18814/epiiugs/2009/v32i4/002.]

Cook, R.B., 2010, Connoisseur's choice—Calaverite, Cripple Creek, Colorado: Rocks and Minerals, v. 85, no. 5, p. 426–433. [Also available at https://doi.org/10.1080/00357529.2010.494151.]

Cooke, D.R., and McPhail, D.C., 2001, Epithermal Au-Ag-Te mineralization, Acupan, Baguio district, Philippines—Numerical simulations of mineral deposition: Economic Geology and the Bulletin of the Society of Economic Geologists, v. 96, no. 1, p. 109–131. [Also available at https://doi.org/10.2113/gsecongeo.96.1.109.]

Cooke, D.R., and Simmons, S.F., 2000, Characteristics and genesis of epithermal gold deposits: Reviews in Economic Geology, v. 13, p. 221–244.

Cooke, D.R., Tosdale, D., Chamberlain, C., and Deyell, C., 2006, Alkalic porphyry and epithermal deposits, *in* Sydney Minerals Exploration Discussion Group, Mines and Wines Conference 2006: Cessnock, New South Wales, Mineral Exploration Geoscience in NSW, Extended Abstracts, p. 7–10. [Also available at https://smedg.org.au/M&W06AllAbs.pdf.]

Cooke, D.R., Wilson, A.J., House, M.J., Wolfe, R.C., Walshe, J.L., Lickfold, V., and Crawford, A.J., 2007, Alkalic porphyry Au-Cu and associated mineral deposits of the Ordovician to Early Silurian Macquarie Arc, New South Wales: Australian Journal of Earth Sciences, v. 54, no. 2–3, p. 445–463. [Also available at https://doi.org/10.1080/08120090601146771.]

Cox, D.P., and Bagby, W.C., 1986, Descriptive model of Au-Ag-Te veins, *in* Cox, D.P., and Singer, D.A., eds., Mineral deposit models: U.S. Geological Survey Bulletin 1693, p. 124.

Cox, D.P., and Singer, D.A., eds., 1986, Mineral deposit models, U.S. Geological Survey Bulletin 1693, 379 p. [Also available at https://doi.org/10.3133/b1693.]

Craig, H., 1961, Isotopic variations in meteoric waters: Science, v. 133, no. 3465, p. 1702–1703. [Also available at https://doi.org/10.1126/science.133.3465.1702.]

Craig, H., 1963, The isotopic geochemistry of water and carbon in geothermal areas, *in* Tongiorgi, E., ed., Nuclear geology on geothermal areas: Pisa, Consiglio Nazionale dell Richerche, p. 17–53. [Also available at http://pubs.geothermal-library.org/lib/grc/1020382.pdf.]

Demopoulos, G.P., and Cheng, T.C., 2004, A case study of CIP tailings slurry treatment—Comparison of cyanide recovery to cyanide destruction: The European Journal of Mineral Processing and Environmental Protection, v. 4, no. 1, p. 1–9.

Denny, E.H., Marshall, K.L., Fieldner, A.C., Emery, A.H., Yant, W.P., and Selvig, W.A., 1930, Rock-strata gases of the Cripple Creek district, Colo. and their effect on mining: U.S. Department of Commerce Bureau of Mines Bulletin 317, 74 p.

Dentith, M.C., and Mudge, S.T., 2014, Geophysics for the mineral exploration geoscientist: Cambridge, Cambridge University Press, 438 p. [Also available at https://doi.org/10.1017/CBO9781139024358.]

Diggles, M.F., Rytuba, J.R., Moring, B.C., Wrucke, C.T., Cox, D.P., Ludington, S., Ashley, R.P., Pickthorn, W.J., Hillman, C.T., and Miller, R.J., 1996, Geology and mineral issues, chap. 18 *of* Erman, D.C., ed., Status of the Sierra Nevada—The Sierra Nevada Ecosystem Project: U.S. Geological Survey Digital Data Series DDS-43, v. 2, 28 p.

Dold, B.S., 1999, Mineralogical and geochemical changes of copper flotation tailings in relation to their original composition and climatic setting—Implications for acid mine drainage and element mobility: Geneva, Université de Genève, Section des Sciences de la Terre, Terre & Environment Series, n. 18, 230 p.

Dold, B.S., and Fontbote, L., 2001, Element cycling and secondary mineralogy in porphyry copper tailings as a function of climate, primary mineralogy, and mineral processing: Journal of Geochemical Exploration, v. 74, no. 1–3, p. 3–55. [Also available at https://doi.org/10.1016/S0375-6742(01)00174-1.]

Douglass, S.E., and Campbell, A.R., 1994, Characterization of alkaline rock-related mineralization in the Nogal mining district, Lincoln County, New Mexico: Economic Geology and the Bulletin of the Society of Economic Geologists, v. 89, no. 6, p. 1306–1321. [Also available at https://doi.org/10.2113/gsecongeo.89.6.1306.]

du Bray, E.A., ed., 1995, v. 95–831. Preliminary compilation of descriptive geoenvironmental mineral deposit models, U.S. Geological Survey Open-File Report, 275 p. [Also available at https://doi.org/10.3133/ofr95831.]

Dye, M.D., 2015, Mineralogical characterization and paragenesis of the Cripple Creek deposit, Colorado: Golden, Colo., Colorado School of Mines, M.S. thesis, 115 p. [Also available at https://mountainscholar.org/handle/11124/20103.]

Eaton, P.C., and Setterfield, T.N., 1993, The relationship between epithermal and porphyry hydrothermal systems within the Tavua Caldera, Fiji: Economic Geology and the Bulletin of the Society of Economic Geologists, v. 88, no. 5, p. 1053–1083. [Also available at https://doi.org/10.2113/gsecongeo.88.5.1053.]

Eckel, E.B., 1949, Geology and ore deposits of the La Plata district, Colorado: U.S. Geological Survey Professional Paper 219, 179 p. [Also available at https://doi.org/10.3133/pp219.]

Enns, S.G., Thompson, J.F.H., Stanley, C.R., and Yarrow, E.W., 1995, The Galore Creek porphyry copper-gold deposits, Northwest British Columbia, *in* Schroeter, T.G., ed., Porphyry deposits of the northwestern Cordillera of North America: Canadian Institute of Mining, Metallurgy, and Petroleum Special Volume, v. 46, p. 640–644.

Fehr, M.A., Hammond, S.J., and Parkinson, I.J., 2018, Tellurium stable isotope fractionation in chondritic meteorites and some terrestrial samples: Geochimica et Cosmochimica Acta, v. 222, p. 17–33. [Also available at https://doi.org/10.1016/j.gca.2017.10.010.]

Fey, D.L., Desborough, G.A., and Church, S.E., 2000, Comparison of two leach procedures applied to metal-mining related wastes in Colorado and Montana and a relative ranking method for mine wastes, *in* Fifth International Conference on Acid Rock Drainage, Littleton, Colo., 2000, Proceedings: Englewood, Colo., Society for Mining, Metallurgy, and Exploration, Inc., v. 2, p. 1477–1488.

Fey, D.L., Wirt, L., Besser, J.M., and Wright, W.G., 2002, Water quality and aquatic toxicity data of 2002 spring thaw conditions in the upper Animas River watershed, Silverton, Colorado: U.S. Geological Survey Open-File Report 02–0488, 20 p. [Also available at https://doi.org/10.3133/ofr02488.]

Finlayson, D.M., Korsch, R.J., Glen, R.A., Leven, J.H., and Johnstone, D.W., 2002, Seismic imaging and crustal architecture across the Lachlan Transverse Zone, a possible early cross-cutting feature of eastern Australia: Australian Journal of Earth Sciences, v. 49, no. 2, p. 311–321. [Also available at https://doi.org/10.1046/j.1440-0952.2002.00917.x.]

Ford, K., Keating, P., and Thomas, M.D., 2007, Overview of geophysical signatures associated with Canadian ore deposits: Canada Geological Association, Mineral Deposits Division, Special Publication 5, p. 939–970.

Fornadel, A.P., Spry, P.G., Hagneghadar, M.A., Schauble, E.A., Jackson, S.E., and Mills, S.J., 2017, Stable Te isotope fractionation in tellurium-bearing minerals from precious metal hydrothermal ore deposits: Geochimica et Cosmochimica Acta, v. 202, p. 215–230. [Also available at https://doi.org/10.1016/j.gca.2016.12.025.]

Fornadel, A.P., Spry, P.G., and Jackson, S.E., 2019, Geological controls on the stable tellurium isotope variation in tellurides and native tellurium from epithermal and orogenic gold deposits—Application to the Emperor gold-telluride deposit, Fiji: Ore Geology Reviews, v. 313, no. 103076, 9 p., accessed November 3, 2019, at https://doi.org/10.1016/j.oregeorev.2019.103076.

Fornadel, A.P., Spry, P.G., Jackson, S.E., Mathur, R.D., Chapman, J.B., and Girard, I., 2014, Methods for the determination of stable Te isotopes of minerals in the system Au-Ag-Te by MC-ICP-MS: Journal of Analytical Atomic Spectrometry, v. 29, no. 4, p. 623–637. [Also available at https://doi.org/10.1039/C3JA50237F.]

Fornadel, A.P., Voudouris, P.Ch., Spry, P.G., and Melfos, V., 2012, Mineralogical, stable isotope, and fluid inclusion studies of spatially related porphyry Cu and epithermal Au-Te mineralization, Fakos Peninsula, Limnos Island, Greece: Mineralogy and Petrology, v. 105, p. 85–111. [Also available at https://doi.org/10.1007/s00710-012-0196-8.]

Forrest, R.A., 1971, Geology and mineral deposits of the Warm Springs-Giltedge district, Fergus County, Montana: Butte, Mont., Montana College of Mineral Science and Technology, M.S. thesis, 191 p.

Forsythe, D.L., 1971, Vertical zoning of gold-silver tellurides in the Emperor gold mine, Fiji: Australian Institute of Mining and Metallurgy, Proceedings, 1971, v. 240, p. 25–31.

Forsythe, D.L., Spry, P.G., and Thompson, M.L., 2019, Petrological and mineralogical aspects of epithermal low-sulfidation Au- and porphyry Cu-style mineralization, Navilawa Caldera, Fiji: Geosciences, v. 9, no. 42, 25 p., accessed March 25, 2020, at https://doi.org/10.3390/geosciences9010042.

Foster, D.A., Mueller, P.A., Mogk, D.W., Wooden, J.L., and Vogl, J.J., 2006, Proterozoic evolution of the western margin of the Wyoming craton—Implications for the tectonic and magmatic evolution of the northern Rocky Mountains: Canadian Journal of Earth Sciences, v. 43, no. 10, p. 1601–1619. [Also available at https://doi.org/10.1139/e06-052.]

Foster, F., and Childs, J.F., 1993, An overview of significant lode gold systems in Montana, and their regional geologic setting: Exploration and Mining Geology, v. 2, no. 3, p. 217–244.

Fulignati, P., and Sbrana, A., 1998, Presence of native gold and tellurium in the active high-sulfidation hydrothermal system of the La Fossa volcano (Vulcano, Italy): Journal of Volcanology and Geothermal Research, v. 86, no. 1–4, p. 187–198. [Also available at https://doi.org/10.1016/S0377-0273(98)00078-X.]

Gantumur, H., Batulzii, D., Lijuan, W., and Heping, Z., 2005, Tsav—A shoshonite-hosted intermediate sulfidation epithermal Ag-Pb-Zn deposit, eastern Mongolia, *in* Mao, J., and Bierlein, F.P., eds., Mineral deposit research—Meeting the global challenge: Berlin, Springer, p. 389–392. [Also available at https://doi.org/10.1007/3-540-27946-6_102.]

Gast, P.W., 1968, Trace element fractionation and the origin of tholeiitic and alkaline magma types: Geochimica et Cosmochimica Acta, v. 32, no. 10, p. 1057–1086. [Also available at https://doi.org/10.1016/0016-7037(68)90108-7.]

Geller, B.A., 1994, Mineralogy and origin of telluride deposits in Boulder County, Colorado: Boulder, Colo., University of Colorado, Ph.D. dissertation, 731p.

Geoscience Australia, 2018, Geoscience Australia website, accessed January 5, 2018, at http://www.ga.gov.au/.

Glen, R.A., Korsch, R.J., Direen, N.G., Jones, L.E.A., Johnstone, D.W., Lawrie, K.C., Finlayson, D.M., and Shaw, R.D., 2002, Crustal structure of the Ordovician Macquarie Arc, Eastern Lachlan Orogen, based on seismic-reflection profiling: Australian Journal of Earth Sciences, v. 49, no. 2, p. 323–348. [Also available at https://doi.org/10.1046/j.1440-0952.2002.00925.x.]

Gott, G.B., McCarthy, J.H., Van Sickel, G.H., and McHugh, J.B., 1969, Distribution of gold and other metals in the Cripple Creek District, Colorado: U.S. Geological Survey Professional Paper 625-A, p. A1–A17. [Also available at https://doi.org/10.3133/pp625A.]

Greenland, L.P., and Aruscavage, P., 1986, Volcanic emission of Se, Te, and As from Kilauea Volcano, Hawaii: Journal of Volcanology and Geothermal Research, v. 27, no. 1–2, p. 195–201. [Also available at https://doi.org/10.1016/0377-0273(86)90086-7.]

Griswold, G.B., 1959, Mineral deposits of Lincoln County, New Mexico: New Mexico Bureau of Mines and Mineral Resources Bulletin 67, 117 p. [Also available at https://geoinfo.nmt.edu/publications/monographs/bulletins/downloads/67/Bulletin67.pdf.]

Gröpper, H., Calvo, M., Crespo, H., Bisso, C.R., Cuadra, W.A., Dunkerley, P.M., and Aguirre, E., 1991, The epithermal gold-silver deposit of Choquelimpie, northern Chile: Economic Geology and the Bulletin of the Society of Economic Geologists, v. 86, no. 6, p. 1206–1221. [Also available at https://doi.org/10.2113/gsecongeo.86.6.1206.]

Grundler, P.V., Brugger, J., Etschmann, B.E., Helm, L., Liu, W., Spry, P.G., Tian, Y., Testemale, D., and Pring, A., 2013, Speciation of aqueous tellurium (IV) in hydrothermal solutions and vapors, and the role of oxidized tellurium species in Te transport and gold deposition: Geochimica et Cosmochimica Acta, v. 120, p. 298–325. [Also available at https://doi.org/10.1016/j.gca.2013.06.009.]

Gunn, P.J., Mackey, T., and Meixner, A.J., 2009a, Magnetic, radiometric and gravity signatures of localities of epithermal gold deposits in Fiji, *in* Petterson, M.G., ed., Pacific minerals in the new millennium—Science, Exploration, Mining, and Community—The Jackson Lum Volume: Pacific Islands Applied Geoscience Commission, Technical Bulletin 11 p. 77–84.

Gunn, P.J., Mackey, T., and Meixner, A.J., 2009b, The Fiji airborne geophysical survey project, *in* Petterson, M.G., ed., Pacific minerals in the new millennium—Science, Exploration, Mining, and Community—The Jackson Lum Volume: Pacific Islands Applied Geoscience Commission, Technical Bulletin 11 p. 53–75.

Hastings, J.S., 1988, Gold deposits of the Zortman-Landusky, Little Rocky Mountains, Montana, *in* Schafer, R.W., Cooer, J.J., and Vikre, P.G., eds., Bulk mineable precious metal deposits of the western United States: The Geological Society of Nevada, p. 187–205.

Hayashi, K., and Ohmoto, H., 1991, Solubility of gold in NaCl-and H_2S-bearing aqueous solutions at 250–350°C: Geochimica et Cosmochimica Acta, v. 55, no. 8, p. 2111–2126. [Also available at https://doi.org/10.1016/0016-7037(91)90091-I.]

Hayba, D.O., Bethke, P.M., Heald, P., and Foley, N.K., 1985, Geologic, mineralogic, and geochemical characteristics of volcanic-hosted epithermal precious-metal deposits: Reviews in Economic Geology, v. 2, p. 129–167.

Heald, P., Foley, N.K., and Hayba, D.O., 1987, Comparative anatomy of volcanic-hosted epithermal deposits; acid-sulfate and adularia-sericite types: Economic Geology and the Bulletin of the Society of Economic Geologists, v. 82, no. 1, p. 1–26. [Also available at https://doi.org/10.2113/gsecongeo.82.1.1.]

Heald-Wetlaufer, P., Hayba, D.O., Foley, N.K., and Gross, J.A., 1983, Comparative anatomy of epithermal precious- and base-metal districts hosted by volcanic rocks—A talk presented at the GAC/MSC/GGU joint annual meeting, May 11–13, 1983, Victoria, British Columbia: U.S. Geological Survey Open-File Report 83–710, 20 p. [Also available at https://doi.org/10.3133/ofr83710.]

Hedenquist, J.W., 1987, Mineralization associated with volcanic-related hydrothermal systems in the Circum-Pacific Basin, chap. 44 *of* Horn, M.K., ed., Transactions of the Fourth Circum-Pacific Energy and Mineral Resources Conference—August 17–22, 1986: Singapore, Circum-Pacific Council for Energy and Mineral Resources, American Association of Petroleum Geologists, p. 513–524.

Hedenquist, J.W., Arribas, A., Jr., and Reynolds, T.J., 1998, Evolution of an intrusion-centered hydrothermal system—Far southeast-Lepanto porphyry and epithermal Cu-Au deposits, Philippines: Economic Geology and the Bulletin of the Society of Economic Geologists, v. 93, no. 4, p. 373–404. [Also available at https://doi.org/10.2113/gsecongeo.93.4.373.]

Heithersay, P.S., and Walshe, J.L., 1995, Endeavour 26 North—A porphyry copper-gold deposit in the Late Ordovician, shoshonitic Goonumbla Volcanic Complex, New South Wales, Australia: Economic Geology and the Bulletin of the Society of Economic Geologists, v. 90, no. 6, p. 1506–1532. [Also available at https://doi.org/10.2113/gsecongeo.90.6.1506.]

Holley, E.A., Bissig, T., and Monecke, T., 2016, The Veladero high-sulfidation epithermal gold deposit, El Indio-Pascua Belt, Argentina—Geochronology of alunite and jarosite: Economic Geology and the Bulletin of the Society of Economic Geologists, v. 111, no. 2, p. 311–330. [Also available at https://doi.org/10.2113/econgeo.111.2.311.]

Holliday, J.R., and Cooke, D.R., 2007, Advances in geological models and exploration methods for copper ± gold porphyry deposits, *in* Milkereit, B., ed., Exploration 07—Exploration in the new Millenium, 5th Decennial International Conference on Mineral ExplorationToronto, 2007, Proceedings: Toronto, Decennial Mineral Exploration Conferences, p. 791–809. [Also available at http://www.dmec.ca/ex07-dvd/E07/pdfs/53.pdf.]

Holliday, J.R., Wilson, A.J., Blevin, P.L., Tedder, I.J., Dunham, P.D., and Pfitzner, M., 2002, Porphyry gold–copper mineralisation in the Cadia district, eastern Lachlan Fold Belt, New South Wales, and its relationship to shoshonitic magmatism: Mineralium Deposita, v. 37, p. 100–116. [Also available at https://doi.org/10.1007/s00126-001-0233-8.]

Hu, H.B., Mao, J.W., Niu, S.Y., Li, Y.F., and Li, M.W., 2006, Geology and geochemistry of telluride-bearing Au deposits in the Pingyi area, Western Shandong, China: Mineralogy and Petrology, v. 87, p. 209–240. [Also available at https://doi.org/10.1007/s00710-006-0126-8.]

Hynes, T.P., Harrison, J., Bonitenko, E., Doronina, T.M., Baikowitz, H., James, M., and Zinck, J.M., 1998, The International Scientific Commission's assessment of the impact of the cyanide spill at Barskaun, Kyrgyz Republic, May 20, 1998: CANMET Mining and Mineral Sciences Laboratories Report MMSL 98-039(CR), 111 p.

International Institute for Environment and Development, 2002, Mining for the future, Appendix 1—Porgera riverine disposal case study: International Institute for Environment and Development, MMSD Working Paper Series no. 68b, 16 p., accessed June 16, 2014, at https://pubs.iied.org/pdfs/G00562.pdf.

Irvine, T.N., and Baragar, W.R.A., 1971, A guide to the chemical classification of the common volcanic rocks: Canadian Journal of Earth Sciences, v. 8, no. 5, p. 523–548. [Also available at https://doi.org/10.1139/e71-055.]

Jago, C.P., Tosdal, R.M., Cooke, D.R., and Harris, A.C., 2014, Vertical and lateral variation of mineralogy and chemistry in the Early Jurassic Mt. Milligan alkalic porphyry Au-Cu deposit, British Columbia, Canada: Economic Geology and the Bulletin of the Society of Economic Geologists, v. 109, no. 4, p. 1005–1033. [Also available at https://doi.org/10.2113/econgeo.109.4.1005.]

Jenkins, T.T., and Carter, J.L., 1997, Soil tellurium and other elements as geochemical guides to gold, silver, and tellurium deposits, Rex Mine, Gold Hill mining district, Boulder County, Colorado: Geological Society of America Abstracts with Programs, v. 29, no. 6, p. 443–444.

Jensen, E.P., 2003, Magmatic and hydrothermal evolution of the Cripple Creek gold deposit, Colorado, and comparisons with regional and global magmatic-hydrothermal systems associated with alkaline magmatism: Tucson, Ariz., University of Arizona, Ph.D. dissertation, 846 p. [Also available at https://repository.arizona.edu/handle/10150/280422.]

Jensen, E.P., and Barton, M.D., 2000, Gold deposits related to alkaline magmatism: Reviews in Economic Geology, v. 13, p. 279–314. [Also available at https://doi.org/10.5382/Rev.13.08.]

John, D.A., Vikre, P.G., du Bray, E.A., Blakely, R.J., Fey, D.L., Rockwell, B.W., Mauk, J.L., Anderson, E.D., and Graybeal, F.T., 2018, Descriptive models for epithermal gold-silver deposits: U.S. Geological Survey Scientific Investigations Report 2010–5070–Q, 247 p. [Also available at https://doi.org/10.3133/sir20105070Q.]

Kadel-Harder, I., and Price, P., 2017, Remote sensing of alteration signatures associated with epithermal and porphyry-related mineral deposits using WorldView-3, ASTER, and Hyperion data, *in* Kleinhans, L.C., Little, M.L., and Modreski, P.J., eds., Gold and Silver Deposits in Colorado Symposium, Golden, Colo., 2017: Golden, Colo., Colorado School of Mines, p. 104–105.

Kelley, K.D., Armbrustmacher, T.J., and Klein, D.P., 1995, Au-Ag-Te vein deposits, chap. 15 *in* du Bray, E.A., ed., Preliminary compilation of descriptive geoenvironmental mineral deposit models: U.S. Geological Survey Open-File Report 95–0831, p. 130–136. [Also available at https://pubs.usgs.gov/of/1995/ofr-95-0831/.]

Kelley, K.D., Jensen, E.P., Rampe, J.S., and White, D., 2020, Epithermal gold deposits related to alkaline igneous rocks in the Cripple Creek district: Society of Economic Geologists Special Publication 23, in press.

Kelley, K.D., and Ludington, S., 2002, Cripple Creek and other alkaline-related gold deposits in the southern Rocky Mountains, USA—Influence of regional tectonics: Mineralium Deposita, v. 37, p. 38–60. [Also available at https://doi.org/10.1007/s00126-001-0229-4.]

Kelley, K.D., Romberger, S.B., Beaty, D.W., Pontius, J.A., Snee, L.W., Stein, H.J., and Thompson, T.B., 1998, Geochemical and geochronological constraints on the genesis of Au-Te deposits at Cripple Creek, Colorado: Economic Geology and the Bulletin of the Society of Economic Geologists, v. 93, no. 7, p. 981–1012. [Also available at https://doi.org/10.2113/gsecongeo.93.7.981.]

Kelley, K.D., and Spry, P.G., 2016, Critical elements in alkaline igneous rock-related epithermal gold deposits, chap. 9 *of* Verplanck, P.L., and Hitzman, M.W., eds., Rare earth and critical elements in ore deposits: Reviews in Economic Geology, v. 18, p. 195–216. [Also available at https://doi.org/10.5382/Rev.18.09.]

Kelly, W.C., and Goddard, E.N., 1969, Telluride ores of Boulder County, Colorado: Geological Society of America Memoir 109, 237 p. [Also available at https://doi.org/10.1130/MEM109-p1.]

Kleinkopf, M.D., Peterson, D.L., and Gott, G., 1970, Geophysical studies of the Cripple Creek mining district, Colorado: Geophysics, v. 35, no. 3, p. 490–500. [Also available at https://doi.org/10.1190/1.1440110.]

Koschmann, A.H., 1949, Structural control of the gold deposits of the Cripple Creek district Teller County, Colorado: U.S. Geological Survey Bulletin 995B, 60 p. [Also available at https://pubs.usgs.gov/bul/0955b/report.pdf.]

Kovalenker, V.A., Plotinskaya, O.Y., Prokof'ev, V.Y., Gertman, Y.L., Koneev, R.I., and Pomortsev, V.V., 2003, Mineralogy, geochemistry, and genesis of gold-sulfide-selenide-telluride ores from the Kairagach deposit (Uzbekistan): Geology of Ore Deposits, v. 45, no. 3, p. 171–200.

Kovalenker, V.A., Safonov, Y.G., Naumov, V.B., and Rusinov, V.L., 1997, The epithermal gold-telluride Kochbulak deposit (Uzbekistan): Geology of Ore Deposits, v. 39, no. 2, p. 127–152.

Kruse, F.A., Bedell, R.L., Taranik, J.V., Peppin, W.A., Weatherbee, O., and Calvin, W.M., 2012, Mapping alteration minerals at prospect, outcrop and drill core scales using imaging spectrometry: International Journal of Remote Sensing, v. 33, no. 6, p. 1780–1798. [Also available at https://doi.org/10.1080/01431161.2011.600350.]

Kwak, T.A.P., 1990, Geochemical and temperature controls on ore mineralization at the Emperor gold mine, Vatukoula, Fiji: Journal of Geochemical Exploration, v. 36, no. 1–3, p. 297–337. [Also available at https://doi.org/10.1016/0375-6742(90)90059-J.]

Lang, J.R., Lueck, B., Mortensen, J.K., Russel, J.K., Stanley, C.R., and Thompson, J.F.H., 1995, Triassic-Jurassic silica-undersaturated and silica-saturated alkalic intrusions in the cordillera of British Columbia—Implications for arc magmatism: Geology, v. 23, no. 5, p. 451–454. [Also available at https://doi.org/10.1130/0091-7613(1995)023<0451:TJSUAS>2.3.CO;2.]

Lapakko, K., and Lawrence, L.W., 1993, Modification of the net acid production (NAP) test, *in* Mine Reclamation, Building Confidence—The 17th annual British Columbia Mine Reclamation Symposium, Port Hardy, British Columbia, 1993, Proceedings: British Columbia, Canada, British Columbia Technical and Research Committee on Reclamation, p. 145–159.

Le Bas, M.J., Le Maitre, R.W., Streckeisen, A., and Zenettin, B., 1986, A chemical classification of volcanic rocks based on the total alkali-silica diagram: Journal of Petrology, v. 27, no. 3, p. 745–750. [Also available at https://doi.org/10.1093/petrology/27.3.745.]

Lee, D.C., and Halliday, A.N., 1995, Precise determinations of the isotopic compositions and atomic weights of molybdenum, tellurium, tin and tungsten using ICP magnetic sector multiple collector mass spectrometry: International Journal of Mass Spectrometry and Ion Processes, v. 146–147, p. 35–46. [Also available at https://doi.org/10.1016/0168-1176(95)04201-U.]

LeFort, D., Hanley, J., and Guillong, M., 2011, Subepithermal Au-Pd mineralization associated with an alkalic porphyry Cu-Au deposit, Mount Milligan, Quesnel Terrane, British Columbia, Canada: Economic Geology and the Bulletin of the Society of Economic Geologists, v. 106, no. 5, p. 781–808. [Also available at https://doi.org/10.2113/econgeo.106.5.781.]

Levett, J., and Logan, K.J.F., 1998, Geophysics of the Porgera gold mine, Papua New Guinea: Exploration Geophysics, v. 29, no. 3–4, p. 472–476. [Also available at https://doi.org/10.1071/EG998472.]

Lihir Gold Limited, 2006, Environmental Annual Report 2006, vol.1 (Main report) and vol. 2 (apps.): Melbourne, Australia, Newcrest Mining Limited, 108 p., accessed June 16, 2014, at http://lihir.ipb.icemedia.com.au/data/portal/.../93206001182987243642.pdf.

Lindgren, W., and Ransome, F.L., 1906, Geology and gold deposits of the Cripple Creek district, Colorado: U. S. Geological Survey Professional Paper 54, 516 p. [Also available at https://doi.org/10.5962/bhl.title.150479.]

Lindsey, D.A., 1985, A gold-mineralized breccia zone at Kendall, North Moccasin Mountains, Fergus County, Montana: U.S. Geological Survey Professional Paper 1301-C, p. 43–56. [Also available at https://doi.org/10.3133/pp1301.]

Lindsey, D.A., and Fisher, F.S., 1985, Mineralized breccias in intrusive complexes of Late Cretaceous and Paleocene age, north-central Montana: U.S. Geological Survey Professional Paper 1301-A, p. 1–34. [Also available at https://doi.org/10.3133/pp1301.]

Lindsey, D.A., and Naeser, C.W., 1985, Relation between igneous intrusion and gold mineralization in the North Moccasin Mountains, Fergus County, Montana: U.S. Geological Survey Professional Paper 1301-B, p. 35–41. [Also available at https://doi.org/10.3133/pp1301.]

Lisenbee, A.L., 1981, Studies of the Tertiary intrusions of the northern Black Hills uplift, South Dakota and Wyoming—A historical review, *in* Rich, F.J., ed., Geology of the Black Hills, South Dakota and Wyoming: American Geological Institute, p. 106–125.

Liu, J., Bai, X., Zhao, S., Tran, M., Zhang, Z., Zhao, Z., Zhao, H., and Lu, J., 2011, Geology of the Sandaowanzi telluride gold deposit of the northern Great Xing'an Range, NE China—Geochronology and tectonic controls: Journal of Asian Earth Sciences, v. 41, no. 2, p. 107–118. [Also available at https://doi.org/10.1016/j.jseaes.2010.12.011.]

Liu, J., Zhao, S., Cook, N.J., Bai, X., Zhang, Z., Zhao, Z., Zhao, H., and Lu, J., 2013, Bonanza-grade accumulations of gold tellurides in the Early Cretaceous Sandaowanzi deposit, northeast China: Ore Geology Reviews, v. 54, p. 110–126. [Also available at https://doi.org/10.1016/j.oregeorev.2013.03.003.]

Livo, E.K., 1994, Use of remote sensing to characterize hydrothermal alteration of the Cripple Creek area, Colorado: Golden, Colo., Colorado School of Mines, Department of Geology and Geological Engineering, M.S. thesis, 139 p.

Logsdon, M.J., Hagelstein, K., and Mudder, T.I., 1999, The Management of cyanide in gold extraction: Ottawa, Canada, International Council on Metals and the Environment, 44 p.

Longo, A.A., Dilles, J.H., Grunder, A.L., and Duncan, R., 2010, Evolution of calc-alkaline volcanism and associated hydrothermal gold deposits at Yanacocha, Peru: Economic Geology and the Bulletin of the Society of Economic Geologists, v. 105, no. 7, p. 1191–1241. [Also available at https://doi.org/10.2113/econgeo.105.7.1191.]

Loughlin, G.F., and Koschmann, A.H., 1935, Geology and ore deposits of the Cripple Creek district, Colorado: Lakewood, Colo., Colorado Scientific Society Proceedings, v. 13, p. 217–435.

Lovering, T.S., and Tweto, O.L., 1953, Geology and ore deposits of the Boulder County tungsten district, Colorado: U.S. Geological Survey Professional Paper 245, 199 p. [Also available at https://pubs.usgs.gov/pp/0245/report.pdf.]

Lowenstern, J.B., 2001, Carbon dioxide in magmas and implications for hydrothermal systems: Mineralium Deposita, v. 36, no. 6, p. 490–502. [Also available at https://doi.org/10.1007/s001260100185.]

Mao, J., Wang, Y., Ding, T., Chen, Y., Wei, J., and Yin, J., 2002, Dashuigou tellurium deposit in Sichuan Province, China—S, C, O, and H isotope data and their implications on hydrothermal mineralization: Resource Geology, v. 52, no. 1, p. 15–23. [Also available at https://doi.org/10.1111/j.1751-3928.2002.tb00113.x.]

Margolis, J., 1993, Geology and intrusion-related copper-gold mineralization, Sulphurets, British Columbia: Eugene, Oreg., University of Oregon, Ph. D. thesis, 289 p.

Maynard, S.R., 1995, Gold mineralization associated with mid-Tertiary magmatism and tectonism, Ortiz Mountains, Santa Fe County, New Mexico, *in* Bauer, P.W., Kues, B.S., Dunbar, N.W., Karlstrom, K.E., and Harrison, B., eds., Geology of the Santa Fe region: New Mexico Geological Society, 46th field conference guidebook, p. 161–166. [Also available at https://nmgs.nmt.edu/publications/guidebooks/downloads/46/46_p0161_p0166.pdf.]

McEwan, C.J.A., Fallick, A.E., and Rice, C.M., 1996, The Rosita Hills epithermal Ag-base metal deposits, Colorado, USA—A stable isotope and fluid inclusion study: Mineralium Deposita, v. 31, no. 1, p. 41–51. [Also available at https://doi.org/10.1007/BF00225394.]

McInnes, B.I.A., Evans, N.J., McBride, J.S., and Lambert, D.D., 1998, Osmium isotope and noble metal enrichment of the mantle source region of the Ladolam gold deposit Lihir Island, PNG: Boulder, Colo., Geological Society of America, 1998 Annual Meeting and Exposition, v. 30, p. 302.

McLemore, V.T., 1996, Great Plains Margin (alkaline-related) gold deposits in New Mexico, *in* Coyner, A.R., Fahey, P.L., eds., Geology and ore deposits of the American Cordillera: Geological Society of Nevada Symposium Proceedings, v. 2, p. 935–950.

McLemore, V.T., 2001, RM-21—Silver and gold in New Mexico: New Mexico Bureau of Geology & Mineral Resources, Resource Map 21, 62 p. [Also available at https://geoinfo.nmt.edu/publications/maps/resource/21/.]

McLemore, V.T., 2010, Geology and mineral deposits of the Gallinas Mountains, Lincoln and Torrance Counties, New Mexico—Preliminary report: New Mexico Bureau of Geology and Mineral Resources Open–File Report OF–532, 92 p. [Also available at https://geoinfo.nmt.edu/publications/openfile/downloads/500-599/532/ofr_532.pdf.]

McLemore, V.T., 2015, Great Plains Margin (alkaline-related) gold deposits in New Mexico—Twenty years later, *in* New Concepts and Discoveries—The Geological Society of Nevada Symposium, Sparks, Nev., 2015, Proceedings: Reno, Nev., Geological Society of Nevada.

McLemore, V.T., 2018, Rare earth elements (REE) deposits associated with Great Plain Margin deposits (alkaline-related), southwestern United States and eastern Mexico: Socorro, N. Mex., New Mexico Bureau of Geology and Mineral Resources, Resources, v. 7, no. 1, 44 p. [Also available at https://doi.org/10.3390/resources7010008.]

McLemore, V.T., and North, R.M., 1987, Metallic mineral deposits in Colfax and Union Counties, northeastern New Mexico, *in* Lucas, S.G., and Hunt, A.P., eds., Northeastern New Mexico—Guidebook to the 38th Field Conference: Socorro, N.Mex., New Mexico Geological Society, p. 323–329. [Also available at https://nmgs.nmt.edu/publications/guidebooks/downloads/38/38_p0323_p0329.pdf.]

McPhail, D.C., 1995, Thermodynamic properties of aqueous tellurium species between 25 and 350°: Geochimica et Cosmochimica Acta, v. 59, no. 5, p. 851–866. [Also available at https://doi.org/10.1016/0016-7037(94)00353-X.]

Mindat, 2014, Dongping Mine, Dongping Au-Te ore field, Chongli Co., Zhangjiakou Prefecture, Hebei Province, China: Mindat website, accessed June 14, 2014, at https://www.mindat.org/loc-135170.html.

MiningLink, 2014, Porgera: MiningLink website, accessed June 16, 2014, at http://mininglink.com.au/mine/porgera.

Moyle, A.L., Doyle, B.J., Hoogvliet, H., and Ware, A.R., 1990, Ladolam gold deposit, Lihir Island: Australian Institute of Mining and Metallurgy Monograph Series, v. 14, p. 1793–1805.

Mudd, G.M., 2007, Global trends in gold mining—Towards quantifying environmental and resource sustainability: Resources Policy, v. 32, no. 1–2, p. 42–56. [Also available at https://doi.org/10.1016/j.resourpol.2007.05.002.]

Mudder, T.I., Botz, M.M., and Smith, A., 2001, Chemistry and treatment of cyanidation wastes, 2nd ed.: London, Mining Journal Books, 391 p. [Also available at http://dana6.free.fr/3%20060713%20English%20Compendium.pdf.]

Müller, D., Franz, L., Herzig, P.M., and Hunt, S., 2001, Potassic igneous rocks from the vicinity of epithermal gold mineralization, Lihir Island, Papua New Guinea: Lithos, v. 57, no. 2–3, p. 163–186. [Also available at https://doi.org/10.1016/S0024-4937(01)00035-4.]

Müller, D., and Groves, D.I., 2019, Potassic igneous rocks and associated gold-copper mineralization, 5th ed: Switzerland, Springer Nature, 398 p. [Also available at https://doi.org/10.1007/978-3-319-92979-8.]

Mutschler, F.E., 1992, Alkaline igneous systems and related mineral deposits, in Annual Pacific Northwest Mining and Metals Conference, 1992, Short Course Notes: Spokane, Wash., Northwest Mining Association.

Mutschler, F.E., Griffen, M.E., Stevens, D.S., and Shannon, S.S., Jr., 1985, Precious metal deposits related to alkaline rocks in the North American Cordillera—An interpretive review: South African Journal of Geology, v. 88, no. 2, p. 355–377.

Mutschler, F.E., Larson, E.E., and Ross, M.L., 1998, Potential for alkaline igneous rock-related gold deposits in the Colorado Plateau Laccolithic Centers, *in* Friedman, J.D., and Huffman, A.C., Jr., Laccolith complexes of southeastern Utah; time of emplacement and tectonic setting—Workshop proceedings: U.S. Geological Survey Bulletin 2158, p. 233–252.

Mutschler, F.E., and Mooney, T.C., 1995, Precious metal deposits related to alkaline igneous rocks—Provisional classification, grade-tonnage data, and exploration frontiers: Canada Geological Association Special Paper, IAGOD 1990 Symposium on Ore Deposit Models, 22 p.

Mutschler, F.E., Mooney, T.C., and Johnson, D.C., 1991, Precious metal deposits related to alkaline igneous rocks—A space-time trip through the Cordillera: Mining Engineering, v. 43, no. 3, p. 304–309.

Nash, J.T., and Cunningham, C.G., 1973, Fluid-inclusion studies of the fluorspar and gold deposits, Jamestown district, Colorado: Economic Geology and the Bulletin of the Society of Economic Geologists, v. 68, no. 8, p. 1247–1262. [Also available at https://doi.org/10.2113/gsecongeo.68.8.1247.]

Nixon, G.T., and Archibald, D.A., 2001, Age of platinum-group-element mineralization in the Sappho alkaline complex, south-central British Columbia: British Columbia Geological Survey Paper 2002–1, p. 171–176.

Nordstrom, D.K., and Alpers, C.N., 1997, Geochemistry of acid mine waters, *in* Plumlee, G.S., Logsdon, M.J., and Filipek, L.F., eds., The environmental geochemistry of mineral deposits—Part A—Processes, techniques, and health issues: Society of Economic Geologists, Reviews in Economic Geology, v. 6, p. 161–182. [Also available at https://doi.org/10.5382/Rev.06.06.]

Norgate, T., and Haque, N., 2012, Using life cycle assessment to evaluate some environmental impacts of gold production: Journal of Cleaner Production, v. 29–30, p. 53–63. [Also available at https://doi.org/10.1016/j.jclepro.2012.01.042.]

Oldenburg, D.W., Li, Y., and Ellis, R.G., 1997, Inversion of geophysical data over a copper gold porphyry deposit—A case history for Mt. Milligan: Geophysics, v. 62, no. 5, p. 1419–1431. [Also available at https://doi.org/10.1190/1.1444246.]

Oyer, N., Childs, J., and Mahoney, J.B., 2014, Regional setting and deposit geology of the Golden Sunlight Mine—An example of responsible resource extraction, *in* Shaw, C.A., and Tikoff, B., eds., Exploring the northern Rocky Mountains: Geological Society of America Field Guide, v. 37, p. 115–144. [Also available at https://doi.org/10.1130/2014.0037(06).]

Pals, D.W., and Spry, P.G., 2003, Telluride mineralogy of the low-sulfidation epithermal Emperor gold deposit, Vatukoula, Fiji: Mineralogy and Petrology, v. 79, no. 3, p. 285–307. [Also available at https://doi.org/10.1007/s00710-003-0013-5.]

Pals, D.W., Spry, P.G., and Chryssoulis, S., 2003, Invisible gold and tellurium in arsenic-rich pyrite from the Emperor gold deposit, Fiji—Implications for gold distribution and deposition: Economic Geology and the Bulletin of the Society of Economic Geologists, v. 98, no. 3, p. 479–493. [Also available at https://doi.org/10.2113/gsecongeo.98.3.479.]

Paterson, C.J., Uzunlar, N., Groff, J., and Longstaffe, F.J., 1989, A view through an epithermal-mesothermal precious metal system in the northern Black Hills, South Dakota—A magmatic origin for the ore-forming fluids, *in* Keays, R.R., Ramsay, W.R.H., and Groves, D.I., eds., The geology of gold deposits—The perspective in 1988: Economic Geology Monograph Series, v. 6, p. 564–570. [Also available at https://doi.org/10.5382/Mono.06.43.]

Peccerillo, A., and Taylor, S.R., 1976, Geochemistry of the Eocene calc-alkaline volcanic rocks in the Kastamonu area, northern Turkey: Contributions to Mineralogy and Petrology, v. 58, no. 1, p. 63–81. [Also available at https://doi.org/10.1007/BF00384745.]

Phillips, R.S., 1990, Geochemistry of hydrothermal Th-U-REE quartz/fluorite veins, Capitan pluton, New Mexico—Evidence for a magmatic/hydrothermal origin: Socorro, N. Mex., New Mexico Institute of Mining and Technology, M.S. thesis, 214 p.

Phillips, R.S., Campbell, A.R., and McLemore, V.T., 1991, Th-U-REE quartz/fluorite veins, Capitan pluton, New Mexico—Evidence for a magmatic/hydrothermal origin: New Mexico Geological Society Guidebook, v. 42, p. 129–136.

Pilet, S., Baker, M.B., and Stolper, E.M., 2008, Metasomatized lithosphere and the origin of alkaline lavas: Science, v. 320, no. 5878, p. 916–919. [Also available at https://doi.org/10.1126/science.1156563.]

Pitkin, J.A., and Long, C.L., 1977, Interpretation of data from an aerial gamma-ray survey in the Cripple Creek district, Teller County, Colorado: U.S. Geological Survey Open-File Report 77–534, 12 p. [Also available at https://doi.org/10.3133/ofr77534.]

Plumlee, G.S., 1999, The environmental geology of mineral deposits, *in* Plumlee, G.S., Logsdon, M.J., and Filipek, L.F., eds., The environmental geochemistry of mineral deposits—Part A—Processes, techniques, and health issues: Society of Economic Geologists, Reviews in Economic Geology, v. 6, p. 71–116. [Also available at https://doi.org/10.5382/Rev.06.03.]

Plumlee, G.S., Smith, K.S., Montour, M.R., Ficklin, W.H., and Mosier, E.L., 1999, Geologic controls on the composition of natural waters and mine waters draining diverse mineral-deposit types, *in* Plumlee, G.S., Logsdon, M.J., and Filipek, L.F., eds., The environmental geochemistry of mineral deposits—Part B–Case studies and research topics: Society of Economic Geologists, Reviews in Economic Geology, v. 6, p. 373–432. [Also available at https://doi.org/10.5382/Rev.06.19.]

Poblete, J.A., Bissig, T., Mortensen, J.K., Gabites, J., Friedman, R., and Rodriguez, M., 2014, The Cerro Bayo district, Chilean Patagonia—Late Jurassic to Cretaceous magmatism and protracted history of epithermal Ag-Au mineralization: Economic Geology and the Bulletin of the Society of Economic Geologists, v. 109, no. 2, p. 487–502. [Also available at https://doi.org/10.2113/econgeo.109.2.487.]

Porter, E.W., and Ripley, E.M., 1985, Petrologic and stable isotope study of the gold-bearing breccia pipe at the Golden Sunlight deposit, Montana: Economic Geology and the Bulletin of the Society of Economic Geologists, v. 80, no. 6, p. 1689–1706. [Also available at https://doi.org/10.2113/gsecongeo.80.6.1689.]

Pour, A.B., and Hashim, M., 2012, The application of ASTER remote sensing data to porphyry copper and epithermal gold deposits: Ore Geology Reviews, v. 44, p. 1–9. [Also available at https://doi.org/10.1016/j.oregeorev.2011.09.009.]

Price, W.A., Morin, K., and Hutt, N., 1997, Guidelines for the prediction of acid rock drainage and metal leaching for mines in British Columbia—Part II—Recommended procedures for static and kinetic testing, *in* Fourth International Conference on Acid Rock Drainage, 1997, Vancouver, British Columbia, Proceedings: Ottawa, Canada, Mine Environmental Neutral Drainage Programme, p. 15–30.

Rahfeld, A., 2013, Mineralogical and geochemical fingerprints of alteration associated with the Cripple Creek alkaline-magmatic Au-Te deposit: Golden Colo., Colorado School of Mines, M.S. thesis, 151 p. [Also available at http://hdl.handle.net/11124/79020.]

Ratajeski, K., and Campbell, A.R., 1994, Distribution of fluid inclusions in igneous quartz of the Capitan pluton, New Mexico, USA: Geochimica et Cosmochimica Acta, v. 58, no. 3, p. 1161–1174. [Also available at https://doi.org/10.1016/0016-7037(94)90579-7.]

Rice, C.M., Harmon, R.S., and Shepherd, T.J., 1985, Central City, Colorado—The upper part of an alkaline porphyry molybdenum system: Economic Geology and the Bulletin of the Society of Economic Geologists, v. 80, no. 7, p. 1769–1796. [Also available at https://doi.org/10.2113/gsecongeo.80.7.1769.]

Richards, J.P., 1990, Petrology and geochemistry of alkalic intrusives at the Porgera gold deposit, Papua New Guinea: Journal of Geochemical Exploration, v. 35, no. 1–3, p. 141–199. [Also available at https://doi.org/10.1016/0375-6742(90)90038-C.]

Richards, J.P., 1995, Alkalic-type epithermal gold deposits—A review, *in* Thompson, J.F.H., ed., Magmas, fluids, and ore deposits: Canada Mineralogical Association Short Course Series, v. 23, p. 367–400.

Richards, J.P., 2009, Postsubduction porphyry Cu-Au and epithermal Au deposits—Products of remelting of subduction-modified lithosphere: Geology, v. 37, no. 3, p. 247–250. [Also available at https://doi.org/10.1130/G25451A.1.]

Richards, J.P., 2013, Giant ore deposits formed by optimal alignments and combinations of geological processes: Nature Geoscience, v. 6, no. 11, p. 911–916. [Also available at https://doi.org/10.1038/ngeo1920.]

Richards, J.P., and Kerrich, R., 1993, The Porgera gold mine, Papua New Guinea—Magmatichydrothermal to epithermal evolution of an alkalic-type precious metal deposit: Economic Geology and the Bulletin of the Society of Economic Geologists, v. 88, no. 5, p. 1017–1052. [Also available at https://doi.org/10.2113/gsecongeo.88.5.1017.]

Richards, J.P., and Ledlie, I., 1993, Alkalic intrusive rocks associated with the Mount Kare gold deposit, Papua New Guinea—Comparison with the Porgera intrusive complex: Economic Geology and the Bulletin of the Society of Economic Geologists, v. 88, no. 4, p. 755–781. [Also available at https://doi.org/10.2113/gsecongeo.88.4.755.]

Richards, J.P., McCulloch, M.T., Chappell, B.W., and Kerrich, R., 1991, Sources of metals in the Porgera gold deposit, Papua New Guinea—Evidence from alteration, isotope, and noble metal geochemistry: Geochimica et Cosmochimica Acta, v. 55, no. 2, p. 565–580. [Also available at https://doi.org/10.1016/0016-7037(91)90013-U.]

Richards, J.P., Wilkinson, D., and Ullrich, T., 2006, Geology of the Sari Gunay epithermal gold deposit, northwest Iran: Economic Geology and the Bulletin of the Society of Economic Geologists, v. 101, no. 8, p. 1455–1496. [Also available at https://doi.org/10.2113/gsecongeo.101.8.1455.]

Rogers, N.W., and Setterfield, T.N., 1994, Potassium and incompatible-element enrichment in shoshonitic lavas from the Tavua volcano, Fiji: Chemical Geology, v. 118, no. 1–4, p. 43–62. [Also available at https://doi.org/10.1016/0009-2541(94)90169-4.]

Ronacher, E., Richards, J.P., Reed, M.H., Bray, C.J., Spooner, E.T.C., and Adams, P.D., 2004, Characteristics and evolution of the hydrothermal fluid in the north zone high-grade area, Porgera gold deposit, Papua New Guinea: Economic Geology and the Bulletin of the Society of Economic Geologists, v. 99, no. 5, p. 843–867. [Also available at https://doi.org/10.2113/gsecongeo.99.5.843.]

Sabins, F.F., 1999, Remote sensing for mineral exploration: Ore Geology Reviews, v. 14, no. 3–4, p. 157–183. [Also available at https://doi.org/10.1016/S0169-1368(99)00007-4.]

Saunders, J.A., 1986, Petrology, mineralogy, and geochemistry of representative gold telluride ores from Colorado: Golden, Colo., Colorado School of Mines, Ph. D. thesis, 182 p. [Also available at https://mountainscholar.org/handle/11124/170211.]

Saunders, J.A., 1991, Gold deposits of the Boulder County gold district, Colorado, *in* Shawe, D.R., Ashley, R.P., and Carter, L.M.H., eds., Epithermal gold deposits—Part II: U.S. Geological Survey Bulletin 1857-I, p. 137–148. [Also available at https://doi.org/10.3133/b1857I.]

Saunders, J.A., and May, E.R., 1986, Bessie G—A high-grade epithermal gold telluride deposit, La Plata County, Colorado, *in* Macdonald, A.J., ed., Gold '86—An International Symposium on the Geology of Gold Deposits, Toronto, Canada, 1986, Proceedings: Toronto, Canada Geological Association, p. 436–444.

Scheibner, E., and Stevens, B.P.J., 1974, The Lachlan River lineament and its relationship to metallic deposits: Quarterly Notes of the Geological Survey of New South Wales, v. 14, p. 8–18. [Also available at https://search.geoscience.nsw.gov.au/product/857.]

Scherbarth, N.L., and Spry, P.G., 2006, Mineralogical, petrological, stable isotope, and fluid inclusion characteristics of the Tuvatu gold-silver telluride deposit, Fiji—Comparisons with the Emperor deposit: Economic Geology and the Bulletin of the Society of Economic Geologists, v. 101, no. 1, p. 135–158. [Also available at https://doi.org/10.2113/gsecongeo.101.1.135.]

Schmidt, P.W., Clark, D.A., and Logan, K.J., 1997, Paleomagnetism, magnetic petrophysics and magnetic signature of the Porgera intrusive complex, Papua New Guinea: Exploration Geophysics, v. 28, no. 1–2, p. 276–280. [Also available at https://doi.org/10.1071/EG997276.]

Schutz, J.L., 1995, Gold mineralization associated with alkaline intrusives at the Carache Canyon breccia pipe prospect, Ortiz Mountains, New Mexico, *in* Bauer, P.W., Kues, B.S., Dunbar, N.W., Karlstrom, K.E., Harrison, B., eds., Geology of the Santa Fe Region—46th Field Conference Guidebook: New Mexico Geological Society, p. 167–173.

Seal, R.R., 2010, Geoenvironmental features, chap. S *of* John, D.A., ed., Porphyry copper deposit model, chap. B *of* Mineral deposit models for resource assessment: U.S. Geological Survey Scientific Investigations Report 2010-5070-B, p 122–125. [Also available at https://doi.org/10.3133/sir20105070B.]

Seal, R.R., and Ayuso, R.A., 2011, Understanding processes affecting mineral deposits in humid environments: U.S. Geological Survey Fact Sheet 2010–3105, 6 p. [Also available at https://doi.org/10.3133/fs20103105.]

Seward, T.M., 1973, Thio complexes of gold and the transport of gold in hydrothermal ore solutions: Geochimica et Cosmochimica Acta, v. 37, no. 3, p. 379–399. [Also available at https://doi.org/10.1016/0016-7037(73)90207-X.]

SGS Mineral Services, 2013, Cyanide recovery: SGS Minerals Technical Document T3 SGS 019, 6 p., SGS website, accessed June 16, 2014, at https://www.sgs.com/~/media/Global/Documents/Flyers%20and%20Leaflets/SGS-MIN-WA016-Cyanide-Recovery-Comparison-EN-11.pdf.

Shackleton, J.M., Spry, P.G., and Bateman, R., 2003, Telluride mineralogy of the Golden Mile deposit, Kalgoorlie, Western Australia: Canadian Mineralogist, v. 41, no. 6, p. 1503–1524. [Also available at https://doi.org/10.2113/gscanmin.41.6.1503.]

Shaw, S.C., 2000, Geochemical characterization and water quality predictions for the Zortman-Landusky reclamation project, *in* Eighth Annual Mine Design, Operations and Closure Conference, Billings, Mont., 2000 Proceedings: Billings, Mont., Mine Design, Operations and Closure Conference, 16 p. [Also available at http://citeseerx.ist.psu.edu/viewdoc/summary?doi=10.1.1.615.1904.]

Sillitoe, R.H., 1979, Some thoughts on gold-rich porphyry copper deposits: Mineralium Deposita, v. 14, no. 2, p. 161–174. [Also available at https://doi.org/10.1007/BF00202933.]

Simmons, E.C., and Hedge, C.E., 1978, Minor-element and Sr-isotope geochemistry of tertiary stocks, Colorado mineral belt: Contributions to Mineralogy and Petrology, v. 67, no. 4, p. 379–396. [Also available at https://doi.org/10.1007/BF00383298.]

Simmons, S.F., and Brown, K.L., 2006, Gold in magmatic hydrothermal solutions and the rapid formation of a giant ore deposit: Science, v. 314, no. 5797, p. 288–291. [Also available at https://doi.org/10.1126/science.1132866.]

Simmons, S.F., White, N.C., and John, D.A., 2005, Geological characteristics of epithermal precious and base metal deposits: Economic Geology—100th Anniversary Volume, p. 485–522. [Also available at https://doi.org/10.5382/AV100.16.]

Smith, A.C.S., and Mudder, T.I., 1997, The environmental geochemistry of cyanide, *in* Plumlee, G.S., Logsdon, M.J., and Filipek, L.F., eds., The environmental geochemistry of mineral deposits–Part A—Processes, techniques, and health issues: Society of Economic Geologists, Reviews in Economic Geology, v. 6, p. 229–248. [Also available at https://doi.org/10.5382/Rev.06.11.]

Smith, C.L., Rosman, K.J.R., and de Laeter, J.R., 1978, The isotopic composition of tellurium: International Journal of Mass Spectrometry and Ion Physics, v. 28, no. 1, p. 7–17. [Also available at https://doi.org/10.1016/0020-7381(78)80065-5.]

Smith, R.J., 2014, Electromagnetic induction methods in mining geophysics from 2008 to 2012: Surveys in Geophysics, v. 35, no. 1, p. 123–156. [Also available at https://doi.org/10.1007/s10712-013-9227-1.]

Smithers, R.M., and Krouse, H.R., 1968, Tellurium isotope fractionation study: Canadian Journal of Chemistry, v. 46, no. 4, p. 583–591. [Also available at https://doi.org/10.1139/v68-096.]

Sobek, A.A., Schuller, W.A., Freeman, J.R., and Smith, R.M., 1978, Field and laboratory methods applicable to overburdens and mine soils: U.S. Environmental Protection Agency, EPA-600/2-78-054, 218 p. [Also available at https://www.resolutionmineeis.us/documents/sobek-1978.]

Sorensen, H., 1974, The alkaline rocks: New York, J. Wiley, 622 p.

Spry, P.G., Chryssoulis, S., and Ryan, C.G., 2004, Process mineralogy of gold—Gold from telluride-bearing ores: JOM, v. 56, no. 8, p. 60–62. [Also available at https://doi.org/10.1007/s11837-004-0185-4.]

Spry, P.G., Foster, F., Truckle, J.S., and Chadwick, T.H., 1997, The mineralogy of the Golden Sunlight gold-silver telluride deposit, Whitehall, Montana, U.S.A: Mineralogy and Petrology, v. 59, no. 3, p. 143–164. [Also available at https://doi.org/10.1007/BF01161857.]

Spry, P.G., Paredes, M.M., Foster, F., Truckle, J.S., and Chadwick, T.S., 1996, Evidence for a genetic link between gold-silver telluride and porphyry molybdenum mineralization at the Golden Sunlight deposit, Whitehall, Montana—Fluid inclusion and stable isotope studies: Economic Geology and the Bulletin of the Society of Economic Geologists, v. 91, no. 3, p. 507–526. [Also available at https://doi.org/10.2113/gsecongeo.91.3.507.]

Spry, P.G., and Scherbarth, N.L., 2006, The gold-vanadium-tellurium association at the Tuvatu gold-silver prospect, Fiji—Conditions of ore deposition: Mineralogy and Petrology, v. 87, no. 3, p. 171–186. [Also available at https://doi.org/10.1007/s00710-006-0128-6.]

Spry, P.G., and Thieben, S.E., 2000, The distribution and recovery of gold in the Golden Sunlight gold-silver telluride deposit, Montana, U.S.A: Mineralogical Magazine, v. 64, no. 1, p. 31–42. [Also available at https://doi.org/10.1180/002646100549111.]

Staatz, M.H., 1983, Geology and description of thorium and rare-earth deposits in the southern Bear Lodge Mountains, northeastern Wyoming: U.S. Geological Survey Professional Paper 1049-D, p. D1–D52. [Also available at https://doi.org/10.3133/pp1049D.]

Stein, H.J., and Crock, J.G., 1990, Late Cretaceous-Tertiary magmatism in the Colorado mineral belt—Rare earth element and samarium-neodymium isotopic studies, chap. 11 *of* Anderson, J.L., ed., The nature and origin of cordilleran magmatism: Geological Society of America Memoirs, v. 174, p. 195–223. [Also available at https://doi.org/10.1130/MEM174-p195.]

Taranik, D.L., 1990, Remote detection and mapping of supergene iron oxides in the Cripple Creek mining district, Colorado: Boulder, University of Colorado, M.S. Thesis, 103 p.

Taylor, H.P., 1997, Oxygen and hydrogen isotope relationships in hydrothermal mineral deposits, *in* Barnes, H.L., ed., Geochemistry of hydrothermal ore deposits 2nd ed.: New York, Wiley Interscience, p. 229–302.

Thieben, S.E., and Spry, P.G., 1995, The geology and geochemistry of Cretaceous-Tertiary alkaline igneous rock-related gold-silver telluride deposits of Montana, USA, *in* Pašava, J., Kríbek, B., and Zák, K., eds., Mineral deposits—From their origin to their environmental impacts: CRC Press, p. 199–202.

Thompson, T.B., Trippel, A.D., and Dwelley, P.C., 1985, Mineralized veins and breccias of the Cripple Creek district, Colorado: Economic Geology and the Bulletin of the Society of Economic Geologists, v. 80, no. 6, p. 1669–1688. [Also available at https://doi.org/10.2113/gsecongeo.80.6.1669.]

U.S. Environmental Protection Agency, 1994, Acid mine drainage prediction: U.S. Environmental Protection Agency, EPA530-R-94-036, 52 p. [Also available at https://www.epa.gov/sites/production/files/2015-09/documents/amd.pdf.]

U.S. Environmental Protection Agency, 2004, Summitville Mine, fact sheet: U.S. Environmental Protection Agency website, accessed June 16, 2014, at https://www.epa.gov/superfund/accomp/factsheets04/summit.htm.

van der Meer, F.D., van der Werff, H.M.A., van Ruitenbeek, F.J.A., Hecker, C.A., Bakker, W.H., Noomen, M.F., van der Meijde, M., Carranza, E.J.M., de Smeth, J.B., and Woldai, T., 2012, Multi- and hyperspectral geologic remote sensing—A review: International Journal of Applied Earth Observation and Geoinformation, v. 14, no. 1, p. 112–128. [Also available at https://doi.org/10.1016/j.jag.2011.08.002.]

Voudouris, P., 2006, A comparative mineralogical study of Te-rich magmatic-hydrothermal systems in northeastern Greece: Mineralogy and Petrology, v. 87, no. 3, p. 241–275. [Also available at https://doi.org/10.1007/s00710-006-0131-y.]

Walshe, J.L., Heithersay, P.S., and Morrison, G.W., 1995, Toward an understanding of the metallogeny of the Tasman fold belt system: Economic Geology and the Bulletin of the Society of Economic Geologists, v. 90, no. 6, p. 1382–1401. [Also available at https://doi.org/10.2113/gsecongeo.90.6.1382.]

Webminerals, 2014, Bilibinskite Mineral Data, Webminerals website, accessed June 16, 2014, at http://webmineral.com/data/Bilibinskite.shtml#.U3YsRJ1MEkQ.

Werle, J.L., Ikramuddin, M., and Mutschler, F.E., 1984, Allard stock, La Plata Mountains, Colorado—An alkaline rock-hosted porphyry copper-precious metal deposit: Canadian Journal of Earth Sciences, v. 21, no. 6, p. 630–641. [Also available at https://doi.org/10.1139/e84-069.]

White, N.C., and Hedenquist, J.W., 1990, Epithermal environments and styles of mineralization—Variations and their causes, and guidelines for exploration: Journal of Geochemical Exploration, v. 36, no. 1–3, p. 445–474. [Also available at https://doi.org/10.1016/0375-6742(90)90063-G.]

White, P., Ussher, G., and Hermoso, D., 2010, Evolution of the Ladolam geothermal system on Lihir Island, Papua New Guinea, *in* World Geothermal Congress, Bali, Indonesia, 2010, Proceedings: International Geothermal Association, p. 1–7. [Also available at https://www.geothermal-energy.org/pdf/IGAstandard/WGC/2010/1226.pdf.]

White, W.W., Lapakko, K.A., and Cox, R.L., 1999, Static-test methods most commonly used to predict acid-mine drainage—Practical guidelines for use and interpretation, *in* Plumlee, G.S., Logsdon, M.J., and Filipek, L.F., eds., The environmental geochemistry of mineral deposits—Part A—Processes, techniques, and health issues: Society of Economic Geologists, Reviews in Economic Geology, v. 6, p. 325–338. [Also available at https://doi.org/10.5382/Rev.06.]

Williams, R.D., Gabelman, J., Shaw, S., Jepson, W., Gammons, C., and Kill Eagle, J.L., 2009, Zortman-Landusky—Challenges in a decade of closure, *in* Barnhisel, R.I., ed., Revitalizing the environment—Proven solutions and innovative approaches, National Meeting of the American Society of Mining and Reclamation, Billings, Mont. 2009, Proceedings: American Society of Mining and Reclamation, p. 1583–1595.

Wilson, A.J., Cooke, D.R., and Richards, T., 2004, Veins, pegmatites and breccias—Examples from the alkalic Cadia Quarry Au–Cu porphyry deposit, NSW, Australia, *in* Cooke, D. R. Deyell, C., and Pongratz, C., eds., 24 carat gold workshop: University of Tasmania, CODES Special Publication v. 5, p. 45–56.

Wilson, M.R., and Kyser, R.K., 1988, Geochemistry of porphyry-hosted Au-Ag deposits in the Little Rocky Mountains, Montana: Economic Geology, v. 83, p. 1329–1346, accessed November 27, 2010, at https://doi.org/10.2113/gsecongeo.83.7.1329.

Wirt, L., Leib, K.J., Bove, D.J., Mast, M.A., Evans, J.B., and Meeker, G.P., 1999, Determination of chemical-constituent loads during base-flow and storm-runoff conditions near historical mines in Prospect Gulch, Upper Animas River Watershed, southwestern Colorado: U.S. Geological Survey Open-File Report 99–159, 43 p. [Also available at https://doi.org/10.3133/ofr99159.]

Woods, K.T., and Webster, S.S., 1985, Geophysical signature of gold and porphyry copper mineral deposits in the Lachlan Fold Belt, NSW: Exploration Geophysics, v. 16, no. 2–3, p. 325–331. [Also available at https://doi.org/10.1071/EG985325.]

Woodward, L.A., 1995, Metallic mineral deposits of the Judith Mountains, central Montana: Montana Bureau of Mines and Geology Memoir 67, 78 p.

Woodward, L.A., and Giles, D.L., 1993, Lode mineralization in the Judith Mountains, *in* Hunter, L.D., ed., Energy and mineral resources of central Montana: Montana Geological Society Guidebook, p. 197–214.

Wyborn, D., 1992, The tectonic significance of Ordovician magmatism in the eastern Lachlan Fold Belt: Tectonophysics, v. 214, no. 1–4, p. 177–192. [Also available at https://doi.org/10.1016/0040-1951(92)90196-D.]

Yang, D., and Oldenburg, D.W., 2012, Three-dimensional inversion of airborne time-domain electromagnetic data with applications to a porphyry deposit: Geophysics, v. 77, no. 2, p. B23–B34. [Also available at https://doi.org/10.1190/geo2011-0194.1.]

Zanbak, C., 2012, Heap leaching technique in mining, within the context of best available techniques (BAT): The European Association of Mining Industries, Metal Ores and Industrial Materials, 36 p. [Also available at https://doi.org/10.13140/RG.2.2.36374.86081.]

Zhang, Q., Liu, Y., He, M., Bai, J., Xu, W., and Zhao, C., 2018, Ore prospecting model and targets for the Dashuigou tellurium deposit, Sichuan Province, China: Acta Geochimica, v. 37, no. 4, p. 578–591. [Also available at https://link.springer.com/article/10.1007/s11631-018-0271-x.]

Zhang, X., Nesbitt, B.E., and Muehlenbachs, K., 1989, Gold mineralization in the Okanagan Valley, southern British Columbia—Fluid inclusion and stable isotope studies: Economic Geology and the Bulletin of the Society of Economic Geologists, v. 84, no. 2, p. 410–424. [Also available at https://doi.org/10.2113/gsecongeo.84.2.410.]

Zhang, X., and Spry, P.G., 1994, Petrological, mineralogical, fluid inclusion, and stable isotope studies of the Gies gold-silver telluride deposit, Judith Mountains, Montana: Economic Geology and the Bulletin of the Society of Economic Geologists, v. 89, no. 3, p. 602–627. [Also available at https://doi.org/10.2113/gsecongeo.89.3.602.]

Zhang, Z., Mao, J., Wang, Y., Pirajno, F., Liu, J., and Zhao, Z., 2010, Geochemistry and geochronology of the volcanic rocks associated with the Dong'an adularia-sericite epithermal gold deposit, Lesser Hinggan Range, Heilongjiang province, NE China—Constraints on the metallogenesis: Ore Geology Reviews, v. 37, no. 3–4, p. 158–174. [Also available at https://doi.org/10.1016/j.oregeorev.2010.03.001.]

Publishing support provided by the Science Publishing Network, Denver Publishing Service Center

For more information concerning the research in this report, contact the

Center Director, USGS Geology, Geophysics, and Geochemistry Science Center

Box 25046, Mail Stop 973

Denver, CO 80225

(303) 236-1800

Or visit Geology, Geophysics, and Geochemistry Science Center website at https://www.usgs.gov/centers/gggsc

ISSN 2328-0328 (online)
https://doi.org/10.3133/sir20105070R